# Photovoltaic Plant and Battery Energy Storage System Integration at NREL's Flatirons Campus

Vahan Gevorgian, Przemyslaw Koralewicz, Shahil Shah, Emanuel Mendiola, Robb Wallen, and Hugo Villegas Pico

*National Renewable Energy Laboratory*

*With collaboration from First Solar*

# Photovoltaic Plant and Battery Energy Storage System Integration at NREL's Flatirons Campus

Vahan Gevorgian, Przemyslaw Koralewicz,
Shahil Shah, Emanuel Mendiola, Robb Wallen,
and Hugo Villegas Pico

*National Renewable Energy Laboratory*

*With collaboration from First Solar*

**NOTICE**

This report is available at no cost from the National Renewable
Energy Laboratory (NREL) at www.nrel.gov/publications.

U.S. Department of Energy (DOE) reports produced after 1991
and a growing number of pre-1991 documents are available
free via www.OSTI.gov.

# Acknowledgments

# List of Acronyms

| | |
|---|---|
| AGC | automatic generation control |
| ARIES | Advanced Research on Integrated Energy Systems |
| BESS | battery energy storage system |
| BMS | battery management system |
| CAISO | California Independent System Operator |
| CGI | controllable grid interface |
| DAS | data acquisition system |
| DOE | U.S. Department of Energy |
| EMS | energy management system |
| ERCOT | Electric Reliability Council of Texas |
| FFR | fast frequency response |
| GHI | global horizontal irradiance |
| GPS | Global Positioning System |
| IBR | inverter-based resource |
| IEEE | Institute of Electrical and Electronics Engineers |
| IESS | Integrated Energy Systems at Scale |
| IR | infrared |
| Li-ion | lithium-ion |
| MPP | maximum power point |
| MPPE | maximum power point estimation |
| MPPT | maximum power point tracking |
| NERC | North American Electric Reliability Corporation |
| NREL | National Renewable Energy Laboratory |
| NWTC | National Wind Technology Center |
| PCC | point of common coupling |
| PCC | point of common coupling |
| PFR | primary frequency response |
| PHIL | power-hardware-in-the-loop |
| PLL | phase-locked loop |
| PMU | phasor measurement unit |
| POD | power oscillation damping |
| POI | point of interconnection |
| PPC | power plant controller |
| PREPA | Puerto Rica Electric Power Authority |
| PSS | power system stabilizer |
| PV | photovoltaic |
| ROCOF | rate of change of frequency |
| RPS | renewables portfolio standards |
| RTAC | Real-Time Automation Controller |
| RTDS | real-time digital simulator |
| SCADA | supervisory control and data acquisition |
| SDS | safety data sheet |
| SETO | Solar Energy Technologies Office |
| SF | synchronous frame |
| SOC | state of charge |

SSI             sinusoidal signal integrator
THD             total harmonic distortion

# Executive Summary

Although utility-scale solar photovoltaic (PV) power plants are becoming a cost-effective energy resource, there is belief within the energy industry that the increasing penetrations of PV technologies could potentially impact grid reliability. This is due to the variability across timescales, the forecast uncertainty of the solar energy resource, and the impacts on both distribution and transmission systems. This can cause utilities to severely limit PV installations or to assign PV integration costs when considering a least-cost portfolio of resources. As California and other regions in the United States are marching toward fulfilling—and probably exceeding—their renewables portfolio standards goals, grid operators are beginning to face operational challenges that could have implications for existing renewable and nonrenewable generators and that will shape opportunities for future projects. In this work, we focused on developing controls and conducting demonstrations for AC-coupled PV-battery energy storage systems (BESS) in which PV and BESS are colocated and share a point of common coupling (PCC). The PV and BESS systems do not share any physical components (such as inverters, transformers, protection, or energy metering equipment), but they have a common controller that can operate both PV and BESS either as a single plant or as two independent systems. The general configuration of a utility-scale PV-BESS plant used to develop and demonstrate many control concepts during this project is shown in Figure ES-1. . As colocated resources, PV generation and BESS naturally share the same infrastructure (substation, PCC, tie-lines) and plant-level controller that operates both technologies as one utility-scale asset interacting with a single market interface.
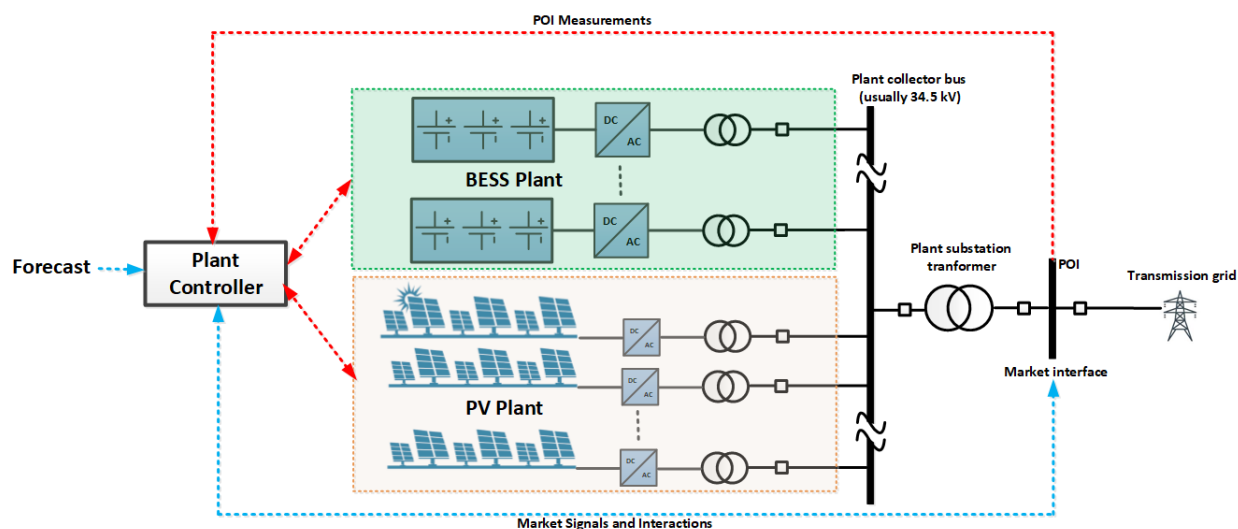


**Figure ES-1. Colocated AC-coupled PV-storage power plant**

The cost of BESS has dramatically declined in recent years, presenting an opportunity for energy storage not only to perform functions currently met by conventional generators that serve peak electricity demand but also to provide new opportunities for economic hybridization with variable generation, including PV. The use of storage can change and customize the "shape" of PV production to better match load and peak demand in many power systems, make PV generation more flexible, and facilitate very high levels of PV generation without curtailment.

vi

This cooperative research-and-development agreement project conducted by the National Renewable Energy Laboratory (NREL) and First Solar leveraged and benefited from the knowledge and field experience accumulated from NREL's previous work with First Solar and other partners—e.g., the California Independent System Operator, the Electric Reliability Council of Texas, AES, Puerto Rica Electric Power Authority (PREPA)—and advanced prior work by:

- Combining PV plant and BESS controls to provide the existing and future projected ancillary service products by various balancing authorities and system operators in U.S. interconnections and island systems
- Developing controls with higher levels of complexity due to the multi-technology nature of PV-BESS operation
- Using an advanced PV power plant controller based on the Schweitzer Engineering Laboratories Real-Time Automation Controller (RTAC) platform supplemented with new control algorithms to include BESS and provide many types of essential reliability services
- Using advanced, smart string PV inverters that provide high performance, robust air-cooled design, easy serviceability, and a quicker return on investment
- Demonstrating controls by the utility-scale PV plant combined with BESS that can qualify for participating in the existing ancillary service spinning and nonspinning reserve markets
- Demonstrating new PV-BESS controls that can be required from variable generation by evolving ancillary service markets, such as primary frequency response (PFR), fast frequency response (FFR), down-ramp control, short-term variability smoothing, and voltage control
- Developing new advanced ancillary service controls by PV-BESS plants for interarea oscillations damping, subsynchronous resonance mitigation, mitigation of control interactions, etc.
- Demonstration of grid-forming controls by BESS to provide resilience services (black start, islanded operation, system restoration) to hybrid PV-plus-storage plants.

The project resulted in the development of a new research asset—a grid-scale PV-storage hybrid system test bed that can be used by the industry and research community for the validation and demonstration of new control concepts, stakeholder engagement, workforce education, and as a validation platform for the future standardization of hybrid technologies. It will lead to the development of both technology and vendor-neutral, "plug-and-play" hybridization guidelines and control architecture openly available at all segments of the stakeholder community. This project was the first research effort that demonstrated the multi-technology aspect of grid integration research possible at NREL's Flatirons Campus and facilitated the shift toward the development of new research platforms, such as Integrated Energy Systems at Scale (IESS) and the Advanced Research on Integrated Energy Systems (ARIES). Capabilities developed under this project were also foundational for continued hybrid systems research conducted at NREL and were used in other U.S. Department of Energy-funded research work, such as the Grid Modernization Laboratory Consortium FlexPower Hybrid Plants project.

The emergence of new integrated energy systems provides many opportunities, and it also presents urgent challenges that must be addressed to ensure that these new integrated energy

systems meet evolving consumer expectations and continue to be economic, reliable, resilient, and secure. From this perspective, integrated PV-BESS systems can play a crucial role for power systems in the transition to high shares of inverter-based resources.

Controls developed and demonstrated under this project for PV-storage plants under both real grid-connected and controlled grid conditions (emulated by NREL's multi-MW grid simulator) include:

- Controls for inertia-like response when the PV-storage plant was responding to the rate of change of frequency
- Controls for FFR
- Controls for PFR
- Ability of PV storage plants to participate in automatic generation control
- Dispatchability controls
- Variability smoothing and ramp-limiting tests
- Advanced power system oscillations damping controls
- Real-time potential available power estimation in curtailed PV plants
- Resilience service controls in the form of black start by grid-forming battery energy storage and the islanded operation of a PV-storage system.

The research and testing activities under this cooperative research-and-development project help address many goals in the areas of achieving a dramatic increase of PV-generated electricity that can be dispatched any time and in maintaining the adequate levels of reliability. The results of this work can be used in designing future ancillary service markets in the United States and abroad to incentivize renewable generators and energy storage to provide such services for enhanced grid stability and reliability.

# Table of Contents

# List of Figures

# List of Tables

# 1 Introduction

## 1.1 Solar PV Integration Challenges

Although utility-scale solar photovoltaic (PV) power plants are becoming a cost-effective energy resource, there is belief within the industry that the increasing penetrations of PV technologies could potentially impact grid reliability. This is due to the variability across timescales and forecast uncertainty of the solar energy resource and the impacts on both distribution and transmission systems. This can cause utilities to severely limit PV installations or assign PV integration costs when considering a least-cost portfolio of resources. With PV's increased proportion of energy to the generation mix, advanced PV controls and grid integration features can minimize grid impacts from variability and, in many cases, improve reliability, stability, and power quality. The deployment of utility-scale, grid-friendly PV power plants that incorporate advanced capabilities to support grid stability and reliability is essential for the large-scale integration of PV generation into the electric power grid.

The rapidly declining cost of PV technology in combination with evolving renewables portfolio standards (RPS) is driving increased PV deployment in many states. A key limiting factor for PV deployment is curtailment due to overgeneration and other constraints. Energy storage can play a crucial role in keeping PV curtailment to acceptable levels, thus the enabling cost-effective integration of larger amounts of PV generation. For example, in fall 2015, the California state legislature passed Senate Bill 350, which requires all utilities in the state to produce 50% of their electricity sales from renewable sources by 2030. In 2018, Senate Bill 100 was signed into law, which increased the RPS to 60% by 2030 and required all the state's electricity to come from carbon-free resources by 2045 [1]. To reach these RPS goals, California operators will need to find additional ways to balance generation and load to manage the variability of increased renewable generation. In combination with the 1,325-GW California energy storage procurement mandate, ancillary services provided by renewables can enhance system flexibility and reliability and reduce needs in spinning reserves by conventional power plants. The exact amount of energy storage needed to meet the RPS goals depends on the complex interdependence of a range of grid flexibility options. One National Renewable Energy Laboratory (NREL) study [2] estimated that under certain scenarios of flexibility and PV levelized cost of energy, nearly 19 GW of energy storage will be required to meet California's 50% RPS goals. Similar studies have been conducted by others looking into the economic and operational impacts of energy storage on PV integration for creating regionally specific low-cost, balanced, and low-carbon generation portfolios; however, the role of energy storage in combination with high levels of variable PV generation when providing a wide range of reliability services in the most cost-effective and co-optimized way is largely unknown to the industry. Many questions are still unknown and depend on future research efforts, including control objectives and architectures, optimization methods, scalability issues, and technology-specific response characteristics. In addition, the lack of publicly available testing and demonstration results for both energy storage and PV technologies operating with the common system-level control objectives at large scales is a significant barrier to bridging the knowledge gaps in the research community and among industry stakeholders.

As California and other regions in the United States are marching toward fulfilling—and probably exceeding—these RPS goals, grid operators are beginning to face operational challenges that could have implications for existing renewable and nonrenewable generators and

1

that will shape opportunities for future projects. One example of such a challenge took place on April 21, 2019, as shown in Figure 1, when up to 4.5 GW of PV generation in California had to be curtailed because of overgeneration. The actual curtailed portion of PV generation on the same day is shown in Figure 2. This curtailed energy was essentially lost, and despite being available as a massive spinning reserve, it was not used to provide any services to California's electric grid. Advanced inverter functions and the design and operation of PV projects can help address grid stability problems during such periods. A typical modern utility-scale PV power plant is a complex system of large PV arrays and multiple power electronic inverters, and it can contribute to mitigating the impacts on grid stability and reliability through sophisticated, automatic grid-supportive controls. Integration with energy storage can assist PV integration in any number of ways by increasing power system flexibility.
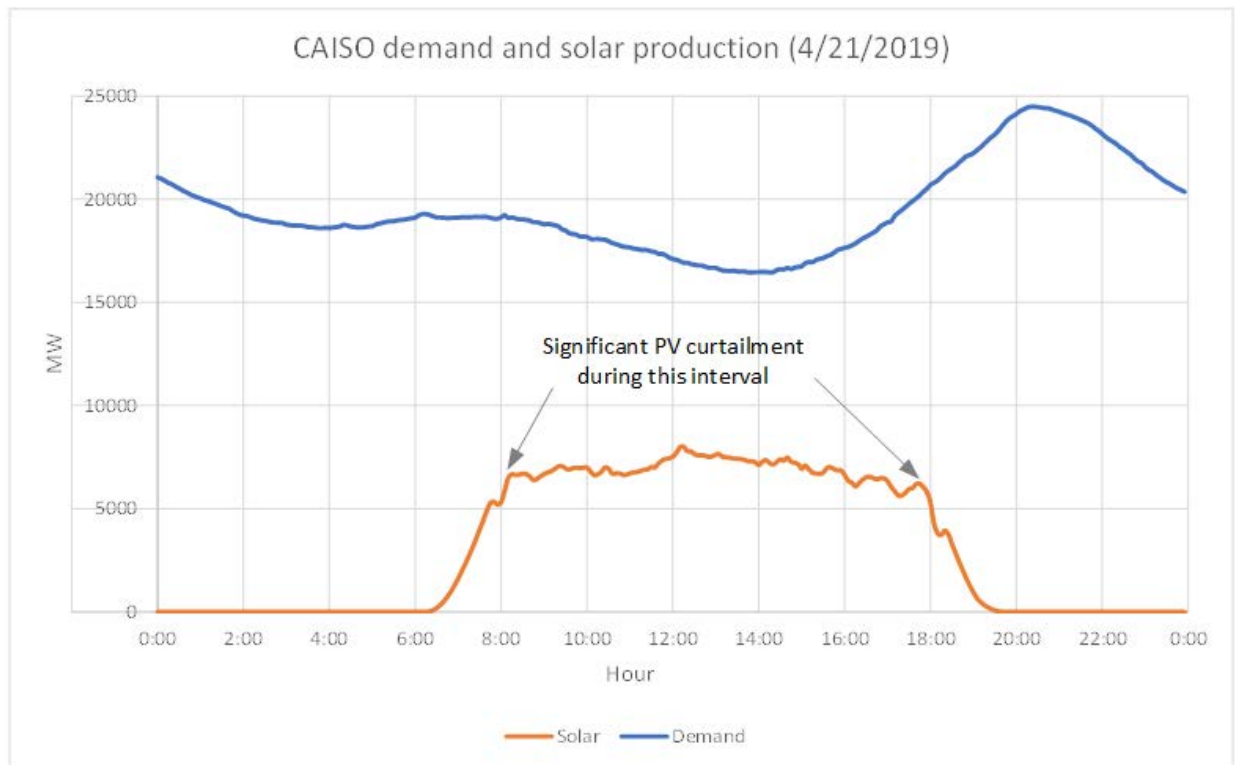


**Figure 1. CAISO generation breakdown for April 21, 2019.**

2
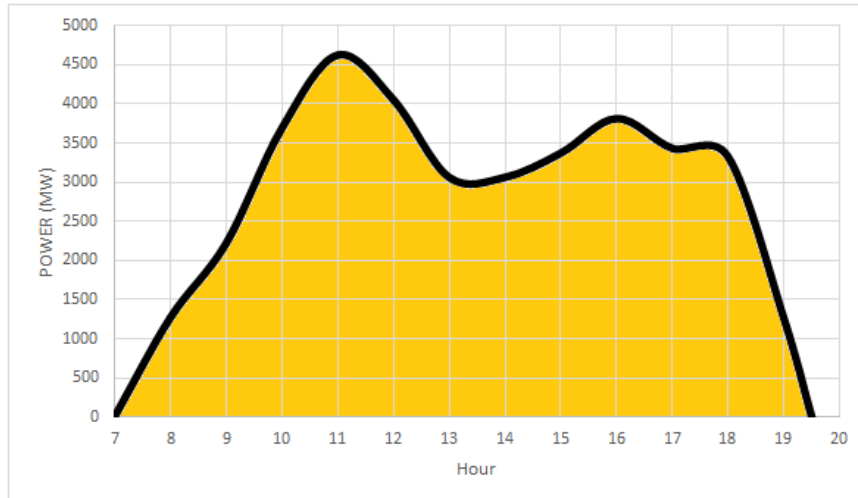
**Figure 2. Curtailed portion of PV generation on April 21, 2019**

It is remarkable that a small portion of this curtailed energy would have been sufficient to cover all California Independent System Operator (CAISO) frequency regulation needs during almost the entire period of curtailment, as shown in Figure 3. The dotted line represents the 600-MW frequency regulation reserve margin that PV generation could have provided if it had been included in CAISO's automatic generation control (AGC). This example shows how curtailed energy could have been used for certain grid services or could have been stored for later use.
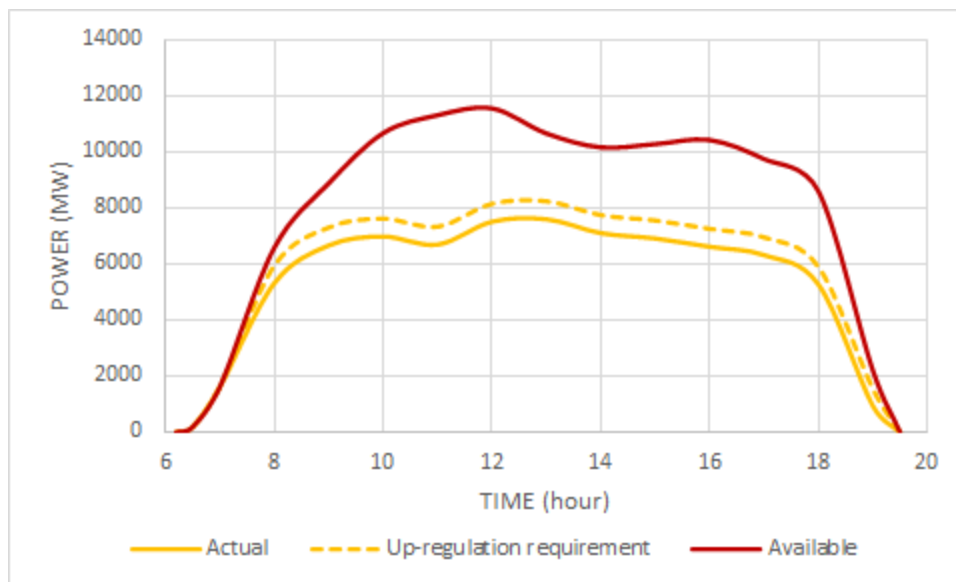


**Figure 3. Available and curtailed PV power on April 21, 2019**

In November 2015, the North American Electric Reliability Corporation (NERC) task force set a framework of reliability services recommended for variable generation (including solar) to provide their share of grid services, including sufficient voltage control, frequency support, and ramping capability—essential components of a reliable bulk power system. The capabilities of utility-scale PV generation technology to provide such services has been demonstrated by NREL and partners in recent U.S. Department of Energy (DOE)-funded groundbreaking demonstration

3

projects conducted in West Texas and Puerto Rico using modern PV plants with rated capacities of +20 MW [3]. In addition, a more recent DOE Solar Energy Technologies Office (SETO)-funded project by NREL in collaboration with CAISO using First Solar's 300-MW PV power plant in California has advanced the industry knowledge even further by demonstrating the ability of PV technology to provide services of unprecedented scale at the system level [4]. Results of these projects are in the public domain and have already triggered significant interest from various stakeholder groups.

The cost of battery energy storage systems (BESS) has dramatically declined in recent years, presenting an opportunity for energy storage not only to perform functions currently met by conventional generators that serve peak electricity demand but also to provide new opportunities for economic hybridization with variable generation, including PV. The use of storage can change and customize the "shape" of PV production to better match load and peak demand in many power systems, make PV generation more flexible, and facilitate very high levels of PV generation without curtailment.

## 1.2  Configurations of PV-Storage Systems

The degree to which the PV and storage are coupled (both physically and operationally) can be divided into four distinct categories:

- Independent: PV and battery are not colocated and do not have a common point of connection, and energy stored in the battery could come from either PV or the grid.
- AC-coupled: PV and battery are colocated and have a common point of connection at the plant substation, and energy stored in the battery could come from either PV or the grid.
- DC-coupled: Battery is connected to the DC side of the PV inverters, and energy stored in the battery could come from either PV or the grid.
- Tightly DC-coupled: Battery is connected to the DC side of PV inverters, and energy stored in the battery could come only from PV.

Each PV-plus-storage configuration has advantages and disadvantages [5]–[9]. Many analyses of PV-plus-storage systems have focused on costs and cost minimization. A sufficient amount of analyses have been done on evaluating the levelized-cost-of-energy metrics for PV-plus-storage systems [10] and on evaluating the economic performance of PV-BESS systems in terms of their cost/benefit ratios [5]. In this work, we focused on developing controls and conducting demonstration testing for AC-coupled PV-BESS systems in which PV and BESS are colocated and share a point of common coupling (PCC). PV and BESS systems do not share any physical components (such as inverters, transformers, protection, or energy metering equipment), but they have a common controller that can operate both PV and BESS either as a single plant or as two independent systems. The general configuration of a utility-scale PV-BESS plant used to develop and demonstrate many control concepts during this project is shown in Figure 4. As colocated resources, PV generation and BESS naturally share the same infrastructure (substation, point of interconnection [POI], tie-lines) and plant-level controller that operates both technologies as one utility-scale asset interacting with a single market interface.
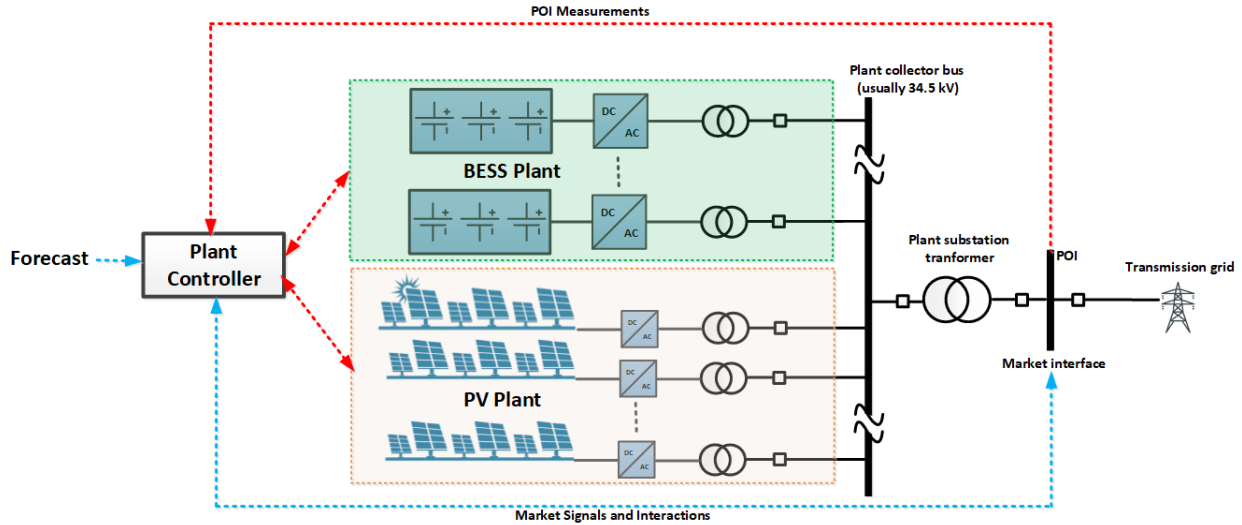
**Figure 4. PV-BESS plant configuration used in this work**

## 1.3 Structure of This Report

To create a fully functional validation testbed for PV-BESS systems, help the industry with developing and demonstrating many types of controls for PV-BESS plants, and establishing a common framework for further discussion, analysis, and advances in PV-plus-storage systems, we developed an "at-scale" system and explored many types of operational aspects of such a system that are hard to evaluate in the field using real commercial installations. The report is intended to demonstrate results of 3-yr activities conducted by NREL and First Solar to address two primary goals:

1. Develop a world-class research facility consisting of an at-scale PV-BESS system at NREL's Flatirons Campus that is capable of providing a wide spectrum of reliability and resilience services when operating under real and simulated grid conditions or as part of stand-alone islanded grids.
2. Develop and demonstrate controls for the provision of such services using this test bed.

The report is structured as follows. Sections 2–6 describe the process of developing and commissioning a PV-BESS validation platform. Sections 7–9 describe results of various types of tests involving different forms of active and reactive power control. Section 10 describes the innovative impedance characterization of PV and BESS inverters developed by NREL. Section 11 describes black-start controls. Section 12 describes the solar resource forecast system implemented at NREL's Flatirons Campus. And Section 13 describes the NREL-developed real-time method for estimating the available power reserve in curtailed PV power plants.

5

# 2 Project Objectives

Emerging hybrid renewable energy systems offer (1) new opportunities for the global renewable energy industry with disruptive market potential and (2) a scalable, economic, and reliable solution applicable to a power system of any size (e.g., large, interconnected power systems, islands, microgrids). The BESS, because of its tremendous range of uses and configurations, can assist PV integration in any number of ways by increasing power system flexibility. These uses include (1) matching generation to loads through time shifting, reducing PV curtailment, managing transmission congestion, and controlling elements of power flow; (2) promoting higher levels of PV penetrations by balancing the grid through ancillary services, load following, ramp limiting, and load levelling; (3) managing forecast uncertainty and short-term variability in PV generation through reserves; (4) smoothing output from individual solar power plants; and (5) enabling islanded and microgrid applications. In addition, in distribution applications, BESS can also play crucial roles in increasing hosting capacities of distribution feeders for large levels of PV penetration by retail energy time shifting, providing voltage support, and improving power quality. This collaborative project aimed toward producing publicly available valid test data and a comprehensive performance evaluation to understand the impacts of combining PV and BESS for all these uses. The project demonstrated many types of services by PV and energy storage systems based on different forms of active and reactive power controls by PV and BESS in both grid-connected mode and under controlled grid conditions emulated by the 7-MVA controllable grid interface (CGI) at NREL's Flatirons Campus.

This cooperative research-and-development agreement project conducted by NREL and First Solar leveraged and benefited from the knowledge and field experience accumulated from NREL's previous work with First Solar and other partners—e.g., CAISO, the Electric Reliability Council of Texas (ERCOT), AES, Puerto Rico Electric Power Authority (PREPA)— and advanced prior work by:

- Combining PV plant and BESS controls to provide the existing and future projected ancillary service products by various balancing authorities and system operators in U.S. interconnections and island systems
- Developing controls with higher levels of complexity due to the multi-technology nature of PV-BESS operation
- Using an advanced PV power plant controller (PPC) based on the SEL Real-Time Automation Controller (RTAC) platform supplemented with new control algorithms to include BESS and provide many types of essential reliability services
- Using advanced, smart string PV inverters that provide high performance, robust air-cooled design, easy serviceability, and a quicker return on investment
- Demonstrating controls by the utility-scale PV plant combined with BESS that can qualify for participating in the existing ancillary service spinning and nonspinning reserve markets
- Demonstrating new PV-BESS controls that can be required from variable generation by evolving ancillary service markets, such as primary frequency response (PFR), fast frequency response (FFR), down-ramp control, short-term variability smoothing, and voltage control

6

- Developing new advanced ancillary service controls by PV-BESS plants for interarea oscillations damping, subsynchronous resonance mitigation, mitigation of control interactions, etc.
- Demonstration of grid-forming controls by BESS to provide resilience services (black start, islanded operation, system restoration) to hybrid PV-plus-storage plants.[1]

The project resulted in the development of a new valuable testing and validation asset—a grid-scale PV-plus-storage hybrid system test bed that can be used by industry and research community for validation and demonstration of new control concepts, stakeholder engagement, workforce education, and as a validation platform for the future standardization of hybrid technologies. In fact, this test bed has already been included as a crucial testing capability in many ongoing research projects and in research proposals led by NREL, industry, and academia in response to various funding opportunity announcements by several DOE programs and requests for proposals from industry. This research is intended to lead development toward both technology- and vendor-neutral, "plug-and-play" hybridization guidelines and control architectures openly available at all segments of the stakeholder community.

This project was the first research effort that demonstrated the multi-technology aspect of grid integration research possible at NREL's Flatirons Campus, and it facilitated the shift toward the development of new research platforms, such as the Integrated Energy Systems at Scale (IESS) and Advanced Research on Integrated Energy Systems (ARIES), as shown in Figure 5. Capabilities developed under this project were also foundational for continued hybrid systems research conducted at NREL and were used in other DOE-funded research work, such as the Grid Modernization Laboratory Consortium FlexPower hybrid plants project.
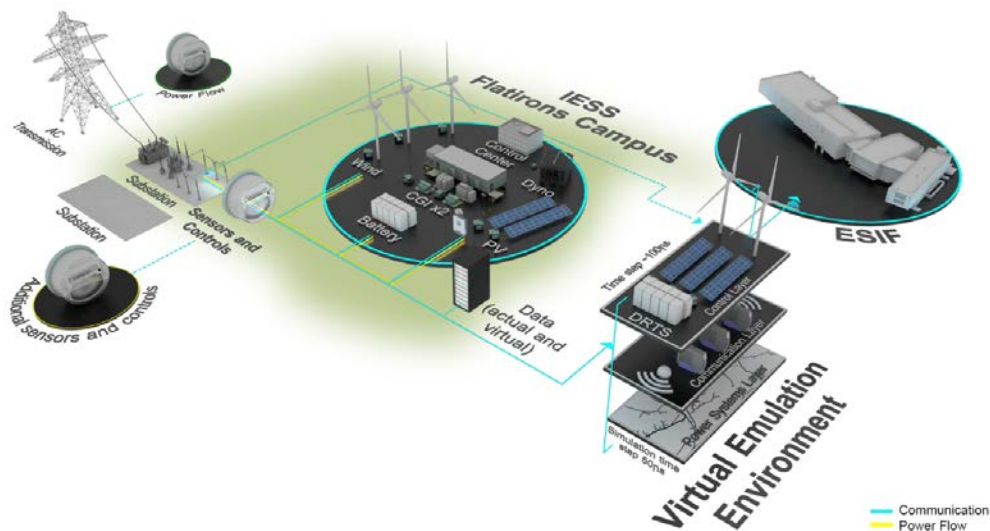


**Figure 5. ARIES virtual emulation platform at NREL's Flatirons Campus**

---

[1] Grid-forming controls by utility-scale PV inverters are being developed and will be tested during 2020–2022 by GE and NREL under another SETO-funded project.

# 3 NREL-First Solar Collaboration

This project was built on NREL and First Solar's prior efforts that demonstrated that large utility-scale PV plants are capable of providing a range of essential grid reliability services [3], [4]. The objective of this research project is to further advance the accumulated controls knowledge from the PV-only area to the multi-technology domain by developing and testing the coordinated controls for PV generation and energy storage cooperation for energy management and ancillary services. This project is unique from other DOE-funded PV-storage integration projects in that the evaluation conditions will be fully controllable because of the distinctive medium-voltage grid emulation capabilities at NREL's Flatirons Campus.

NREL's strategic partnership with First Solar has resulted in the continuation of research collaboration in the area of developing and testing controls for the operation of utility-scale PV generation with energy storage systems for supporting various use cases related to curtailment reduction and reliability services. For this purpose, First Solar installed their 430-KW AC fixed-tilt PV plant at NREL's Flatirons Campus for long-term joint research as a shared resource (estimated cost $350K). In addition, First Solar contributed 3 years of labor to this work ($650K in total). In case of future needs, the First Solar plant is easily expandable to larger capacities because the plant's electrical topology will be based on a scalable advanced string inverter-based configuration (smart air-cooled inverters with advanced grid-friendly controls will be used by First Solar in this project). First Solar is also open to the long-term use of the plant for continued research beyond the scope of this project.

To establish the collaboration framework, NREL and First Solar modified the preexisting cooperative research-and-development agreement to include a new 3-yr research project involving the installation and operation of a new 430-kW array that uses advanced thin-film PV modules with string inverters and NREL's 1-MW/1-MWh BESS. The BESS consists of LG's lithium-ion (Li-ion) batteries with an SMA Storage Central inverter/charger. The technical specifications of NREL's BESS procured for this project are given in the appendix.

# 4  PV Plant Construction at NREL

The construction stage of the project was completed during the second quarter of Fiscal Year (FY) 2018 instead of the originally planned completion time of FY 2017 due to unexpectedly high installation costs quoted by potential contractors. The array was installed at NREL's Flatirons Campus next to the existing and future planned energy storage testing facility for promoting the research of colocated multi-technology hybrid plants. The layout schematic of the plant is shown in Figure 6. The plant uses fixed-tilt PV modules with a 25-degree angle facing south and attached to mounting tables assembled on a number of vertical support posts (Figure 7) combined in 14 parallel rows, as shown in the aerial image of the complete plant (Figure 8). The array was divided into six subarrays, each connected to individual string inverters (Figure 9).
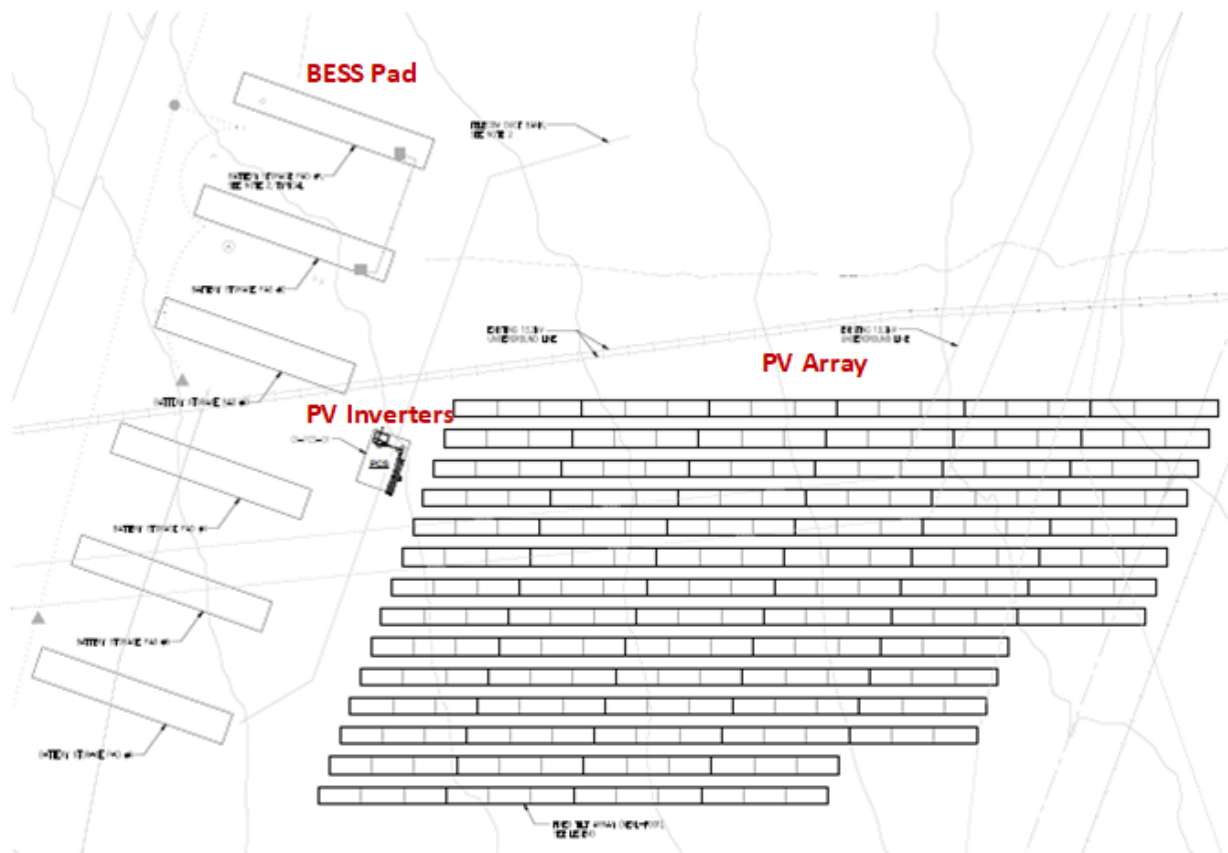


**Figure 6. Physical layout of First Solar's PV plant at NREL's Flatirons Campus**
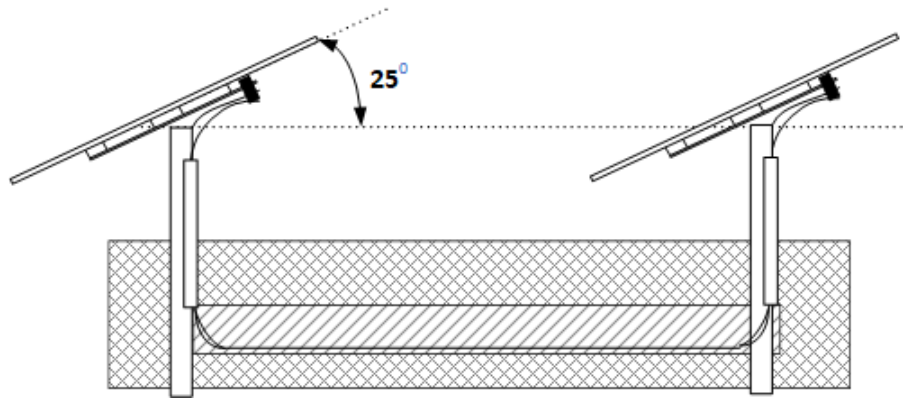
**Figure 7. Array-mounting method**



**Figure 8. Aerial photo of First Solar's PV plant at NREL's Flatirons Campus.**
*Photo by Red Mountain Scientific*
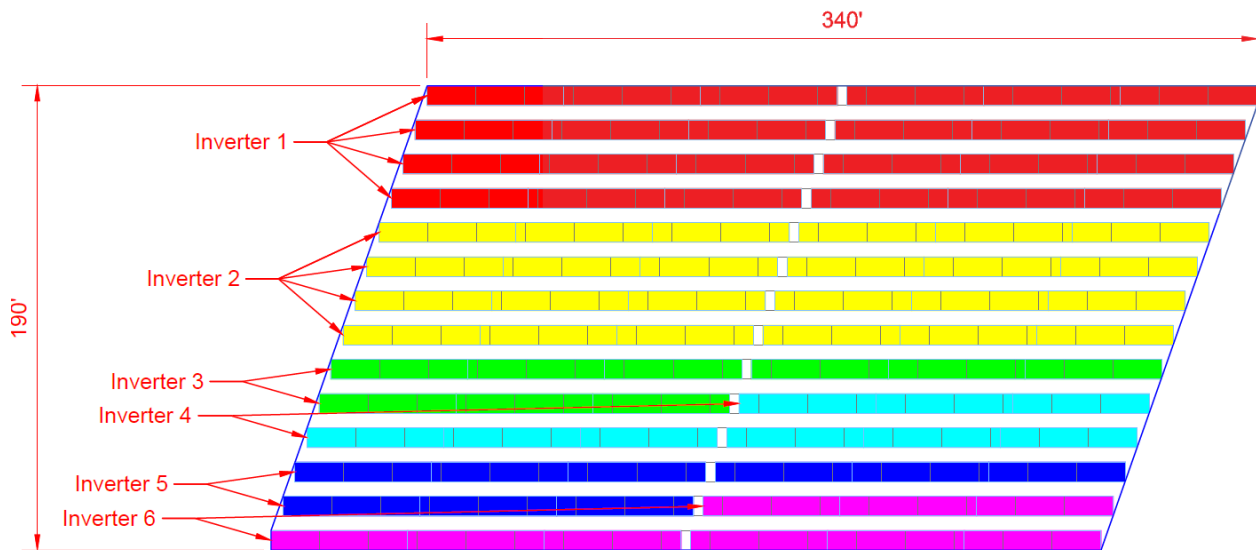


**Figure 9. Layout of First Solar's PV plant site at NREL's Flatirons Campus**

10

The electric design characteristics of the plant are shown in Table 1.

**Table 1. Parameters of First Solar's PV Plant**

| | |
|---|---|
| Power rating | 430 kW AC/480 kW DC |
| DC/AC ratio | 1.14865 |
| Number of rows | 14 |
| PV modules | First Solar Series 4 105-W modules |
| Number of modules in a string | 14 |
| Number of structural tables | 72 |
| DC power per table | 5.88 kW DC |
| Inverter Type A | 4 x 45 kW AC |
| Inverter Type B | 2 x 125 kW AC |

The electric interconnection of all six string inverters with the plant transformer is shown in Figure 10. Inverters, plant communication equipment, and control interfaces are all mounted on a panel located in the northwest corner of the plant.
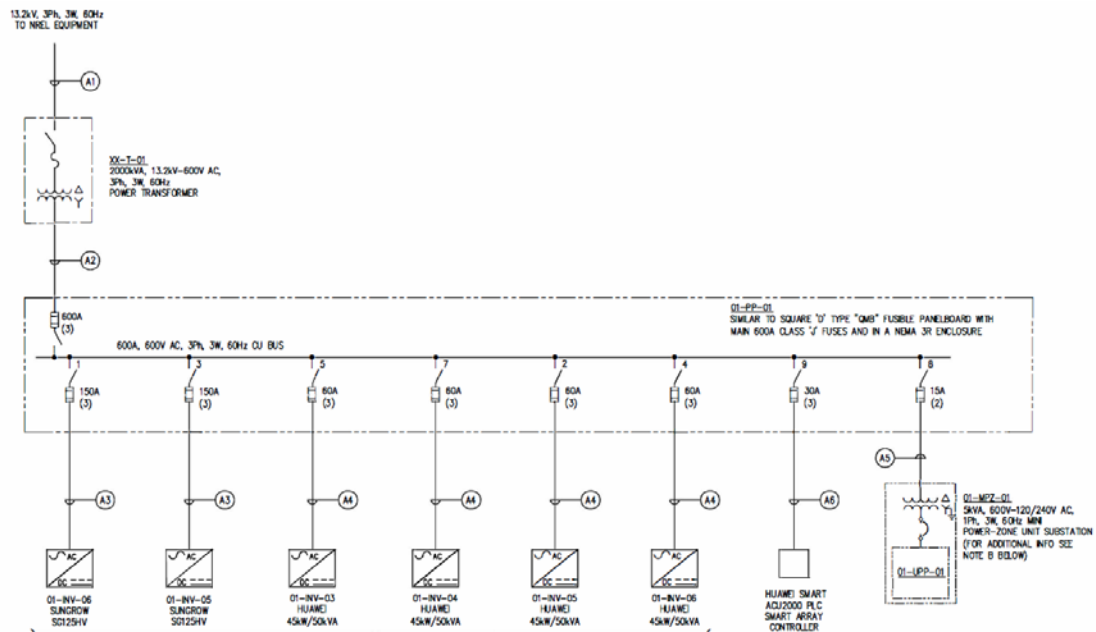


**Figure 10. Interconnection diagram for six string inverters**

The plant electrical design consists of two types of air-cooled string inverters. The first type (Type A) is the SUN2000 50-kVA (45-kW) string inverter (Figure 11), and four of these inverters are installed in total. The electrical diagram of a single SUN2000 inverter with four maximum power point tracking (MPPT) circuits and 1,500-V DC max input voltage is shown in Figure 12.

**Figure 11. A 50-kVA string inverter (SUN2000-45KTL-US-HV)**
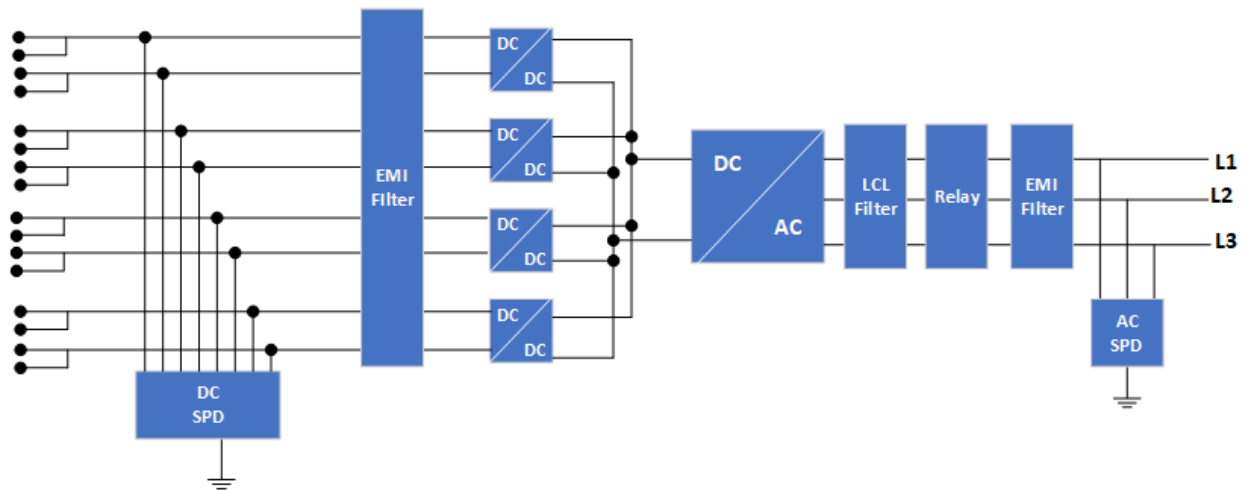


**Figure 12. Circuit diagram of a 45-kW string inverter**

The second type (Type B) of inverter used in the plant is the Sungrow 125-kW string inverter (Figure 13). Two Sungrow inverters are deployed in the plant. This inverter is also designed for 1,500-V DC max voltage (860-V DC nominal) and supports one MPPT circuit.

**Figure 13. A 125-kVA string inverter (Sungrow SG125HV)**

The PV plant was first energized in April 2018, and commissioning activities were conducted during May–June 2018. A ground-level photo of the installation is shown in Figure 14.



**Figure 14. View of First Solar's PV plant at NREL's Flatirons Campus. *Photo by NREL***

13

The battery system was installed at NREL's Flatirons Campus test site in April 2017. Figure 15 shows the aerial photo of the BESS pad, including the battery enclosure, the SMA inverter, the step-up transformer, and the medium-voltage switchgear.



**Figure 15. Aerial photo of BESS.** *Photo by NREL*

# 5  Plant Commissioning

The NREL and First Solar team conducted several commissioning tests and verified that the plant components were operating properly and that the plant could produce expected levels of electric power under various solar resource conditions. In general, the plant operated as expected during the first energizing attempt; however, after several weeks of observation and measurement, a magnetic core saturation effect was observed in the plant transformer causing distortions in current waveforms. After performing PSCAD modeling and experimenting with different transformer tap positions, it was concluded that the transformer nameplate specifications were incorrect, so the decision was made to replace the plant transformer. This caused several months of delays to start the testing activities until the new transformer was delivered, installed, and commissioned. After the transformer replacement, the power quality issue was resolved, and the PV plant operated as expected.

In addition, NREL, in collaboration with Red Mountain Scientific, conducted a survey of the plant under full load using the infrared (IR) camera installed on an unmanned flying vehicle (drone). The purpose of the test was to identify any abnormalities in the temperatures of individual PV modules under load. This way, any defective modules or inconsistent module wiring could be easily identified. The IR-enabled drone flight was conducted on a "clear-sky" day to make sure that the imaging was performed under uniform irradiance conditions across the whole plant.

The aerial inspection consisted of two overlapping IR site images, 69 low-pass IR images, and several visible spectrum images. This inspection required 40 min of flight time and 5 separate flights. The plant was virtually separated into 69 different zones (as shown in Figure 16).
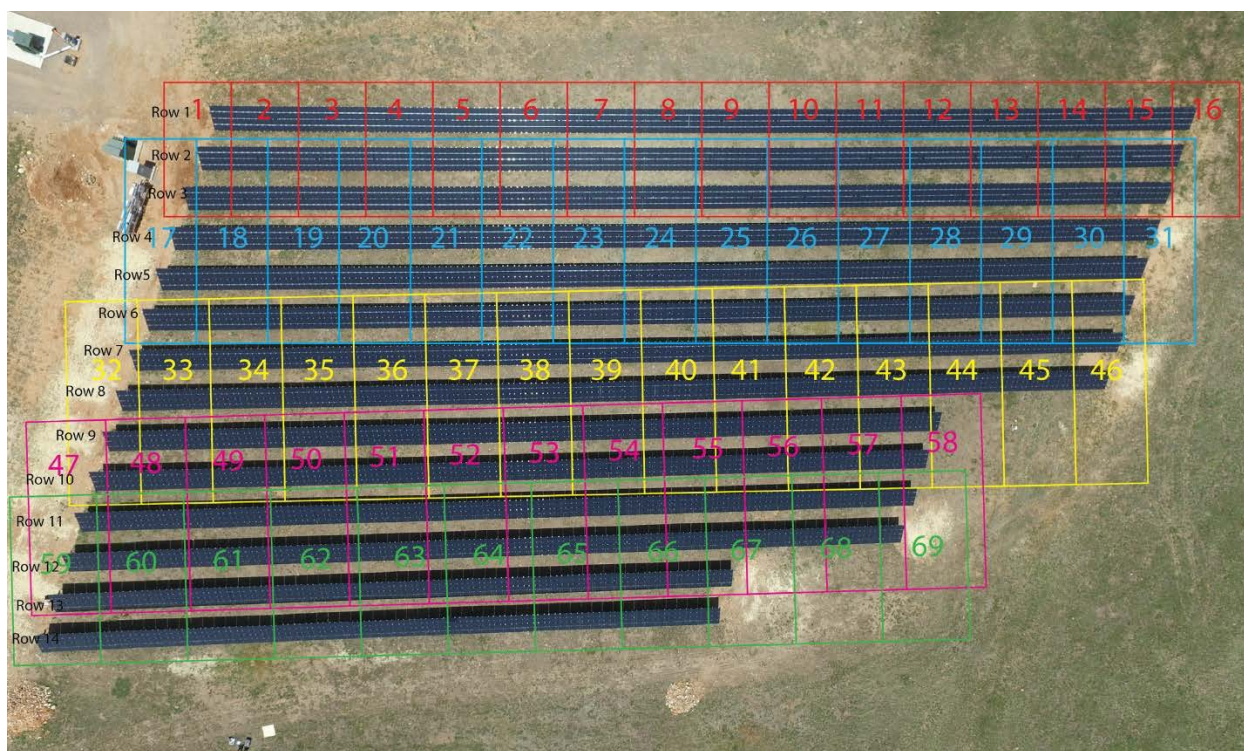


**Figure 16. Virtual plant zones for IR imaging.** *Image by Red Mountain Scientific*

An example of a thermal image taken for the whole plant is shown in Figure 17. More high-resolution detailed analysis was conducted for smaller areas of the plant. Despite the clear-sky conditions, there were some differences in panel temperatures due to the wind conditions present at the site. The wind was strong (gusts up to 12 m/s–13 m/s), causing some temperature differences across the array; however, the detailed thermal analysis did not reveal any abnormalities or hot spots in the array temperatures, proving that the installation was done in accordance with all technical requirements, and there were no factory deficiencies or damaged modules. Note that the ground seems to be warmer than the panels in Figure 17 because the picture shows blackbody radiation temperature, not absolute thermodynamic temperature; thus, it is conceivable that the ground is radiating more than the panels.
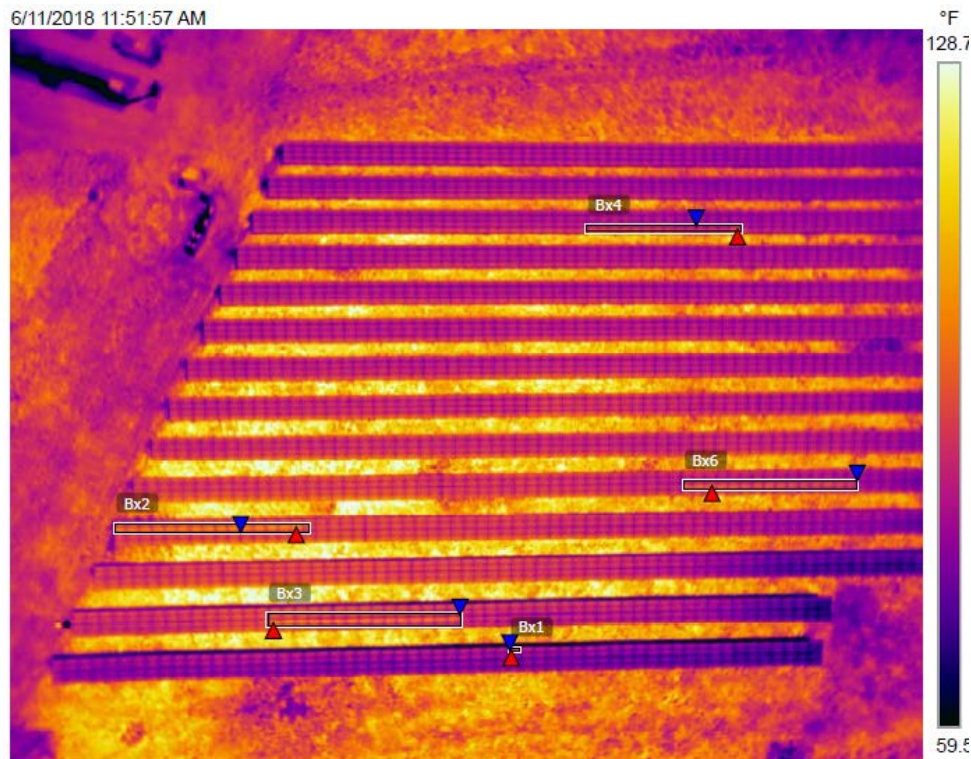


**Figure 17. Thermal image for the whole plant.** *Image by Red Mountain Scientific*

A typical production profile for the individual inverters of the plant under both clear-sky and cloud variability conditions is shown in Figure 18.
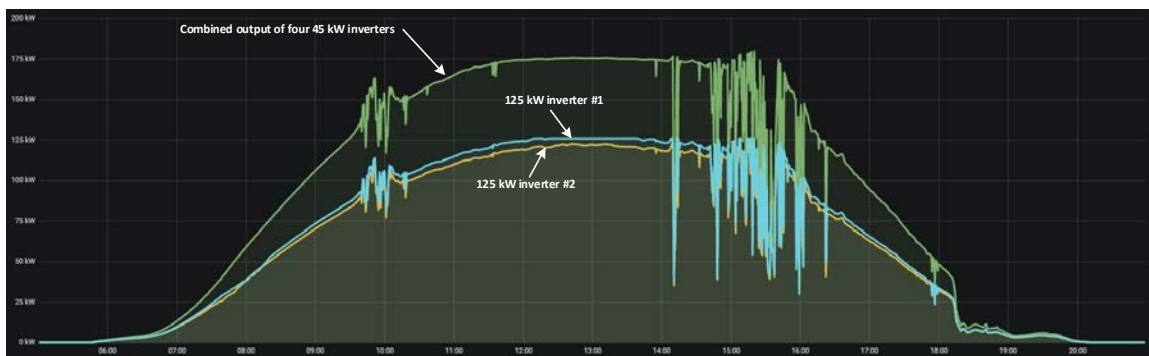


**Figure 18. Typical daily production profile for First Solar's PV plant**

16

# 6 Test Platform and Control Architecture

A test platform was developed combining the PV array and BESS, with both interconnected with the 13.2-kV research bus at NREL's Flatirons Campus. This system has the flexibility to be configured in such a manner, so both the PV plant and the BESS can operate in regular grid-connected mode or can be switched to operate under controlled grid conditions interconnected with the 7-MVA CGI, as shown in Figure 19. The CGI is combined with a real-time digital simulator (RTDS) as a power-hardware-in-the-loop (PHIL) platform, so closed-loop experiments can be conducted for the PV-plus-storage system connected to emulated models of power systems of different sizes. A detailed description of the CGI and characteristics of the PHIL platform are described in detail in [11].
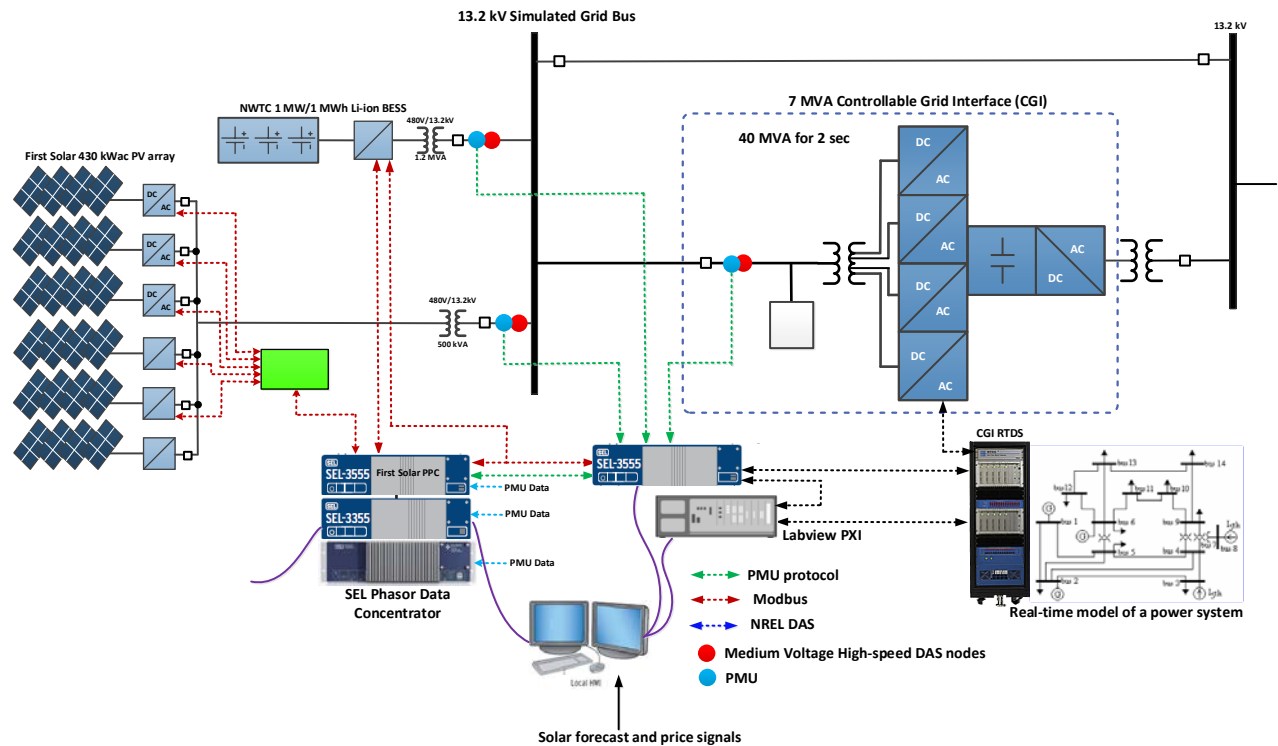


**Figure 19. PV plant and BESS integrated into the hybrid testing platform at NREL's Flatirons Campus**

**Controllable Grid Interface (CGI)**

**Power rating**
- 7 MVA continuous
- 39 MVA short circuit capacity (for 2 sec)
- 4-wire, 13.2 kV

**Possible test articles**
- Types 1, 2, 3 and 4 wind turbines
- Capable of fault testing of largest Type 3 wind turbines
- PV inverters, energy storage systems
- Conventional generators
- Combinations of technologies

**Voltage control (no load THD <3%)**
- Balanced and un-balanced voltage fault conditions (ZVRT and 130% HVRT) – independent voltage control for each phase on 13.2 kV terminals
- Response time – 1 millisecond (from full voltage to zero, or from zero back to full voltage)
- Long-term symmetrical voltage variations (+/- 10%) and voltage magnitude modulations (0-10 Hz) – SSR conditions
- Programmable impedance (strong and weak grids)
- Programmable distortions (lower harmonics 3, 5, 7)

**Frequency control**
- Fast output frequency control (3 Hz/sec) within 45-65 Hz range
- 50/60 Hz operation
- Can simulate frequency conditions for any type of power system
- PHIL capable (coupled with RTDS, Opal-RT, etc.)
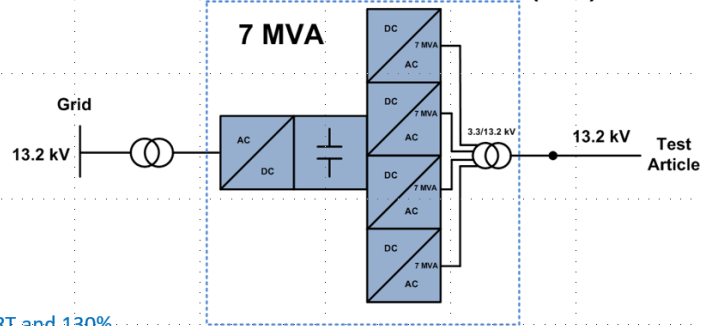
**Capabilities**
- Balanced and unbalanced over and under voltage fault ride-through tests
- Frequency response tests
- Continuous operation under unbalanced voltage conditions
- Grid condition simulation (strong and weak)
- Reactive power, power factor, voltage control testing
- Protection system testing (over and under voltage and frequency limits)
- Islanding operation
- Sub-synchronous resonance conditions
- 50 Hz tests

**Figure 20. Main characteristics of the 7-MVA CGI**

The main characteristics of NREL's 7-MVA CGI are shown in Figure 20. The continuous power rating of the CGI is 7 MVA. It includes a 9-MVA active line-side rectifier unit with filter that allows power to flow from the device under test to the steady grid with a controllable power factor; however, the test-side converter faces many challenges because it needs to provide grid simulator functionality and maintain full controllability under transient conditions that might exist at the PCC. Transient overcurrent capability is one important feature of the grid simulator because certain types of generators under test can inject high short-circuit currents that exceed their nominal rating by many multiples of their nameplate rating. Substantial short-term overcurrent capacity is needed by the grid simulator to maintain stable operation during such transient events. For this purpose, the CGI topology is based on four 3.3-kV medium-voltage, neutral-point-clamped inverter units that are normally used to drive industrial-grade motors and a custom step-up transformer to produce 13.2 kV on the test article terminals. Under continuous 7-MVA operation, the amplitude of the nominal continuous current at the inverter side of the transformer is 500 A. To allow for a significant overcurrent capability, the selected medium-voltage, neutral-point-clamped inverters are based on integrated gate-commutated thyristor devices. Their maximum current is 2.7 kA, which allows for a 540% overcurrent margin assuming a 7-MVA device under test.

CGI's custom transformer is designed to match devices under test with various nominal voltages by using multiple transformer taps. The transformer is rated for 7-MVA continuous operation and 560% short-term overcurrent operation to handle short-circuit currents that might be produced by the test articles. The special configuration of the transformer allows synthesizing 17-level low-distortion voltage waveforms by interleaving 3-level phase voltages.

18

For a given semiconductor device, the power capacity can be increased by decreasing the switching frequency, which, in turn, can lead to voltage waveshape quality degradation, which is normally measured as total harmonic distortion (THD). Normally, the desired THD level in power converters can be maintained by a harmonic filter; however, filters also decrease the dynamic range of operation. To maintain dynamic performance as fast as possible, the CGI uses advanced modulation control methods rather than a hardware filter. Thus, a balance is found among three conflicting requirements of power conversion: multimegawatt power ratings; sub-1% THD; and extremely high response times, typically smaller than 1 ms. The CGI supports two multilevel modulation schemes, each optimized for different objectives. A pulse-width modulated scheme is used for highly dynamic operation, and an optimized pulse pattern modulator is used to achieve minimum line-to-line voltage THD levels. It is possible to transition from one mode to another during operation; therefore, advanced test scenarios using high power quality in normal operation and high dynamic response during faults can be implemented.

Both the PV plant and the BESS supervisory controllers are based on an industrial RTAC (SEL-3555), making it easier to integrate such controls in field systems. In addition, the NREL site supervisory control and data acquisition (SCADA) is implemented in the RTAC controller as well. NREL has a National Instruments LabVIEW PXI RT controller integrated into the system as well for preliminary testing of various control algorithms prior to deploying them in the RTAC. Both the PV plant and the BESS have phasor measurement unit (PMU-)enabled relays installed in 13.2-kV switchgear, so the PMU data streams are sent to all RTACs and a phasor data concentrator (installed in the main control room at the Flatirons Campus). NREL's custom 50-kHz Global Positioning System (GPS)-synchronized data acquisition system (DAS) is deployed in each 13.2-kV node as well, allowing for the capture of high-resolution snapshots of transient events. The control and communication architecture for the whole platform—involving RTACs, network interfaces, and individual inverters—is shown in Figure 21.

**Figure 21. PV-BESS plant communications**

A snapshot of the main SCADA display developed for the whole Flatirons Campus is shown in Figure 22. The PV plant and the BESS are connected to the 13.2-kV grid via circuit breakers ES2 and ES1, respectively. Then, with the desired position combinations in various medium-voltage switches, both the BESS and the PV plant can be connected to either the regular grid (green bus) or the controllable CGI grid (red bus), shown in Figure 22.

The SCADA display of the PV plant control is shown in Figure 23. This SCADA allows for switching the plant control between remote and manual modes, controlling individual inverters, and configuring the sources for external set point signals.

**Figure 22. Flatirons Campus main SCADA display**
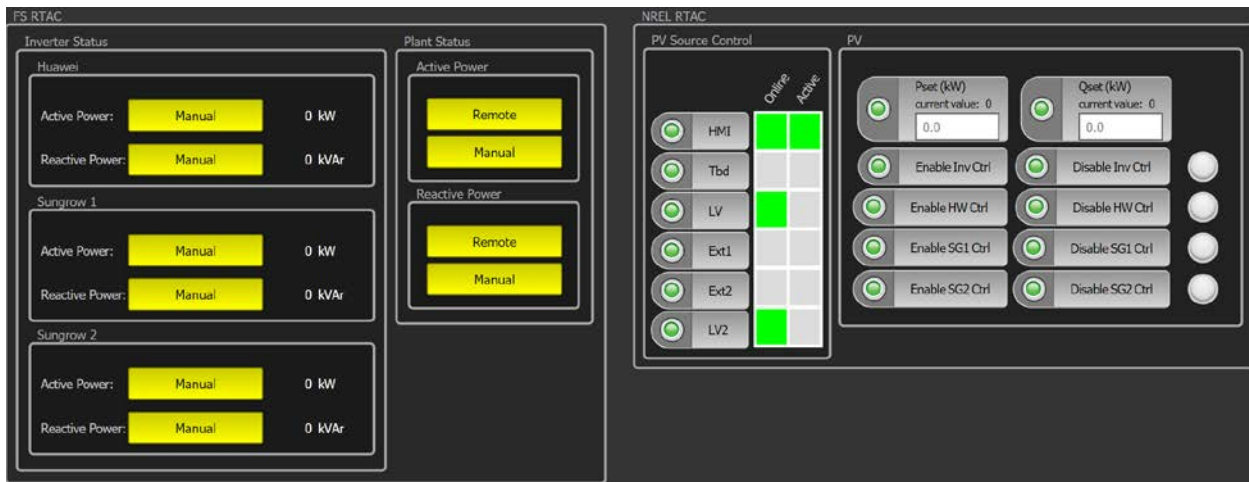


**Figure 23. PV plant SCADA display**

The NREL team developed and implemented a BESS controller based on the standard SEL RTAC industrial controller platform. The BESS RTAC controller is communicating with the First Solar PPC controller, which was developed on the same hardware platform. This makes the integration of the NREL-developed controller with the existing First Solar PPC an easy process. The user interface for the BESS SCADA is shown in Figure 24. It allows for the remote start and stop of the BESS system and the activation of desired control modes, including the ability to switch between grid-following and grid-forming modes.
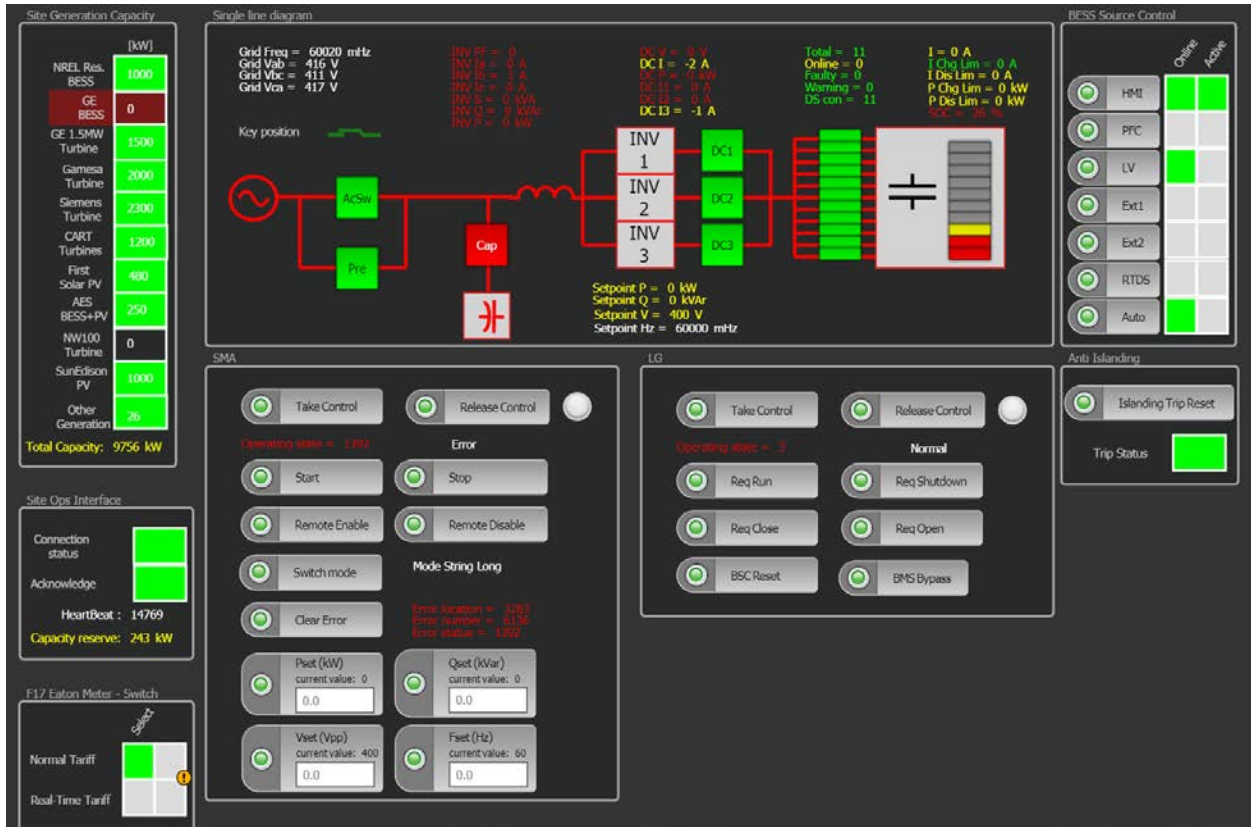
**Figure 24. BESS SCADA display**

The BESS controller is designed to provide various forms of active and reactive power control with the interface shown in Figure 25. It has the capability to provide inertial response, FFR, and PFR by the PV-BESS plant. In addition, the BESS can provide reactive power control in the form of kVAR-voltage droop during dynamic and fault conditions. The implemented control diagram for all these control functions was developed by NREL and is shown in Figure 26.
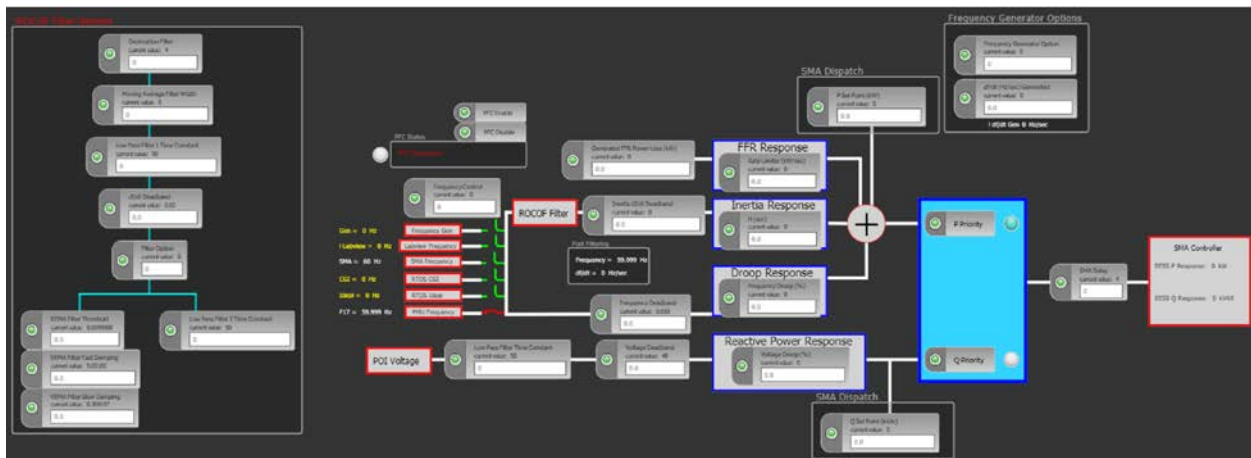


**Figure 25. Controller for the BESS to provide plant services implemented in the RTAC**

22
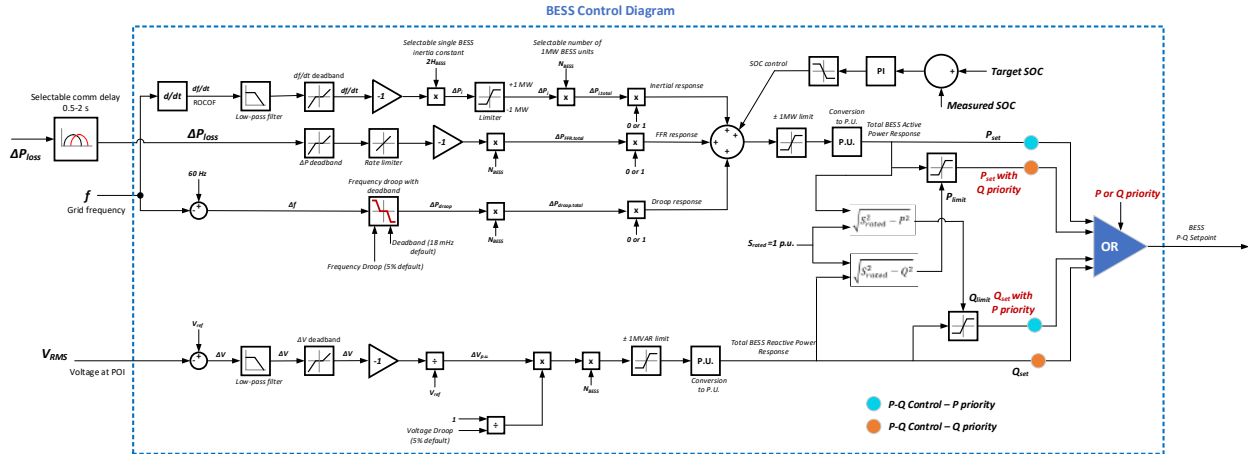
**Figure 26. Controller diagram for the active and reactive power control services by BESS**

All BESS active power controls components can be combined in a single equation, so at any instance in time, the total BESS power (injecting or absorbing) is:

$$P_{bess}(t) = P_o(t) + \Delta P_{soc}(t) + \Delta P_i(t) + \Delta P_{FFR}(t) + \Delta P_{droop}(t) + \Delta P_{AGC}(t) \tag{6.1}$$

where $P_o(t)$ is the BESS dispatch set point; $\Delta P_{soc}(t)$ is the portion of the commanded power set point for the BESS state-of-charge (SOC) control; $\Delta P_i(t)$ is the BESS inertial response (or response proportional to the rate of change of frequency [ROCOF]); $\Delta P_{FFR}(t)$ is BESS FFR response; $\Delta P_{droop}(t)$ is the BESS droop response; and $\Delta P_{AGC}(t)$ is BESS AGC response.

Depending on the types of service that the BESS is providing, the individual components in equation (1) can be activated at the proper times. For example, $\Delta P_i(t)$ will first start at the beginning of the event as soon as a large ROCOF is detected, then either $\Delta P_{FFR}(t)$ or $\Delta P_{droop}(t)$ will kick in (the BESS can provide either FFR or droop response, but it cannot do both at the same time). The $\Delta P_{AGC}(t)$ component will follow the AGC set points from the system operator for secondary frequency control and frequency regulation.

Equation (6.1) can be expanded to show the components of interest in more detail:

$$P_{bess}(t) = P_o(t) + \Delta P_{soc}(t) - 2H\frac{df(t)}{dt} + \Delta P_{FFR}(t) - \frac{f_o - f(t)}{droop} + \Delta P_{AGC}(t) \tag{6.2}$$

where $f_o$ is the scheduled grid frequency, and $f(t)$ is the grid frequency at any point in time.

23

# 7 Measurement of Response Times of the PV-BESS System

The response time of the 430-kW PV plant for the active and reactive power set points was measured in grid-connected mode during the peak PV production hour. The plant controller was set to receive rectangular active and reactive power set points simultaneously, as shown in Figure 27. Before starting this test, the plant was curtailed for testing the active power response in both the up and down directions. The plant was receiving rectangular active and reactive power set points at different frequencies (0.1 Hz and 0.05 Hz, respectively). Several important observations from Figure 27 are:

- The PV plant consisting of string inverters from different vendors is capable of following both the active and reactive power set points with a high level of precision.
- The plant can follow the reactive power set points in both the kVAR injection and absorption modes.
- An approximate delay of 300 ms–350 ms was observed until both the active and reactive power reached the set point due to a combination of communication delays and internal ramp limits in inverters.
- Active and reactive power can be controlled independently of each other and can follow the set points with a high level of precision if the current limits of the inverters are not exceeded.

In this test, both the active and reactive power of the PV plant were measured on the 13.2-kV side of the PV plant transformer.
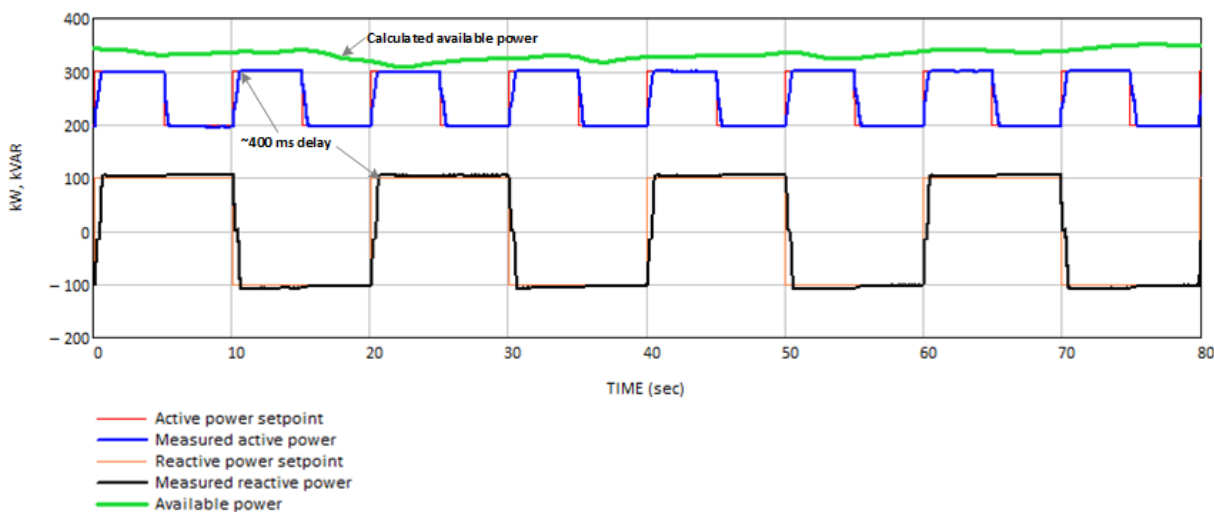


**Figure 27. Measured PV plant response times**

A number of tests for the BESS were conducted as well to measure the ability of the battery system to follow the active and reactive power set points. The BESS response was tested in both grid-following and grid-forming modes of operations. Results of the measured BESS responses to the step changes in the active power set points are shown in Figure 28 and Figure 29 for grid-following and grid-forming modes, respectively. In both tests, the BESS was commanded to

24

inject full rated power (1 MW) starting from zero. In grid-following mode, the measured power reaches the set point within approximately 20 ms after the BESS controller receives the set point from NREL's SCADA. Similarly, in grid-forming mode, the BESS reaches the set point within approximately 50 ms. The BESS power was measured on the 13.2-kV side of the transformer for both tests.
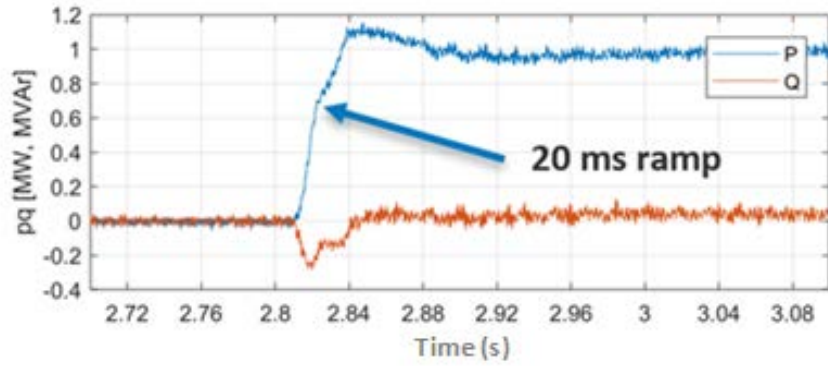


**Figure 28. Measured BESS response time in grid-following mode**
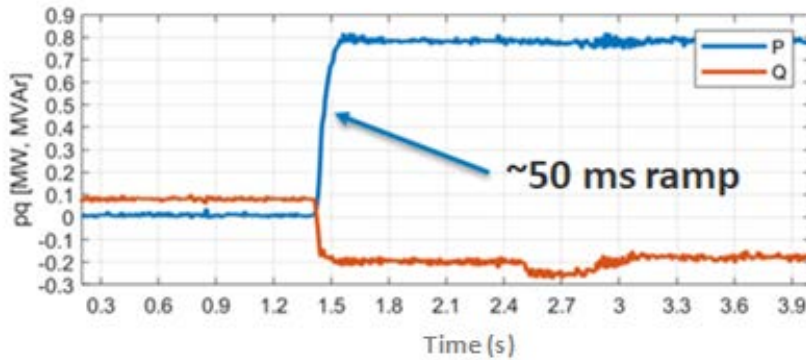


**Figure 29. Measured BESS response time in grid-forming mode**

Additional response time tests were conducted for the BESS during this project. One example of the BESS following rectangular active power set points in grid-following mode is shown in Figure 30.
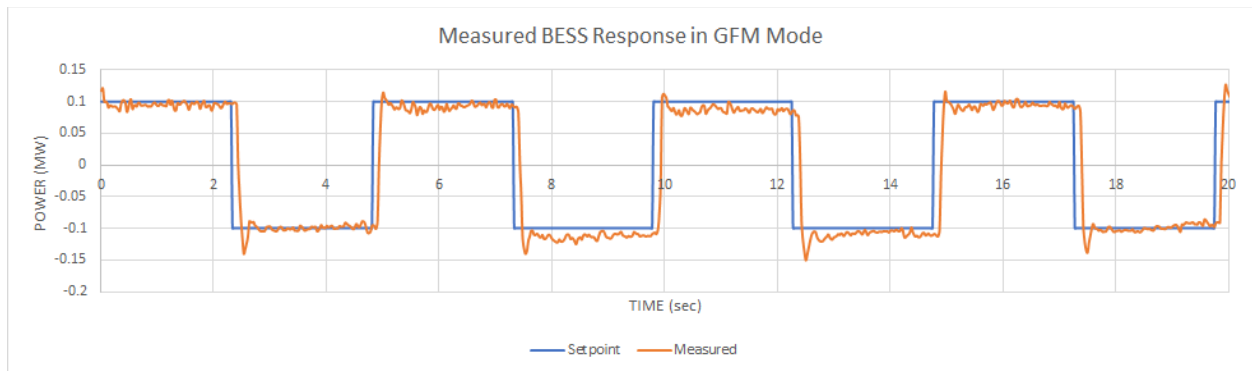


**Figure 30. BESS response to active power set points**

# 8 Active Power Control Tests

To demonstrate several types of active power controls by the PV-BESS system, the NREL team developed a modified real-time model of the Institute of Electrical and Electronics Engineers (IEEE) 9-bus system and used it in the PHIL setup with the 7-MVA CGI (Figure 19). A simplified single-line diagram of the 9-bus system implemented in the RTDS is shown in Figure 31. The real-time model has been modified, so different penetration levels of renewable generation and PV-BESS can be modeled to show how the controls for reliability services by PV-BESS systems can help improve grid stability and frequency response. Also, the model was tuned to replicate frequency responses like that of the Western Interconnection using results of the Western Electricity Coordinating Council Transmission Expansion Planning Policy Committee 2022 positive-sequence load flow model at different penetration levels. This PHIL setup interfaced with the NREL CGI and allows for exposing the PV-BESS system to grid conditions measured at any bus in this RTDS model that represents an approximate 100-GW power system. The model allows for scaling the capacity of the PV-BESS plant to any desired level. Fast active power controls—such as inertial response, FFR, and PFR—by the PV-BESS plants can be tested with this setup by exposing the system to frequency transients caused by the drop of a large conventional power plant (approximate 3% of dispatched capacity). A test system similar to this developed by NREL was used in a project that NREL conducted for the Pacific Gas & Electric Company under the California Energy Commission's Electric Program Investment Charge during 2018 but with focus on BESS only [14]. Individual generation units in the RTDS model can be dispatched to emulate different levels of instantaneous penetration by inverter-coupled resources.

To evaluate the frequency stability impacts of the large-scale deployment of PV-BESS systems, we assumed different PV-BESS plant capacities at different levels of inverter-based resource (IBR) penetration in the test system, as shown in Table 2. The PV-BESS capacity was scaled up in the model from the capacity of the real system at NREL (430-KW PV and 1-MW/1-MWh BESS) to levels shown in Table 2. For each case, we evaluated the frequency response of the system with PV-BESS plants providing various forms of active power controls.

**Table 2. PHIL Scenarios**

| PV-BESS Capacity Deployed in the Model | Level of IBRs (% of Load) | | | |
| --- | --- | --- | --- | --- |
| | 15% | 20% | 40% | 60% |
| 0 GW | Inertia, FFR, PFR | Inertia, FFR, PFR | Inertia, FFR, PFR | Inertia, FFR, PFR |
| 0.6 GW | Inertia, FFR, PFR | Inertia, FFR, PFR | Inertia, FFR, PFR | Inertia, FFR, PFR |
| 1.2 GW | Inertia, FFR, PFR | Inertia, FFR, PFR | Inertia, FFR, PFR | Inertia, FFR, PFR |
| 1.8 GW | Inertia, FFR, PFR | Inertia, FFR, PFR | Inertia, FFR, PFR | Inertia, FFR, PFR |
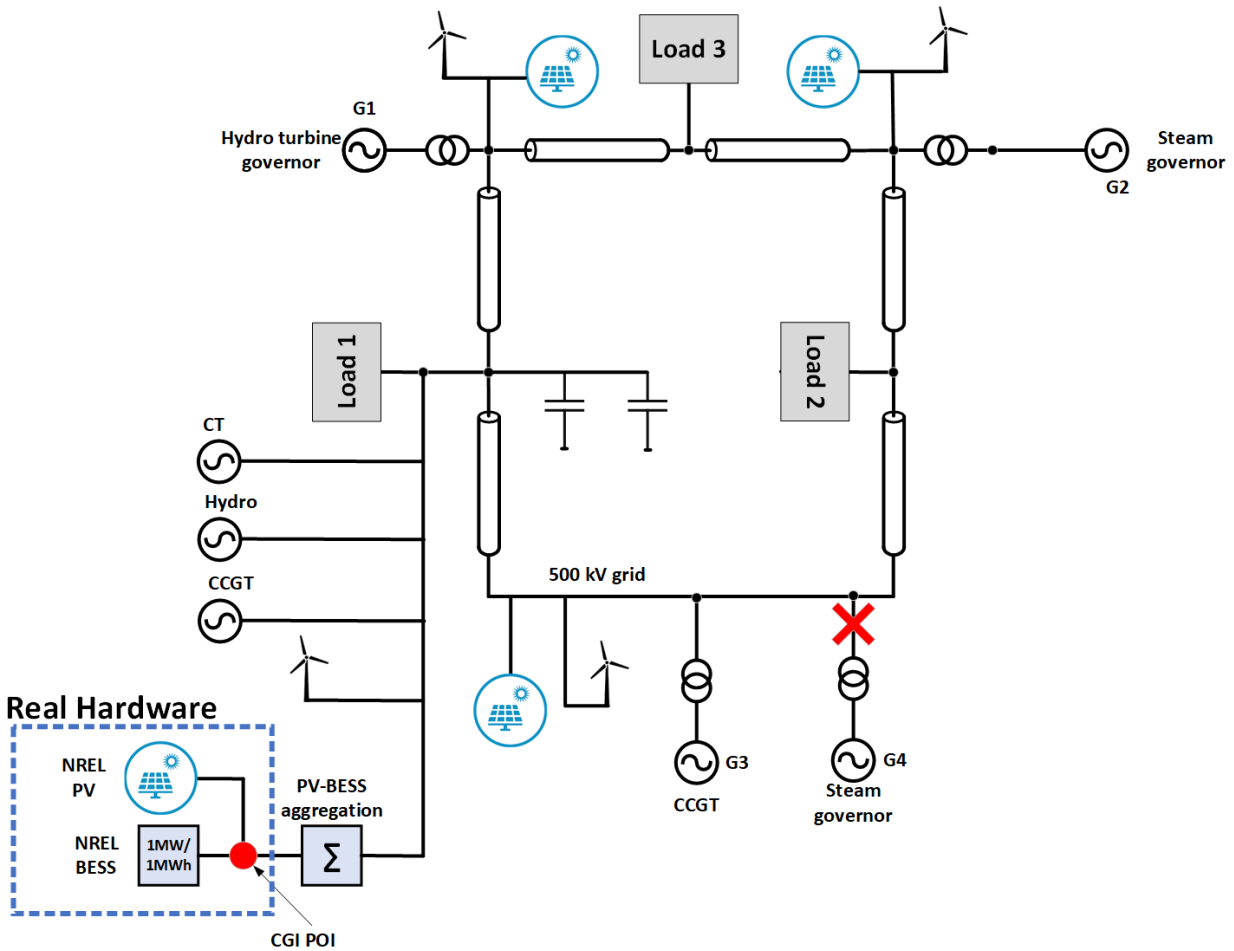
**Figure 31. PHIL setup using 9-bus power system model in RTDS**

## 8.1 Inertial Response Tests

For a PV-BESS plant to provide inertial response like a rotating generator, its output power needs to be modulated to inject/absorb active power proportional to the ROCOF. Inertia-like response can be provided by a BESS only, by a PV plant only if it is curtailed during the frequency event, or by both the PV and BESS; however, note that the maximum level of inertial response by a PV-BESS plant at any time depends on the operating power level of the plant components just before the frequency event occurs. We anticipate that in PV-BESS plants the burden of inertia-like response will be in places mainly on battery storage and not curtailed PV. So, in this experiment, we assumed that the BESS is the only provider of inertial response. Detailed explanations of how the BESS was programmed to provide inertia-like response are given in [11] and [14].

The ROCOF deadband implemented for this test was set at the 20-mHz/s level to avoid unnecessarily triggering the inertial response by the BESS controller. The tests were conducted for four aggregate PV-BESS capacities at each IBR penetration level. The frequency and BESS response time series for each renewable penetration level are consolidated in Figure 32 a, b, c, d, and e for 0%, 15%,20%, 40%, and 60% IBR penetration cases, respectively. The results show continued improvements in the frequency nadir with increased aggregated capacity of PV-BESS

27

plants. Inertial response by the BESS improves the frequency nadir but does not impact the level of the settling frequency because the PFR in the test system remains the same for all test cases. For all cases, except for the 60% IBR penetration case, the inertial response by the PV-BESS plant shifts the frequency nadir above the 59.5-Hz underfrequency load-shedding threshold,

In these tests, the initial BESS power was set to zero at the beginning of the fault, so the battery system had enough headroom to inject the inertia power with a magnitude equal to its full rating (1-MW battery at NREL scaled to the levels shown in Table 2). For this purpose, the inertial constant, H, of the battery was scaled from H=125 s to H=50 s when going from lower to higher penetration levels of IBRs.
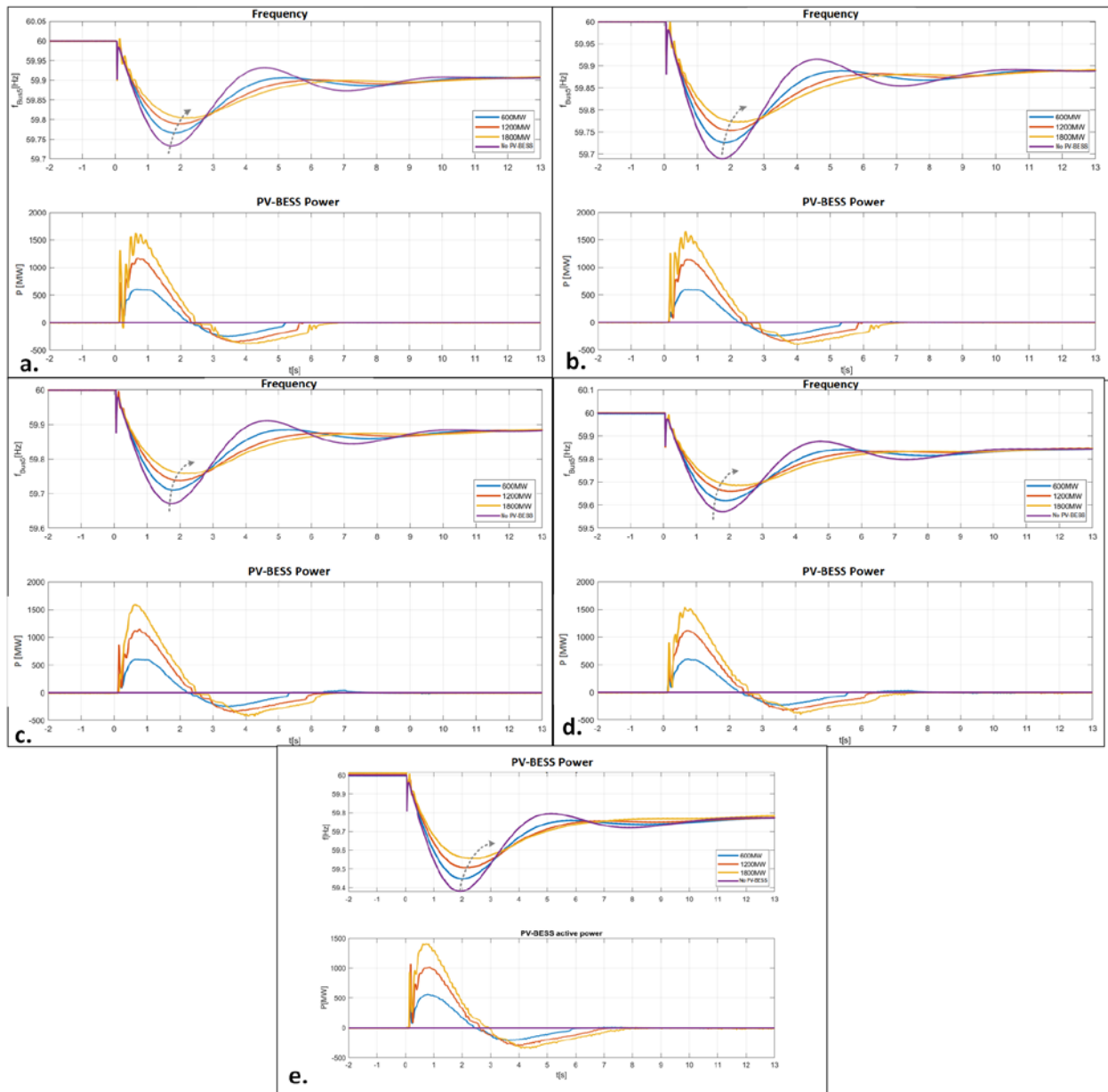


**Figure 32. Results of the PHIL tests for PV-BESS plants providing inertial response at different penetration levels: (a) 0%, (b) 15%, (c) 20%, (d) 40%, and (e) 60%**

28

The accuracy of the frequency measurements is very important for inertial control of IBRs. IBRs should ensure that the frequency measurement and protection settings can ride through without tripping because of phase jumps or other grid disturbances, such as fault events. Phase-locked loops (PLLs) and synchronization techniques used in inverters are important for the reliable operation of IBRs under dynamic and transient conditions in the grid. Different PLL algorithms estimate grid frequency in different ways. Under sinusoidal and balanced grid conditions, they all can be tuned to produce results that are similar to those shown in Figure 33. We modeled and analyzed several PLL methods for comparison, including synchronous-frame PLL (SF-PLL), a PLL method based on instantaneous active and reactive power theory (PQ-PLL), and a sinusoidal signal integrator PLL (SSI-PLL). All these methods are described in detail in [15]. Under unbalanced grid conditions, however, or when voltage harmonics are present, additional filtering delays are needed for PLL algorithms to accurately estimate both grid frequency and ROCOF. An example of frequency estimation by all these PLL algorithms under 5% voltage imbalance is shown in Figure 34, which emphasizes the need for additional filtering of the frequency signal, and which will impact the effective magnitude of the inertial constant, H, emulated by the BESS.
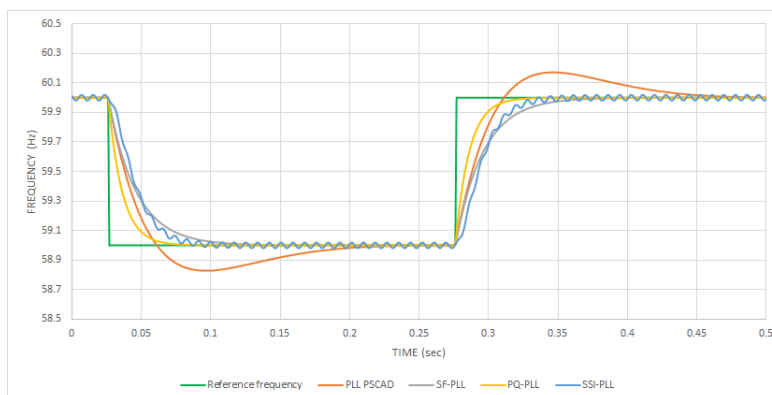


**Figure 33. Comparison of different PLL algorithms under balanced grid conditions**
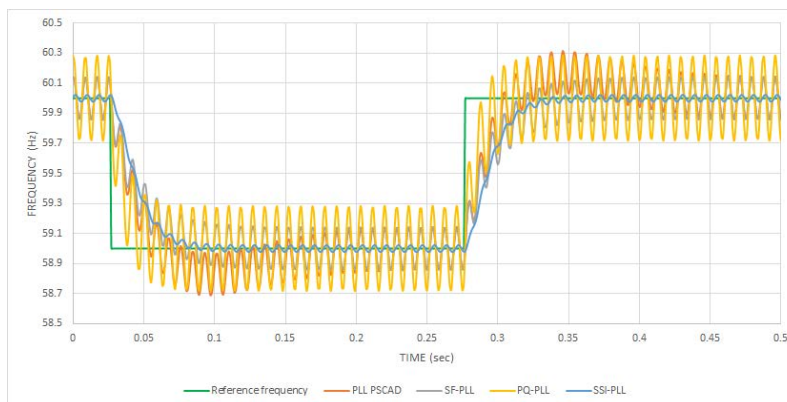


**Figure 34. Comparison of different PLL algorithms under 5% imbalance in grid conditions**

The theoretical range of programmable H for a BESS can be very high, assuming that the frequency and ROCOF can be estimated very fast, and the magnitude of the ROCOF is low. For example, the calculated theoretical inertial constant that can be emulated by the 1-MW BESS at zero power level for the U.S. Western Interconnection is shown in Figure 35 within the range from H= 200 s–800 s; however, the practical range reduces to H= 50 s–125 s if the frequency

filtering delays are applied (a 100-ms delay was applied in the PHIL system). This range for inertia constants is still much higher than one for conventional plants; however, we would like to emphasize that this level of inertial response by the BESS highly depends on the initial conditions of the battery, and care needs to be taken to have adequate power headroom for the desired inertial response if the BESS is expected to provide such service at any time.
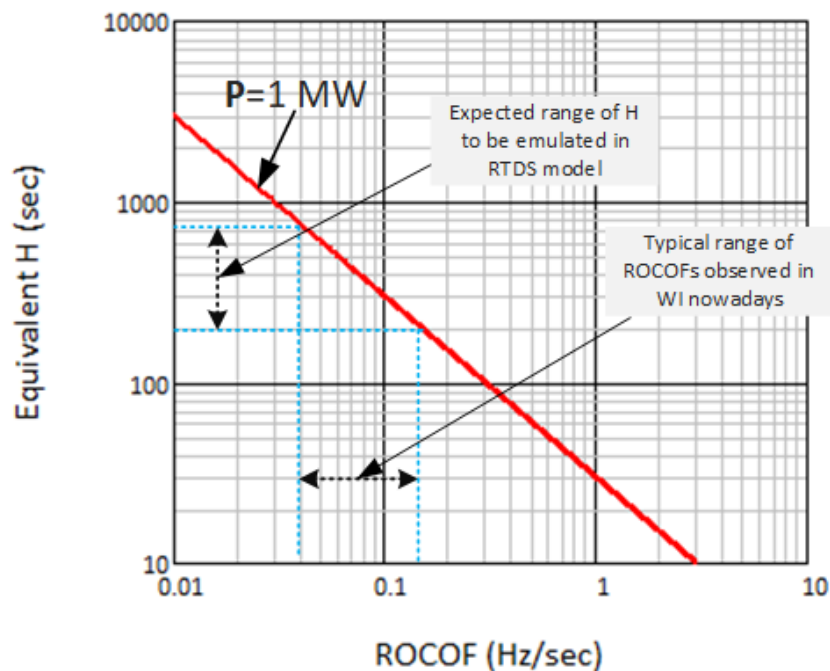


**Figure 35. Calculated range of programmable H for NREL's 1-MW/1-MWh BESS**

## 8.2 Fast Frequency Response Tests

### 8.2.1 FFR-PHIL Simulations

FFR is another method to use PV-BESS systems to compensate for a sudden generation or load loss. This can become a very efficient frequency response tool for system operators, but it requires precise knowledge of the loss of magnitude so participating plants can be commanded to change their power outputs accordingly. This method depends on the ability of the control system to rapidly determine the magnitude of the loss and communicate the set point to the controllers of PV-BESS plants. The required speed of the response (or how fast the PV, BESS, or both deploy available reserves) will depend on the possible impacts on power system stability: BESS and PV plants can deploy their available reserves very fast, which can cause unwanted oscillations in the system. In some cases, FFR activation by PV-BESS plants can be based on frequency thresholds, similar to underfrequency load-shedding schemes, or based on the ROCOF. This will require determining the precise FFR magnitudes based on the measured system frequency or the ROCOF by conducting detailed modeling studies. The main advantage of FFR by PV-BESS plants is that it has the potential to reducing requirements for both primary and secondary reserves due to the fast-acting nature of both resources, allowing for the fast recovery of frequency during the initial stages of the frequency event. Further studies are needed

30

to understand this benefit in terms of a megawatt response comparison that is needed to restore the frequency using a combination of primary and secondary controls compared to FFR.

For this use case, the BESS of the PV-plus-storage plant was programmed to deploy its available power to compensate for the loss of generation. For the first series of FFR tests, a very fast 100-ms response time for the BESS to provide FFR was implemented. Tests were conducted for four BESS capacities at each renewable penetration level. Frequency and plant active response time series for each renewable penetration level are shown consolidated in Figure 36 a, b, c, d, and e for 0%, 15%, 20%, 40%, and 60% IBR penetration cases, respectively.
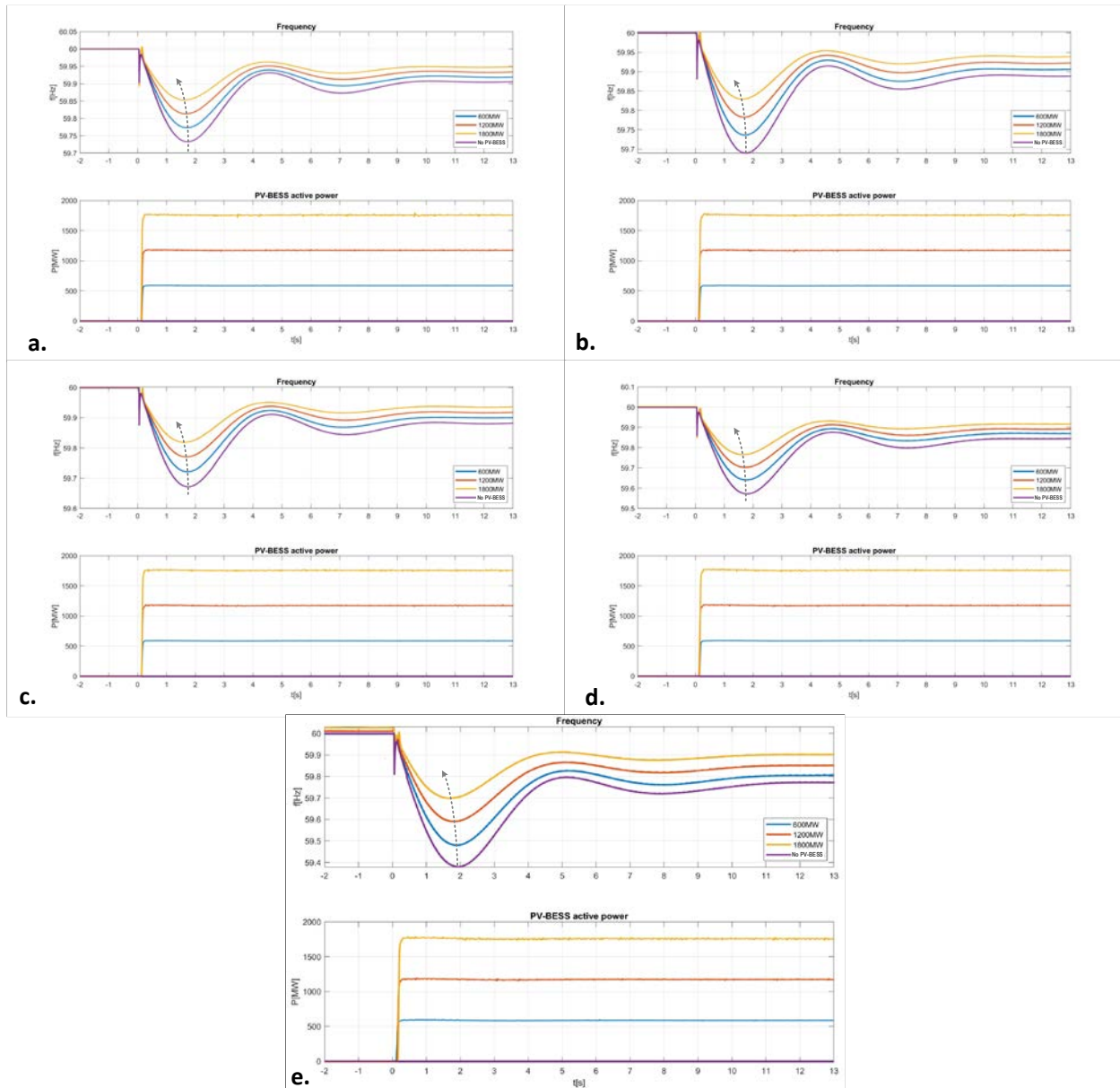


**Figure 36. Result of FFR PHIL tests at different IBR penetration levels: (a) 0%, (b) 15%, (c) 20%, (d) 40%, and (e) 60%**

31

With such FFR, continuous improvements for frequency response can be observed at each penetration level, shifting the frequency nadir well above the 59.5 underfrequency load-shedding threshold for all sizes of PV-BESS plants. Only for extreme 60% penetration cases, a larger amount of storage is needed to keep the nadir securely above the underfrequency load-shedding level. Note that even without the BESS, the system can provide satisfactory frequency response by conventional generation at lower penetration levels; however, it is conceivable that some extreme conditions that were not envisioned in the study could result in unsatisfactory performance. In this regard, the advanced FFR by the BESS can help provide improved frequency response and reliability of the power system.

## 8.2.2  PMU-Based FFR Concept

Reliable FFR by inverter-coupled resources can be realized using the embedded network of PMUs and associated equipment (data concentrators, SCADA, data communication equipment, and data networks), as shown in Figure 37. Such a network can be used in a wide-area FFR control system involving data from PMU units distributed across the network to help detect sudden changes in the system, determine the magnitude of change, and reporting to all participating IBRs (in this case, to all participating PV-BESS systems) to provide precision response for the rapid restoration of any load-generation imbalances that might occur due to disturbances (Figure 38).
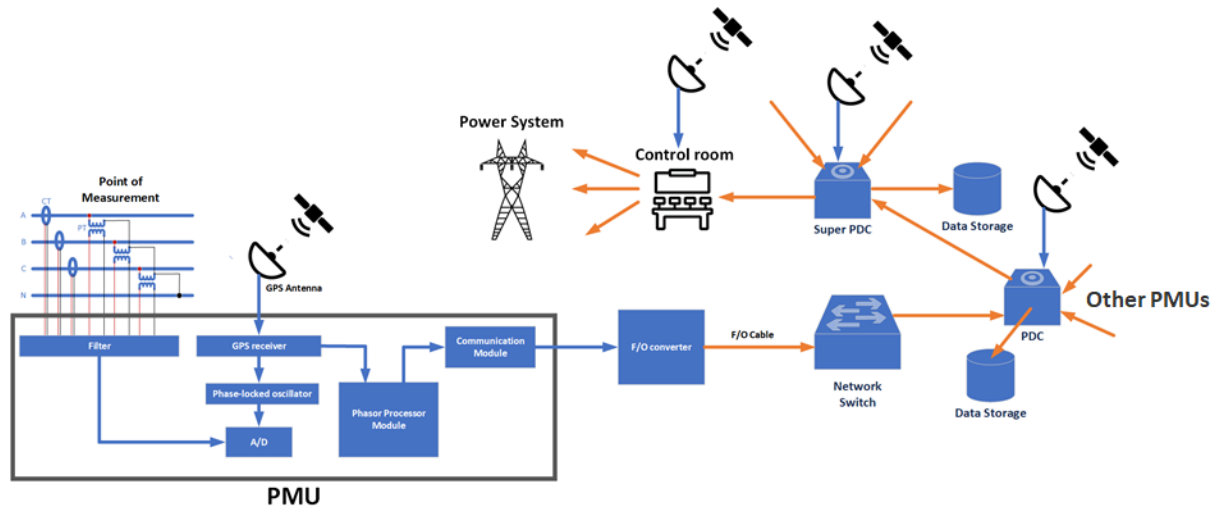


**Figure 37. PMU networks embedded in the power system**
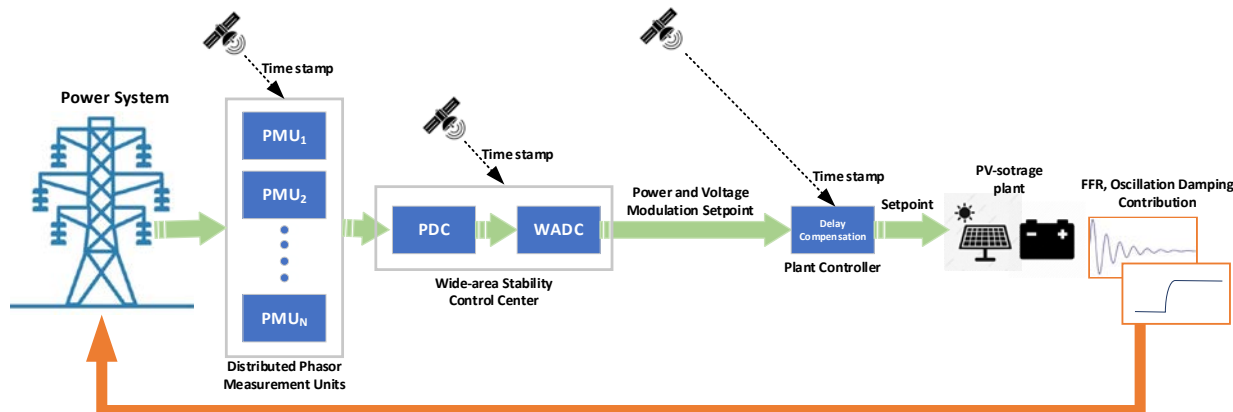
**Figure 38. Concept of PMU-based wide-area reliability service by PV-BESS plants**

Motivated by these considerations, the NREL team developed a PMU-based test bed for characterizing and validating wide-area stability controls by IBRs, including FFR. The diagram of this new fully operational test bed is shown in Figure 39. It consists of a number of GPS-synchronized, SEL PMU-enabled relays installed on the medium-voltage grid across the Flatirons Campus. The diagram in Figure 39 shows a portion of the test bed that has been specifically designed to test wide-area stability services by PV-BESS plants. The test bed includes:

- PMUs installed on the medium-voltage sides of both BESS and PV plant controllers
- PMUs coupled with RTDS, so they can be virtually placed at any bus in a real-time power system model
- RTAC systems
- SEL phasor data concentrator
- PMU fiber-optic communication network
- Network equipment (switches, routers, firewall devices)
- Fully integrated with the Flatirons Campus site controller and synchronized with custom-made, advanced, medium-voltage DAS with 50-kHz sampling rate deployed at the site.
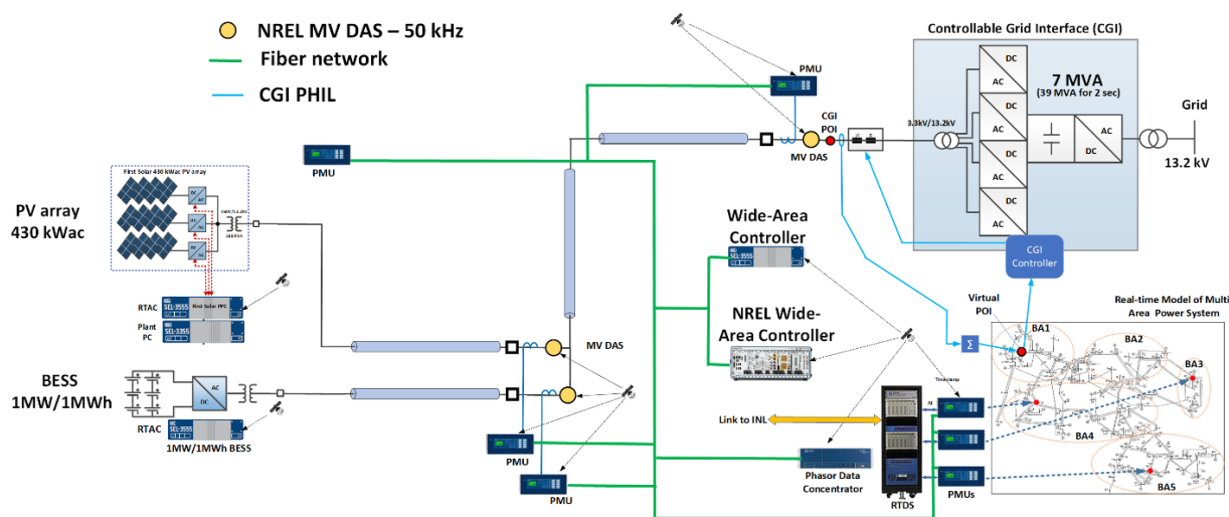


**Figure 39. PMU-controls test bed developed at NREL's Flatirons Campus**

33

This setup was used to characterize and quantify the responses and delays associated with PMU-based controls using real equipment coupled with controlled, repeatable grid conditions emulated using the 7-MVA CGI. During this project, the NREL team conducted characterization testing of PMU-based controls under CGI-emulated voltage, phase angle, and frequency perturbation injections through a RTDS model. Perturbations were captured by both medium-voltage DAS and PMUs in a time-aligned manner to measure the response times and communication delays for all components of the synchrophasor data network (Figure 39):

- PMUs to RTAC
- PMUs to phasor data concentrator
- Phasor data concentrator to RTAC.

The response of the system to various perturbations introduced by the CGI was measured and characterized; the results are shown in Figure 40–Figure 43.
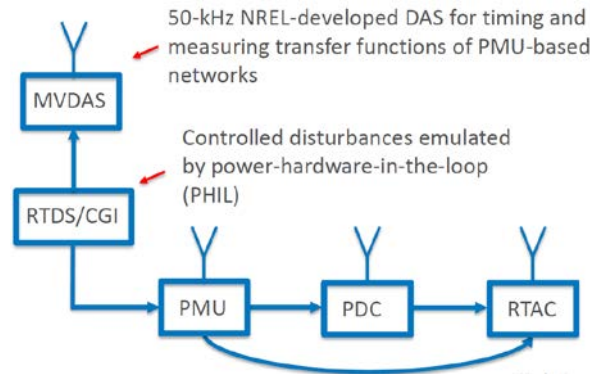


**Figure 40. PMU-based system characterization test setup**
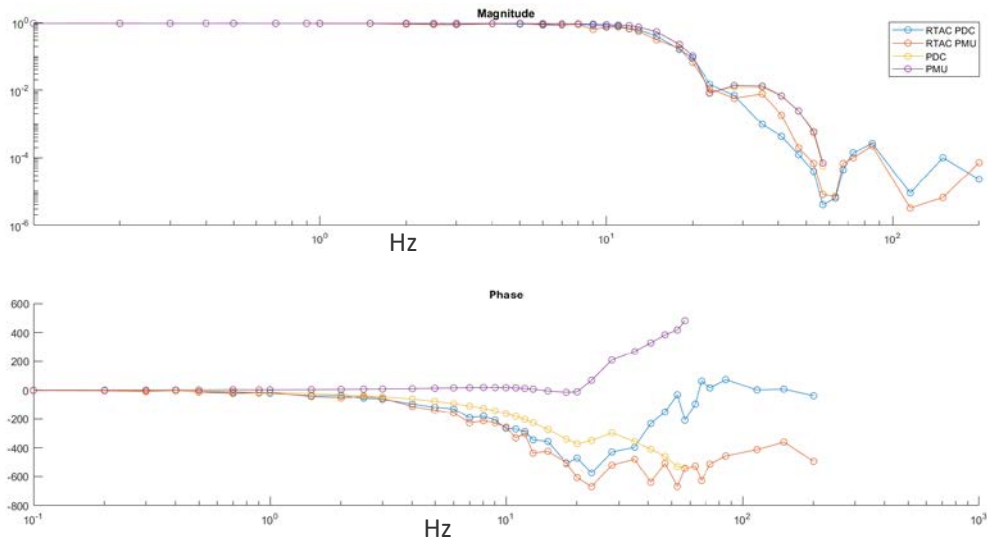


**Figure 41. Transfer function of PMU data flows to 5 % voltage magnitude injection by the CGI**
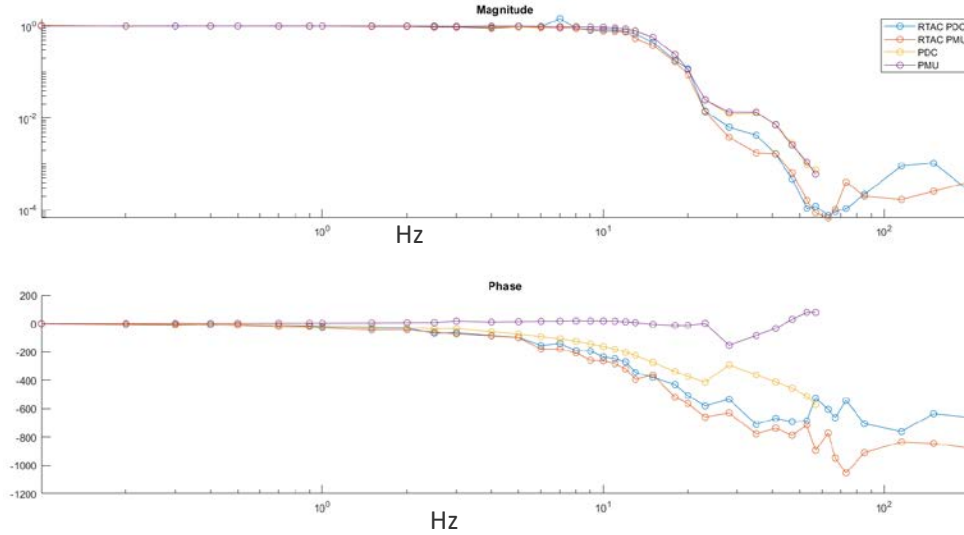
**Figure 42. Transfer functions of PMU data paths in response to the 0.5-Hz frequency injection by the CGI**
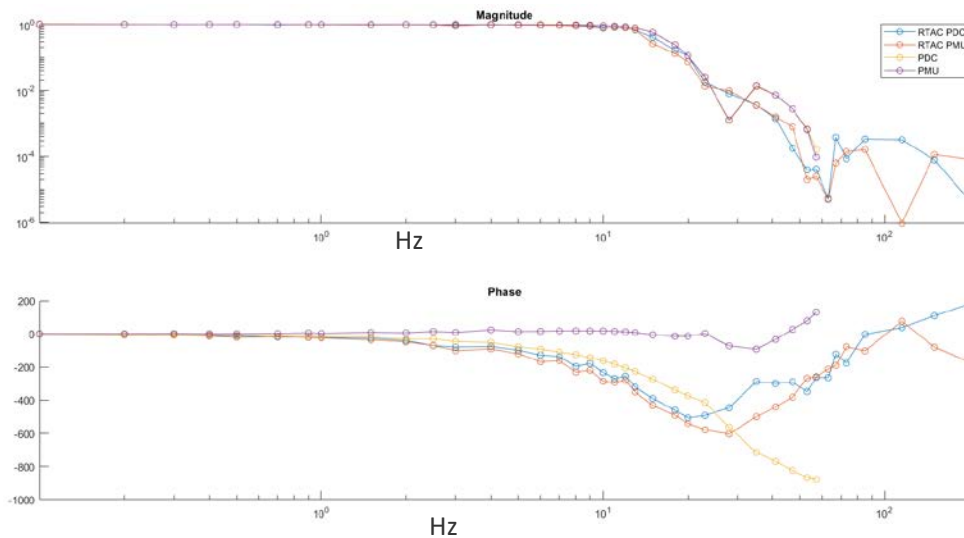


**Figure 43. Transfer functions of PMU data paths in response to the 0.1-rad phase angle injection by the CGI**

It appears that the magnitude response of the whole PMU data flow path is very stable for update frequencies up to 12 Hz (~80-ms update rate). Phase response has some delays at that frequency, but it can be compensated. These types of response times make it possible to consider the use of the proposed method to estimate load-generation imbalances at any bus of a power system and to develop a control strategy to deploy ultrafast frequency response converter-based assets. The objective is to prevent relatively large off-nominal frequency transients by counteracting the impact of sudden imbalances on an electric grid. The implementation of this based on experimental results and using a modified model of the IEEE 39-bus test system is described in [20]. The diagram of the model is shown in Figure 44 and can be used to study the impacts of FFR controls by PV-BESS systems on the frequency stability of the grid.

35
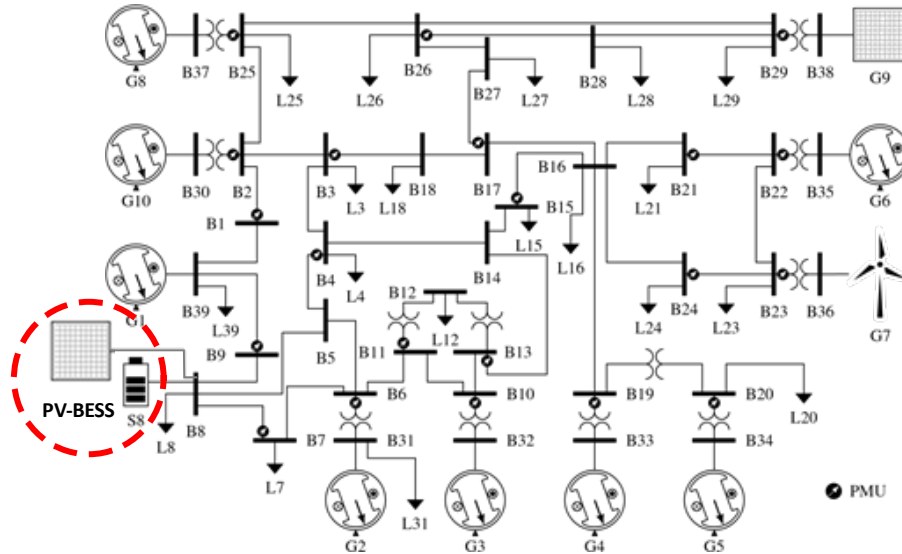
**Figure 44. Modified IEEE 39-bus system for optimally placed PMUs**

The method also addresses the PMU placement problem for maximum system observability and accurate detection of system imbalances. For this purpose, a solution was developed to ensure that all positive-sequence bus voltages, and the currents leaving a bus, become available at a phasor data concentrator facility by direct measurement and/or estimation [20]. One example of simulation results for the 39-bus system under the same contingency event (the loss of a large conventional unit) without and with the proposed FFR method is shown in Figure 45. The proposed FFR method results in a better frequency and voltage response of the system compared to a case with no PMU-based FFR controls. This approach will be investigated further by the NREL team during future research activities.
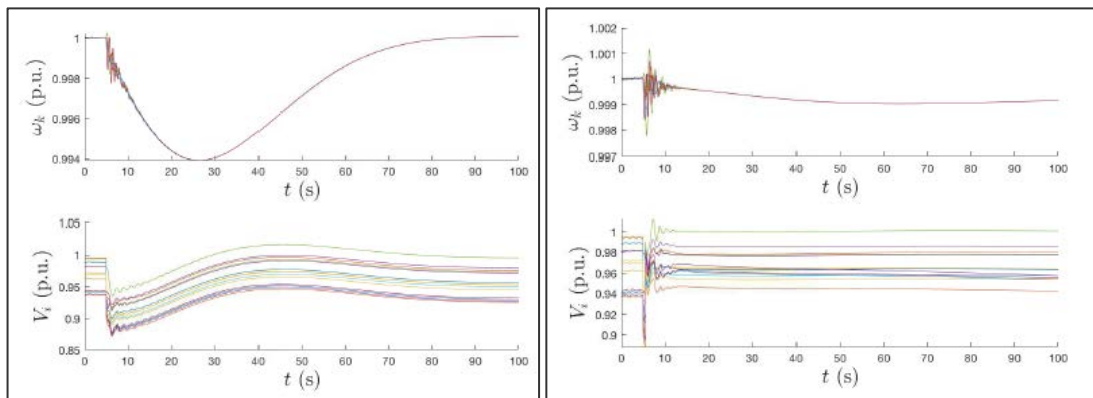


**Figure 45. Frequency and voltage response of 39-bus system: (left) no FFR and (right) with PMU-based FFR**

## 8.3  Frequency Droop Tests

### 8.3.1  *Frequency Droop Test Results by PV-BESS System*

Adequate droop response in combination with inertia is an important reliability factor for any power system and needs to be maintained at levels prescribed by NERC BAL-003-1 for interconnections and individual balancing areas [24]. The most common droop setting used in

36

many power systems is 5%, but in some cases a more aggressive 3% droop is used as well. For example, the Western Electricity Coordinating Council governor droop criterion allows individual generator droop settings within a 3%–5% range [21]. Frequency droop control assumes a linear relationship between power and frequency (with some small deadband). For example, a 5% droop means that a 5% change in frequency would result in a 100% change in power, a 3% droop means that a 3% change in frequency would result in a 100% change in power, etc. Such a linear relationship is theoretical, though, and with real governors, it has many nonlinearities due to various types of control delays, unintentional deadbands, and physical characteristics of prime movers. The ability of large utility-scale PV plants to provide droop response was demonstrated in [4]. For BESS, as was shown by previous testing at NREL [11], the relationship between power and frequency is essentially linear due to the fast response time (less than 50 ms) of the battery inverters; therefore, both PV plants and BESS can provide PFR with much higher levels of precision and speed for a wide range of droop settings (e.g., 1%–5%). However, the ability of BESS to provide adequate droop response is also subject to its initial conditions. For the same per unit of power and depending on the initial conditions, the BESS can provide more benefits to the system's PFR than conventional generators. A theoretical comparison of the frequency droop response of a BESS and a synchronous generator-based unit is shown in Figure 46. In this case, the droop response by the BESS component of the PV-BESS plant is drawn for a case when the BESS happened to be at zero power, so it has equal headroom to inject or absorb power depending on the nature of the transient event (underfrequency or overfrequency). For a PV plant to provide a droop response, it needs to be curtailed to have enough headroom to increase its production to the level determined by the droop settings during underfrequency events. For overfrequency events, a PV plant can provide an aggressive droop response. It is anticipated that the prevailing role of the PFR provision of PV-BESS plants will be based on the BESS components providing such services instead of curtailing the PV components of PV-BESS plants.
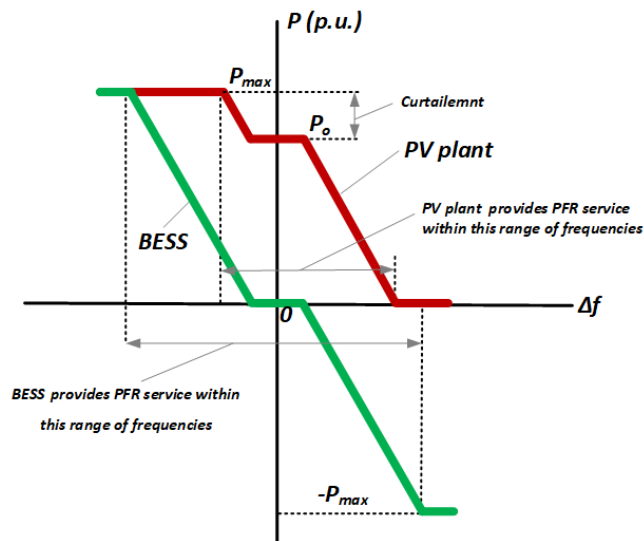


Figure 46. Frequency droop by a PV-BESS system

Several experiments were conducted on the 430-kW PV plant to demonstrate its ability to provide droop response when exposed to real frequency events emulated by the CGI. The PV PPC did not have built-in control for droop response. For this purpose, the external NREL controller was used to command the set points to the PV PPC based on the measured frequency and droop settings, thus introducing an additional delay from 50 ms–100 ms in response. But even then, the PV plant demonstrated good PFR for both the 5% and 3% droop settings, as shown in Figure 47 and Figure 48, respectively. The measured ability of the BESS to provide droop response is shown in Figure 49.
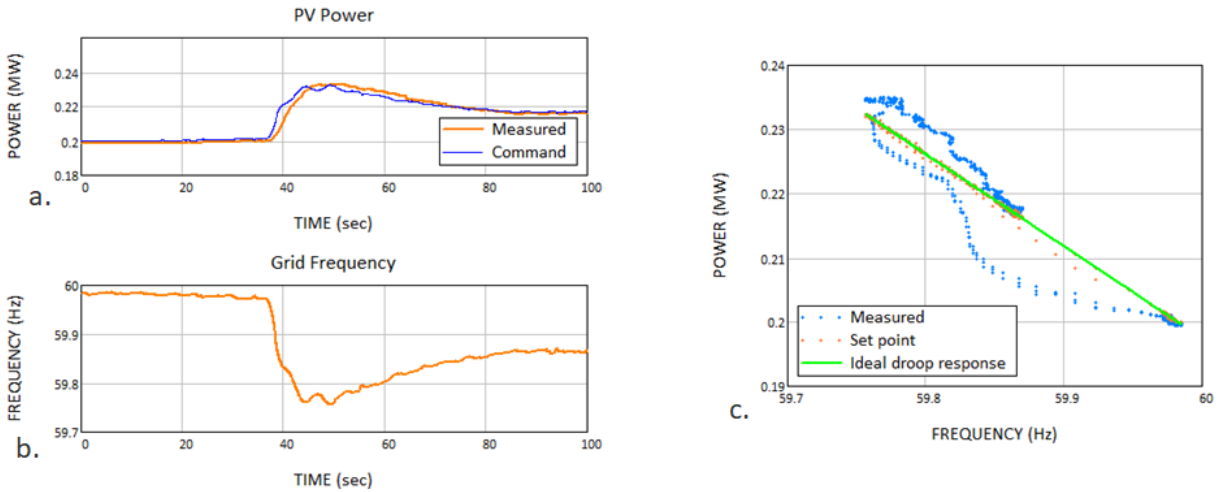


**Figure 47. PV plant providing 5% droop response**
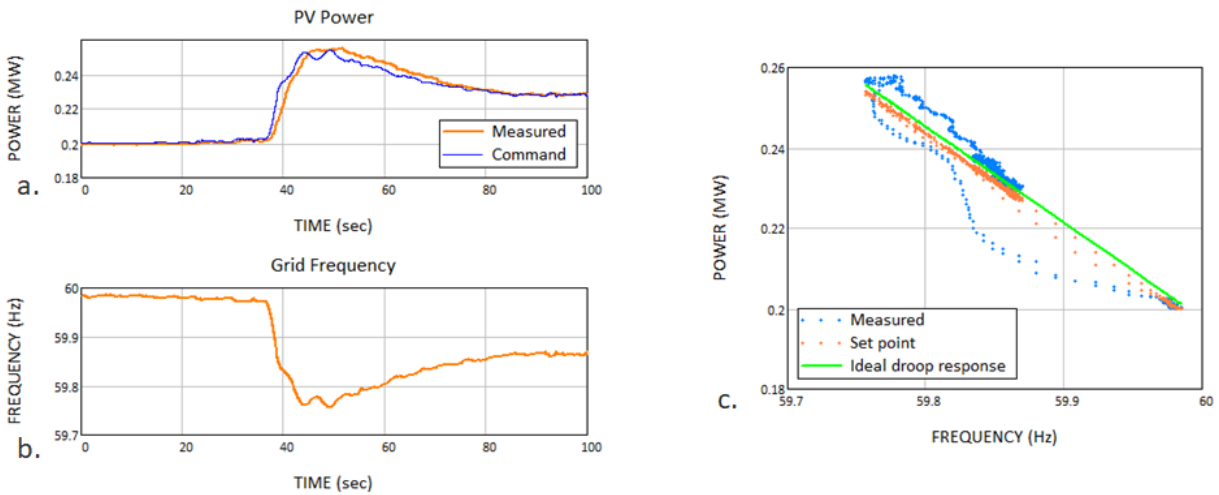


**Figure 48. PV plant providing 3% droop response**
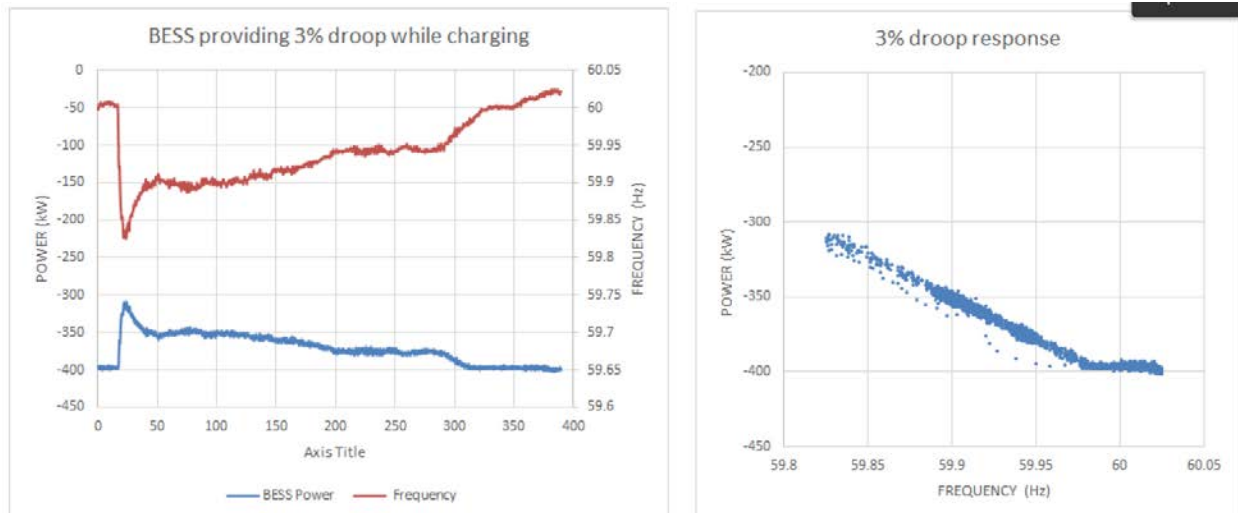
**Figure 49. BESS providing frequency droop response**

### 8.3.2  *Comparison of Frequency Response Methods*

In this section, we analyze the combined results of several PHIL tests to better understand and compare system performance for each method. For this purpose, we selected the most extreme case—corresponding to 60% penetration by IBRs in the power system emulated in PHIL (Figure 31). Figure 50 shows the results for the following test cases:

- No PV-BESS present in the PHIL test case
- Equivalent of 1,800-MW PV-BESS providing inertial response only
- Equivalent of 1,800-MW PV-BESS providing FFR with 0-ms delay
- Equivalent of 1,800-MW PV-BESS providing FFR with 1-s delay
- Equivalent of 1,800-MW PV-BESS providing inertia plus FFR with 1-s delay.

Apparently, the best performance is achieved for the use case with zero-delay FFR ($T_d$=0-s), indicated by the yellow trace; however, as discussed earlier, this is not a realistic situation because actual delays associated with PMU-based FFR controls will exist. After introducing a conservative 1-s delay, the best-performance among all remaining use cases is demonstrated by the use case of "Inertia plus FFR with 1-s delay" (green trace in Figure 50). Even at such a high level of renewable penetration, the combination of inertial response and FFR with a 1-s delay produces the best performance, keeping the frequency nadir securely above underfrequency load-shedding level.
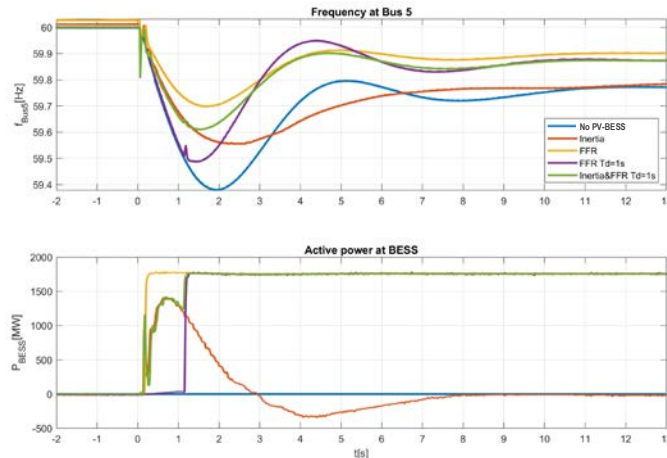
**Figure 50. Comparison of impacts by inertial, FFR, and PFR controls**

## 8.4 AGC Tests

The ability of a large 300-MW PV plant to participate in AGC was successfully demonstrated in [4], with results indicating that PV generation can participate in frequency regulation with much faster speed and higher precision of response than conventional resources when following an AGC signal provided by CAISO. In this section, we show some results of a 430-kW PV plant operation when following the set points generated by the NREL controller. These set points were calculated from the historic 4-s Public Service Company of Colorado area control error time series. The historic area control error data were scaled down by the NREL controller to a level corresponding to the rating of the 430-kW PV plant. The results of such testing are shown in Figure 51 and Figure 52, each for 1 hour of operation. These figures show that the curtailed plant (10% below available peak power) is fully capable of following the AGC signal with a high degree of precision when there is enough headroom between the plant's operational point and the peak available power. During fast cloud movements, however, the plant output can decline rapidly (initial portion of time series in Figure 51). To avoid these types of situations, either a control error correction is needed by using energy storage or a fast real-time peak power estimation method is needed to constantly scale the AGC set points based on the available plant power. Such a method was developed during this project, and it is described in detail in Section 13 of this report.

During less variable conditions, the AGC performance of the plant is much better, as shown in Figure 53 and Figure 54. The ability of the BESS to follow the same AGC set point is shown in Figure 55. The BESS can provide this type of response with a very high degree of precision because it is not subject to resource variability like the PV plant.
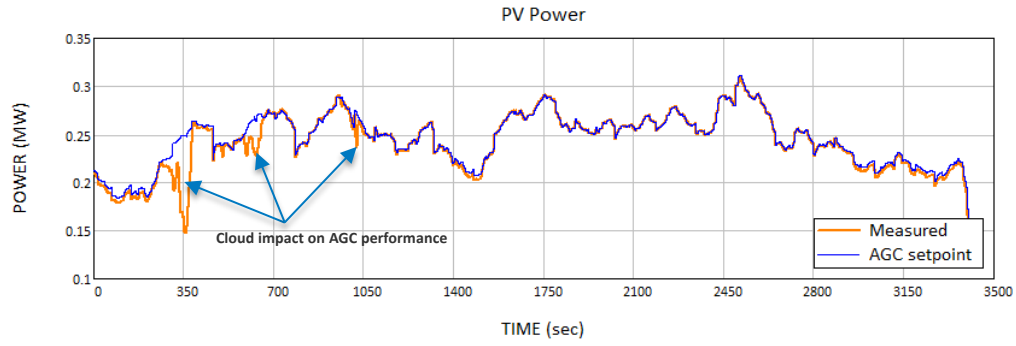
**Figure 51. PV plant following the AGC set point under high-variability conditions**
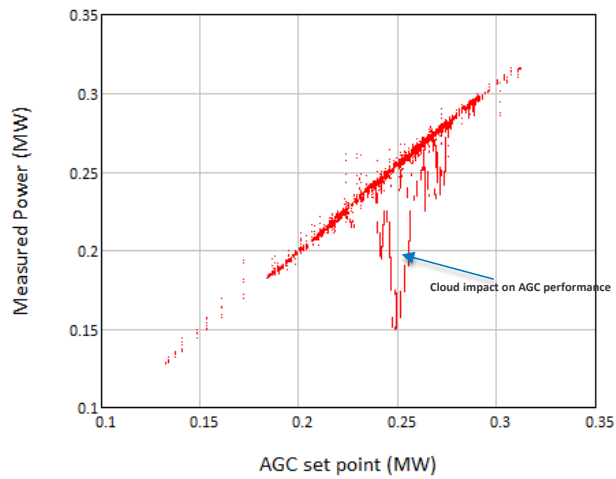


**Figure 52. Correlation between the measured PV plant power and the AGC set points under high-variability conditions**
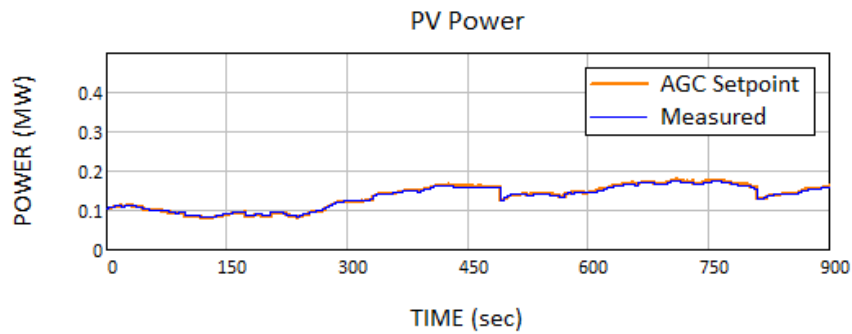


**Figure 53. PV plant following the AGC set point under low variability conditions**

41
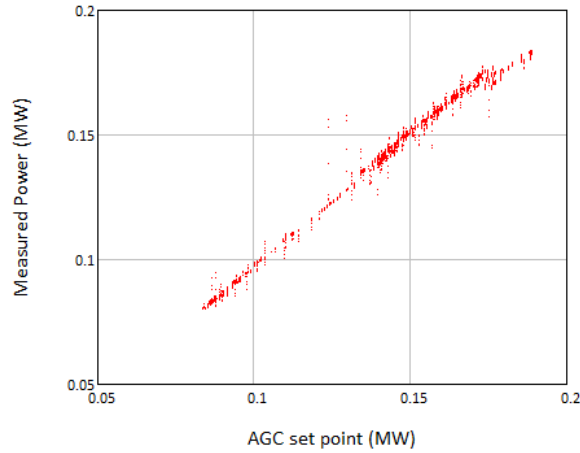
**Figure 54. Correlation between the measured PV plant power and the AGC set points under low variability conditions**
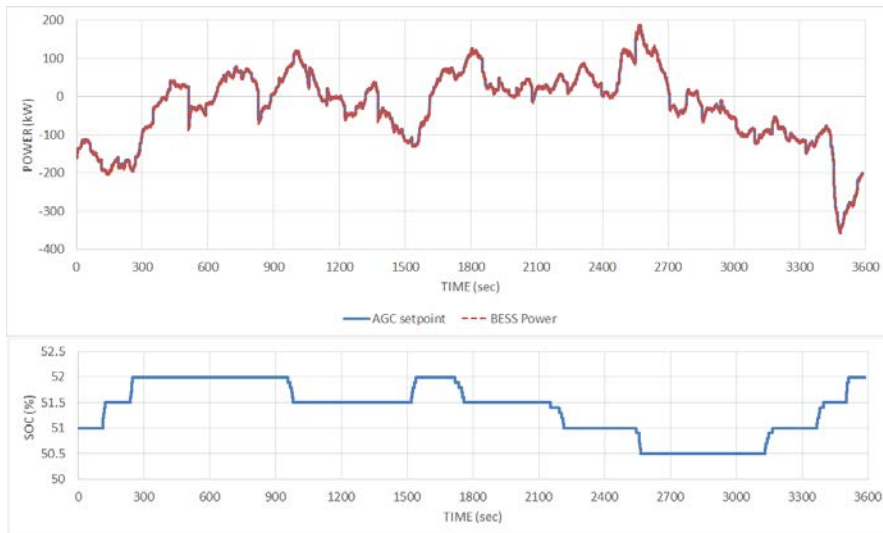


**Figure 55. BESS following the AGC set points—grid-following mode**

## 8.5 Dispatchability of PV-BESS Plant

The combined PV-BESS output can be shaped based on various revenue optimization algorithms, changing electricity prices, dispatch signals from the system operator, and types of reliability services the PV-BESS pant is providing. The NREL PV-BESS system combines an AC-coupled PV array (rated at 430 kW) and a BESS (rated at 1 MW/1 MWh), which creates an opportunity to test algorithms for multihour PV energy shifting and scheduling in addition to output profile shaping with a large degree of flexibility. The plant controller developed at NREL can provide dispatchable operation without PV curtailment while operating within the energy capacity and power rating constraints of the PV-BESS plant. It can be coupled with any external economic dispatch and optimization controller linked to the solar resource forecast system, thus creating the unique platform for industry partners to test, improve, and adapt PV-BESS controls for various market rules, reliability, and resilience metrics. One example of output-shaping operation is shown in Figure 56 for a PV-BESS system with measured PV power output under highly variable solar resource conditions present at NREL's Flatirons Campus. In this example,

42

the BESS is controlled to provide 3-h morning and 5-h evening ramps as well as steady baseload-like operation during the middle of the day. The initial SOC of the BESS happened to be at 70%, and during the day, the BESS is mainly charging (from PV only) in the morning and discharging in the evening while balancing the PV variability throughout the whole day, with the end SOC near 60%.
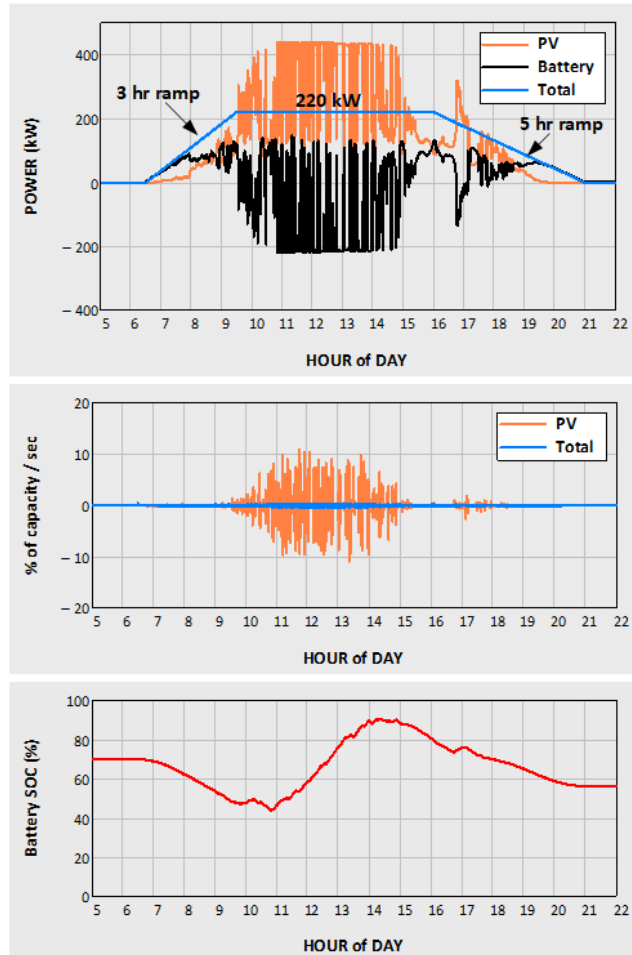


**Figure 56. Example of production profile-shaping PV-BESS system**

Other examples of such dispatchable operation are shown in Figure 57 (a), (b), and (c), with the BESS shifting PV energy into the evening hours following the commanded trapezoidal profile. Figure 57 shows the case when the PV-BESS system is commanded to provide a firm block of energy similar to baseload units.
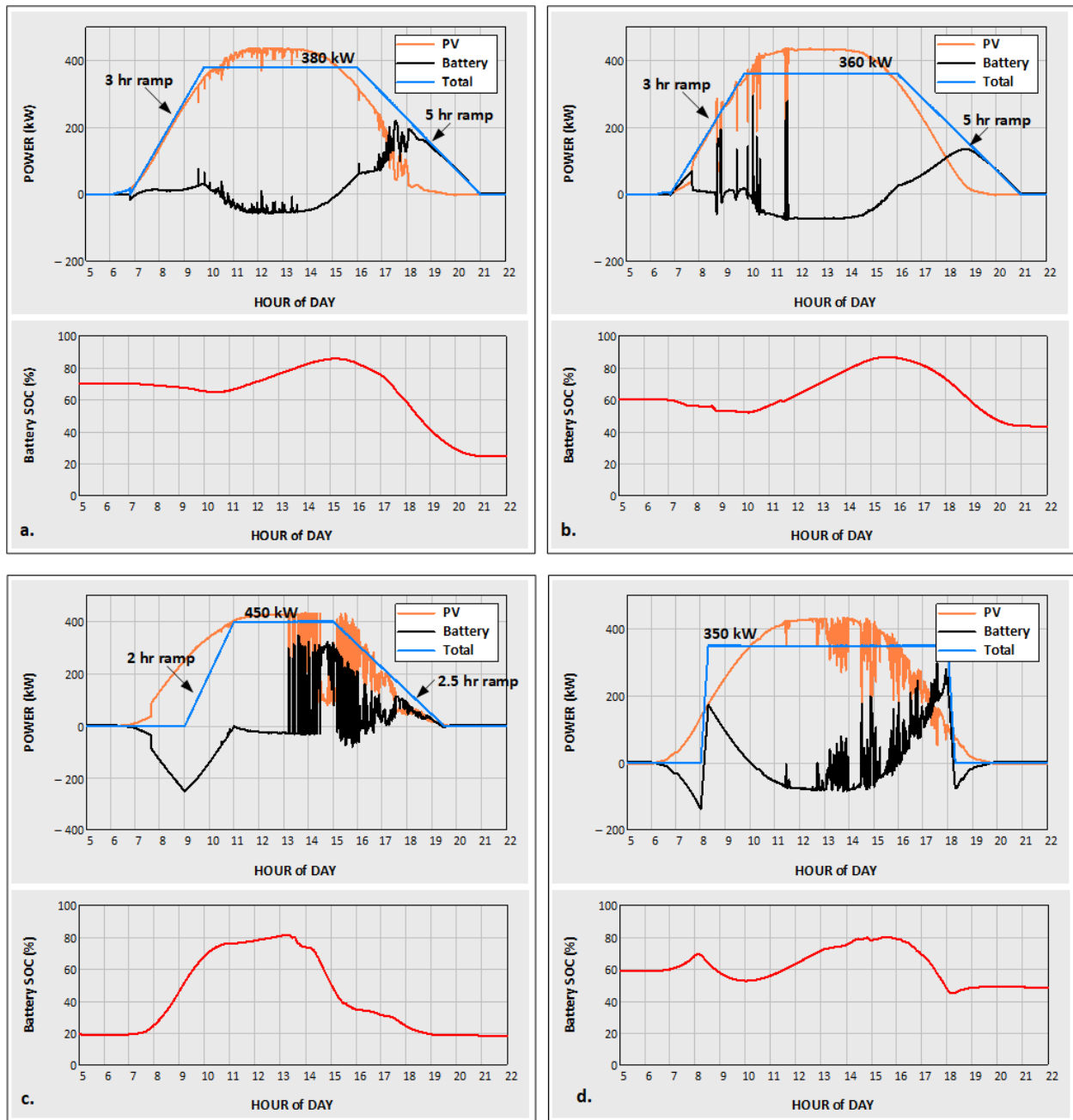
**Figure 57. Examples of dispatchable operation by the PV-BESS system**

In all these cases, the BESS—because of its larger power rating compared to the PV plant—has sufficient headroom to modulate its power above the dispatched level for other services, such as primary response and up-regulation. Any desired aggregate profile of the PV-BESS plant can be achieved similar to the cases shown in Figure 56 and Figure 57 as long as all operational and economic constraints are respected.

## 8.6 Ramp-Limiting Tests

In the bulk power system, short-term variability and instantaneous ramp rates are largely mitigated by the geographic diversity of the solar resource [22]. Despite the attractiveness of a

smoothed and shifted output from each PV plant using energy storage, this approach results in a significant decrease in the efficiency of the entire system and eliminates the benefits of resource aggregation. In fact, operational integration between energy storage and any individual or groups of PV plants would be nonoptimal and would likely result in simultaneous charging and discharging with zero net benefit to the system [22]. From this perspective, we did not consider the variability-smoothing controls an important topic in the context of utility-scale PV operation (the same is true for utility-scale wind as well). In small, stand-alone microgrids or small island systems that do not have the advantage of large spatial resource diversity, however, the variability smoothing of individual plants can still be a useful service. For this purpose, we developed and demonstrated some of the controls that can be used for variability-smoothing and short-term ramp-limiting service by PV-BESS plants. One example of a ramp-limiting test for a PV-BESS plant is shown in Figure 58. In this case, the BESS was controlled to provide ramp limiting for two PV plants at NREL: the 430-kW First Solar PV plant and a 1-MW MaxGen commercial PV plant.[2]
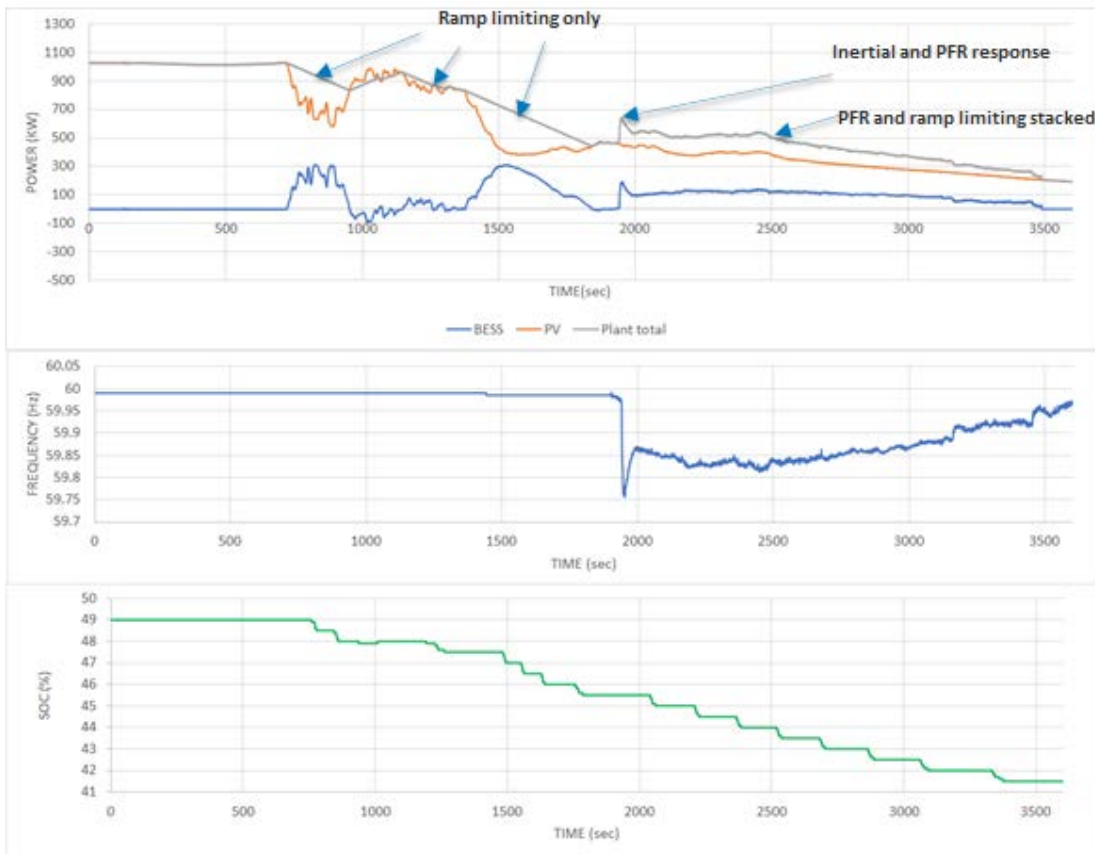


**Figure 58. PV-BESS system in ramp-limiting mode (50-kW/min limit) providing PFR**

---

[2] The MaxGen (formerly SunEdison) PV plant is a commercial 1-MW plant that operates under a PPA with Xcel Energy. NREL does not have control over the inverters of this plant. During most of 2019 and 2020, this plant was malfunctioning and was not used for testing BESS controls related to variability smoothing except for short periods of time when the plant operated properly. (It has problems with the tracking system and inverters.)

At the beginning, the total combined production from the two plants was near 1,000 kW and stable because of clear-sky conditions. The clouds started moving over the plant within approximately 10 min of the beginning of the experiment. The BESS was programmed to provide a 50-kW/min aggregate ramp rate for both plants combined (orange trace), ensuring significant short-term variability smoothing. At t≈1,900 s, a frequency event was simulated by the CGI, so in addition to ramp rate control, the inertial response (H=10 s) and primary frequency control of the BESS became active. From this point, the PV-BESS plant was providing two services at the same time (stacked services): a 50-kW/min ramp rate limit and frequency response. The BESS SOC was declining steadily during the whole test because the BESS was mostly discharging to provide the desired ramp limit.

Another example of a ramp control test is shown in Figure 59. The BESS was set to provide a 100-kW/min ramp limit. This made the total PV-BESS plant output during the periods of cloud variability (time periods near t=60 s and t=150 s). At t=160 min, a large cloud moved in, rapidly collapsing the PV production in only 30 s (yellow trace). The BESS ramp-limiting controls started injecting power to delay the total plant output reduction. This can be a valuable service in some microgrids, allowing sufficient time for backup generation to start and synchronize.
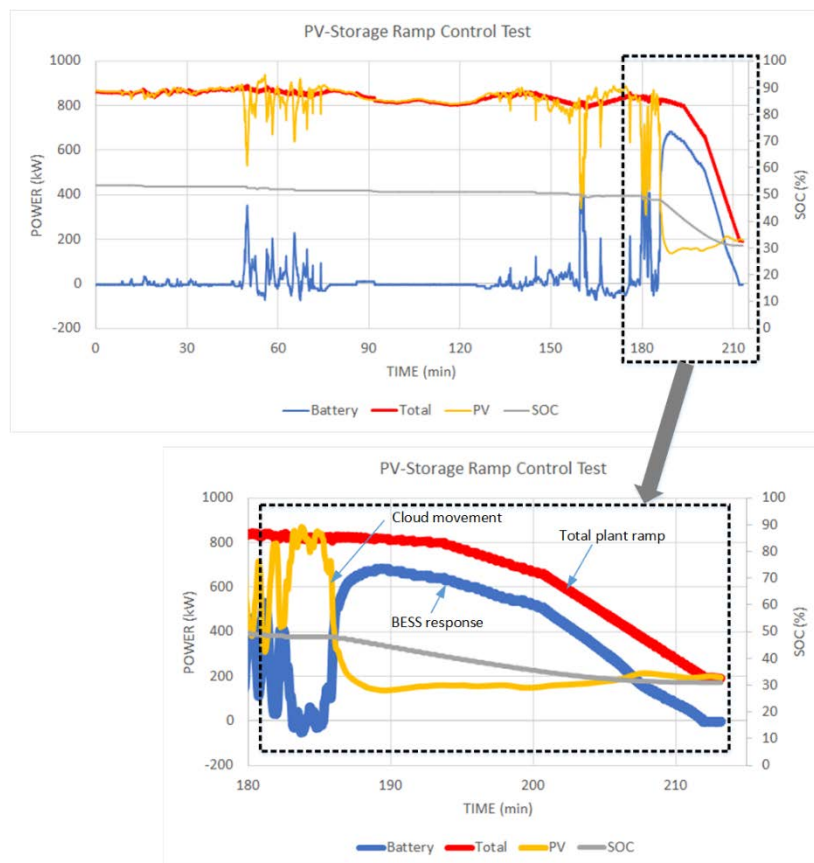


**Figure 59. Ramp-limiting control of the PV-BESS plant (100 k/min)**

The ability of the PV-BESS to provide smoothing services was also tested when the BESS was operating in grid-forming mode. The results of one interesting experiment are shown in Figure 60. In this case, we modulated the output of the PV plant to create a fully controlled variability pattern to explore the response times of the BESS in grid-forming mode when controlled from

the PV-BESS plant controller. In this example, a 60-s averaging filter for PV power was applied in the controller to operate the battery based on a smoothed PV time series. Figure 60 shows that the BESS provided excellent smoothing under this highly variable PV production.
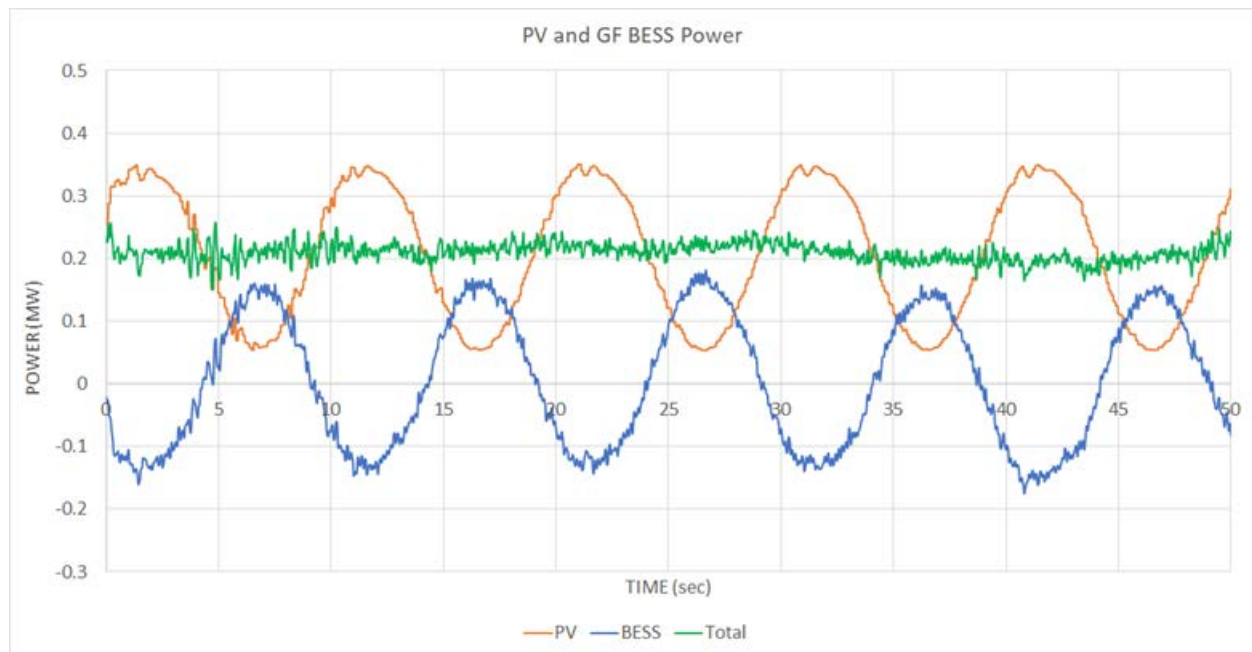


**Figure 60. Example of a variability-smoothing test by the BESS in grid-forming mode**

## 8.7 Oscillation Damping Controls

Power system oscillations triggered by disturbances such as generation outages or transmission line faults can result in system separation because of large swings in the active power flow over intertie lines, potentially leading to major blackout events [44]–[47]. It is critical for the reliable operation of a power system that its interarea oscillation modes remain sufficiently damped under all resource dispatch scenarios. Usually, the interarea modes are damped by installing power system stabilizers (PSS) in the control system of synchronous generators. There is increasing concern that the displacement of synchronous generators by IBRs might negatively impact the damping of the interarea modes. For example, recent studies by ERCOT have shown that it will be important for IBRs to provide PSS-type damping for the reliable operation of the Texas Interconnection as the IBR penetration increases to higher levels [47], [48]. IBRs can provide PSS-like functionality and provide damping to the interarea oscillation modes by modulating their active power output. In this project, we tested the ability of the 430-kW First Solar PV plant to modulate its active power output to evaluate the feasibility of incorporating the PSS-like functionality in the PV plant. The details of this test are provided in the following.

To test the ability of the PV-BESS plant to modulate its active power output, the plant output was slightly curtailed by generating an active power reference slightly less than the maximum available power. In addition to the slow-varying active power reference, sinusoidal modulation of different frequencies was added to the reference. A special control algorithm for testing such modulation characteristics for PV-plus-storage plants was developed in National Instruments LabVIEW software and implemented in a real-time PXI controller during this project (the main user interface is shown in Figure 61).

47

**Figure 61. Main control screen for the P-Q set points and oscillation control**

The results of some sinusoidal active power modulation for both the PV plant (all inverters) and the BESS inverter operating in grid-following mode are shown in Figure 62 and Figure 63, respectively. The frequency sweep was conducted for the sinusoidal modulation frequencies in ranging from 0. Hz–1.5 Hz.
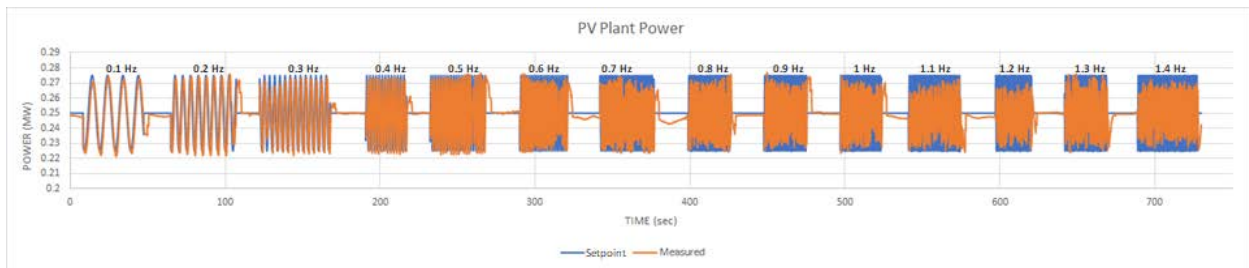


**Figure 62. PV power plant following the sinusoidal set point**
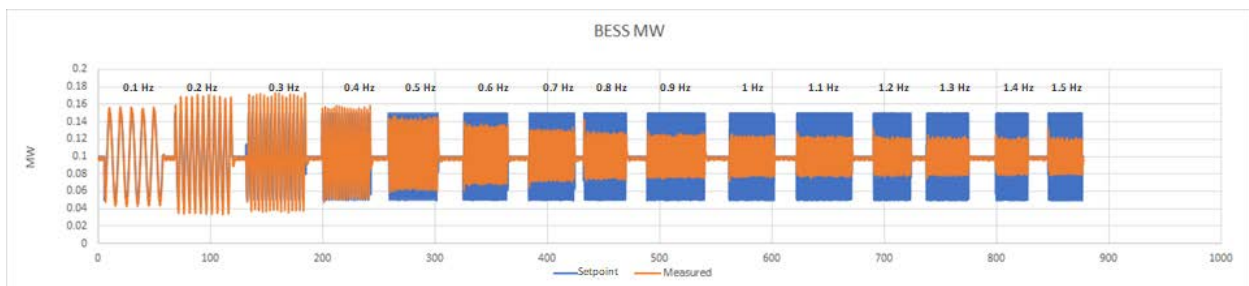


**Figure 63. BESS in grid-following mode following the sinusoidal set point**

Figure 64 and Figure 65 show the active power reference and the plant output for different frequencies of the sinusoidal modulation input individually for the PV and BESS plants. The data captures shown in the figures were used to develop the transfer function gain from the modulating active power reference to the plant output. A similar test was also conducted for a GE 1.5-MW wind turbine.
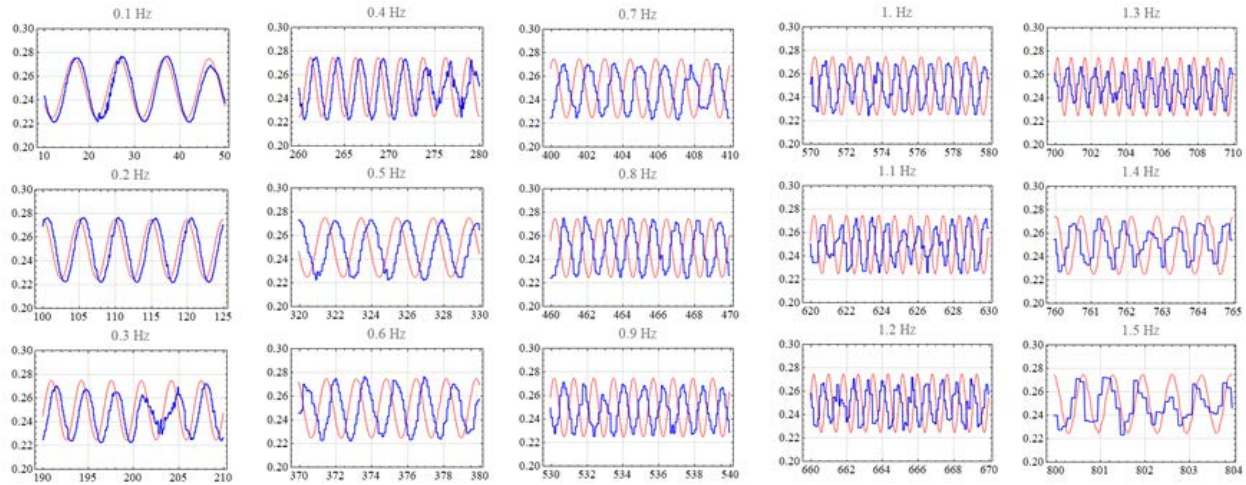


**Figure 64. Time-domain captures for fast Fourier transform analysis for First Solar's 430-kW PV plant**
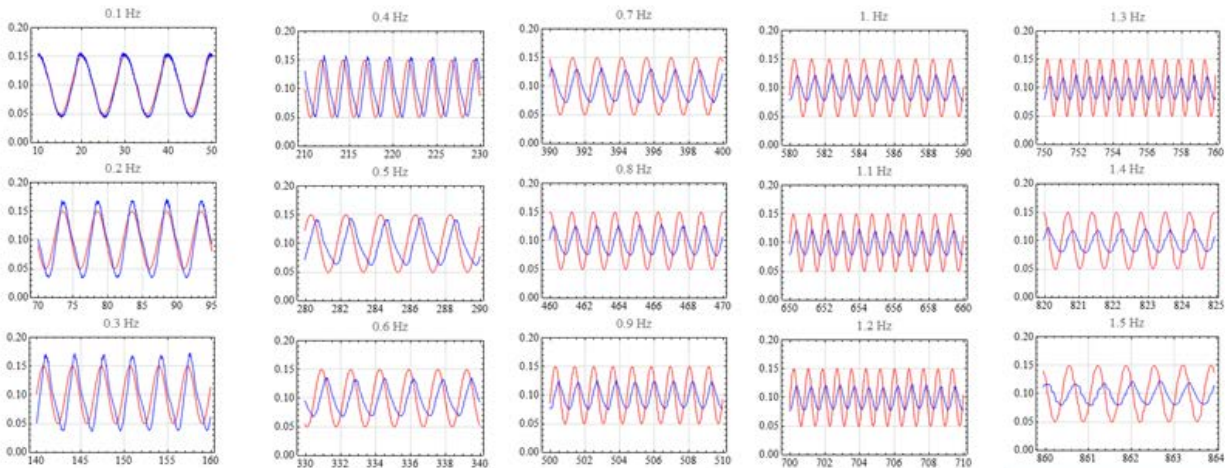


**Figure 65. Time-domain captures for the fast Fourier transform analysis for the BESS**
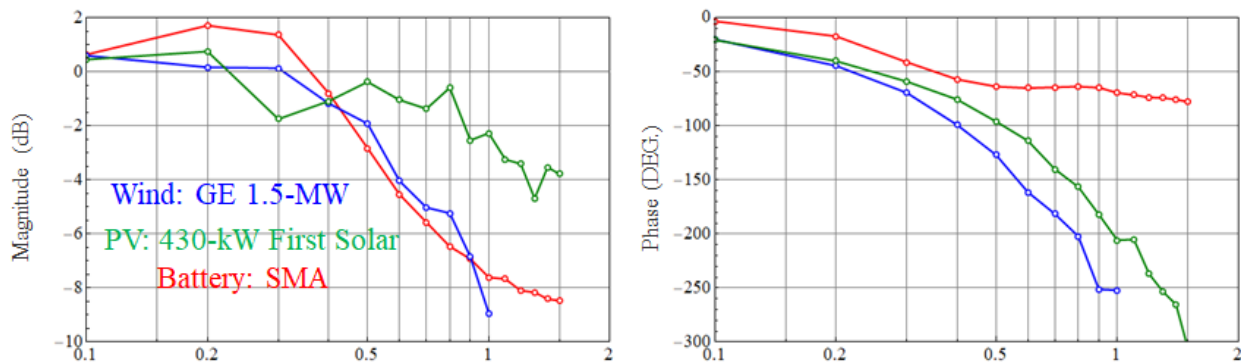


**Figure 66. Gain and phase response bode plot for different resources**

49

Figure 66 shows the transfer function gain from the active power reference to the active power output for the GE 1.5-MW wind turbine, First Solar's 430-kW PV plant, and the 1-MW/1-MWh BESS. It is evident that all three sources can provide active power modulation to near 1 Hz. The PV plant exhibits the maximum bandwidth for the active power modulations—inverter controls can be further tuned to improve performance. The phase response in Figure 66 exhibits the typical behavior of a delay—the phase response can be further improved by reducing the number and amount of delays from the active power reference to the active power output. Future work will implement PSS-like functionality in a PV plant and a BESS, and the performance will be tested using PHIL experiments and later in the field.

## 8.8 Modeling of POD by PV_BESS plants

Multiple approaches have been proposed for damping interarea oscillations. One method using energy storage systems installed in areas that can oscillate against one another and with real power injection at each location using a damping control system is described in [25]. Here, we use the same approach to demonstrate the ability of a PV-BESS plant to provide interarea oscillation damping using the modified two-area power system described in [26]. We show how the PV component of PV-BESS plants can provide such control because the provision of such control by energy storage was investigated in [25]. The damping controller located in the PV-BESS plant in Area 1 controls the power of the curtailed PV plant proportional to the frequency difference between areas 1 and 2 (Figure 67). Generation in both areas is dominated by combined-cycle gas turbine generation.
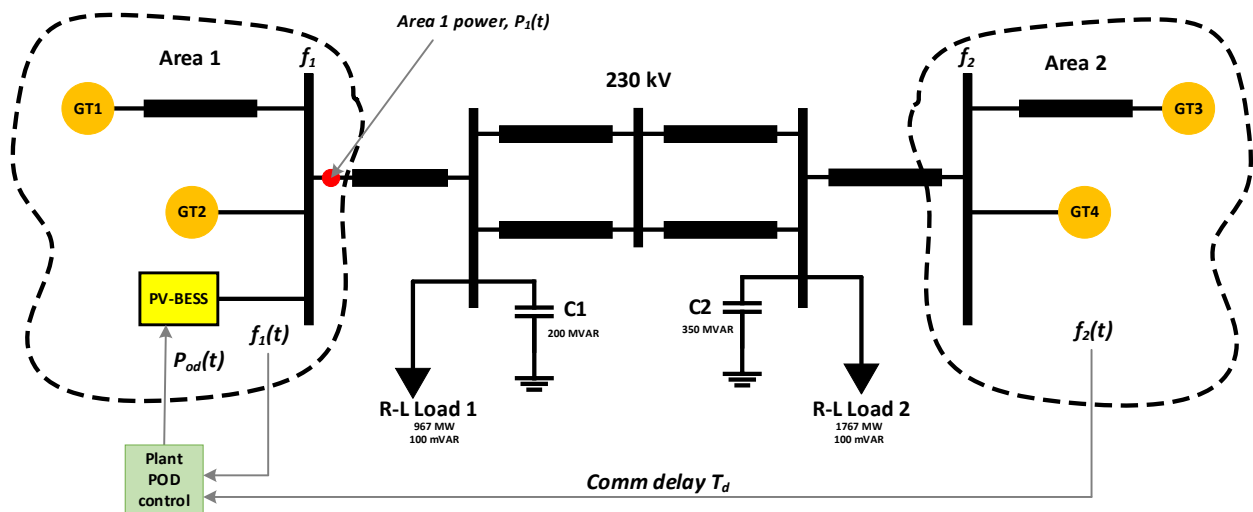


**Figure 67. Modified two-area system model**

Using the same control law described in [25], the output power of the PV plant can be modulated based on the following:

$$P_{pv}(t) = -K_d(f_1(t) - f_2(t - T_d)) \quad (8.1)$$

where $P_{pv}(t)$ is the commanded power of the PV plant, $f_1$ and $f_2$ are the frequencies measured in areas 1 and 2, $K_d$ is the control gain [MW/mHz], and $T_d$ is the communication delay.

Without any damping control (no PSS control implemented in the gas generation models), after a small change in load, the system quickly falls into an unstable oscillatory state, as shown in Figure 68. The upper plot in Figure 68 shows frequency in areas 1 and 2, calculated from the rotational speed of the generation plants. The second plot shows differences in frequency between areas 1 and 2. The third plot shows instantaneous power flow through the tie-line, and the bottom plot shows instantaneous power production of the 120-MW PV plant that was curtailed to the 100-MW level (16% curtailment).
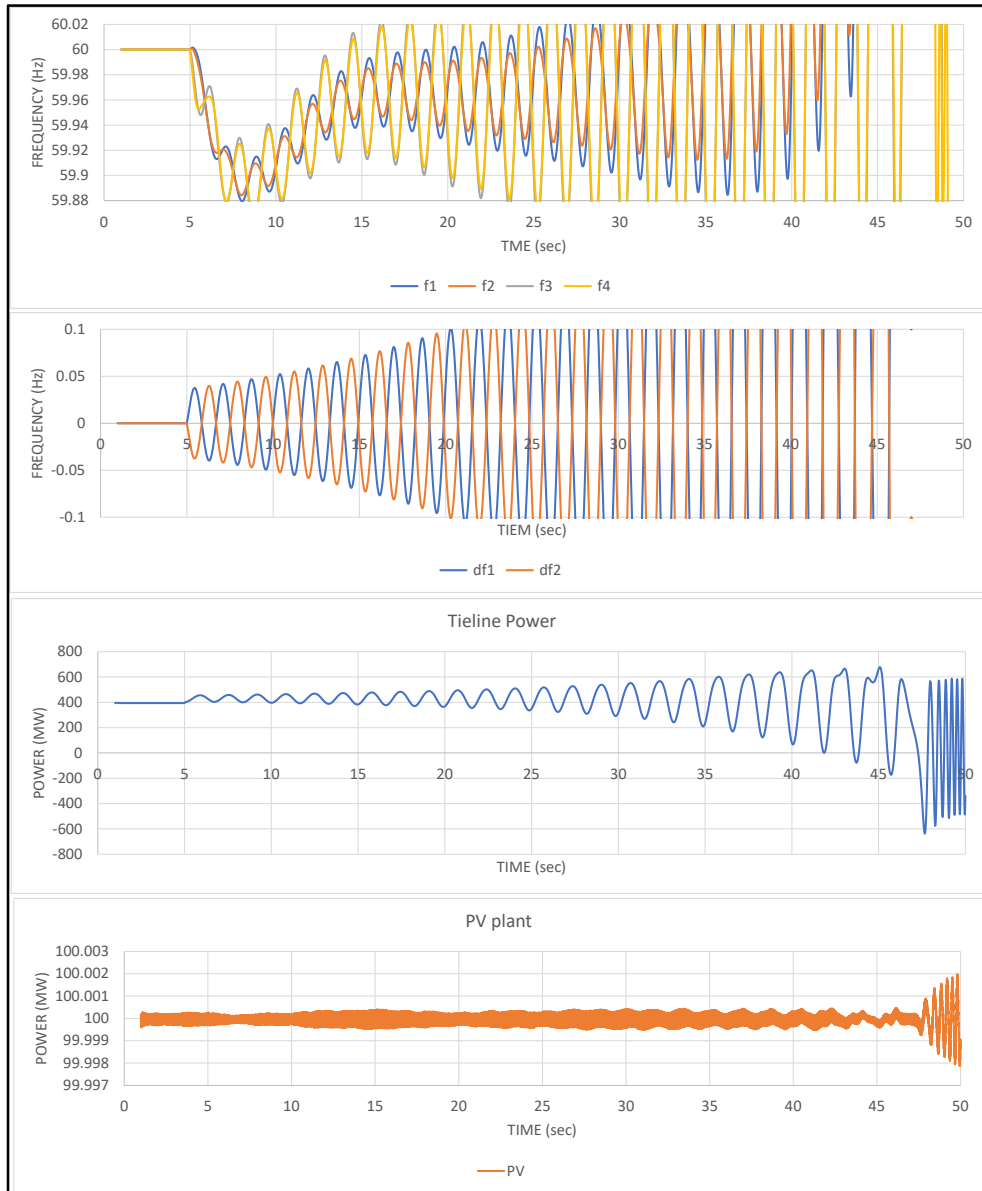


**Figure 68. Undamped oscillations triggered by a small change in load**

The damping behavior of the system changes dramatically after the above control law is applied to the PV plant controller in Area 1, as shown in Figure 69a. Even with a 200-ms communication latency used in this case, the oscillations are effectively damped within 20 s–25 s after the event. With less latency, the damping will be more efficient. If a similar PV plant located in Area 2 had commanded the power set points in accordance with the same control law (with reversed sign), then the damping would be even more efficient.
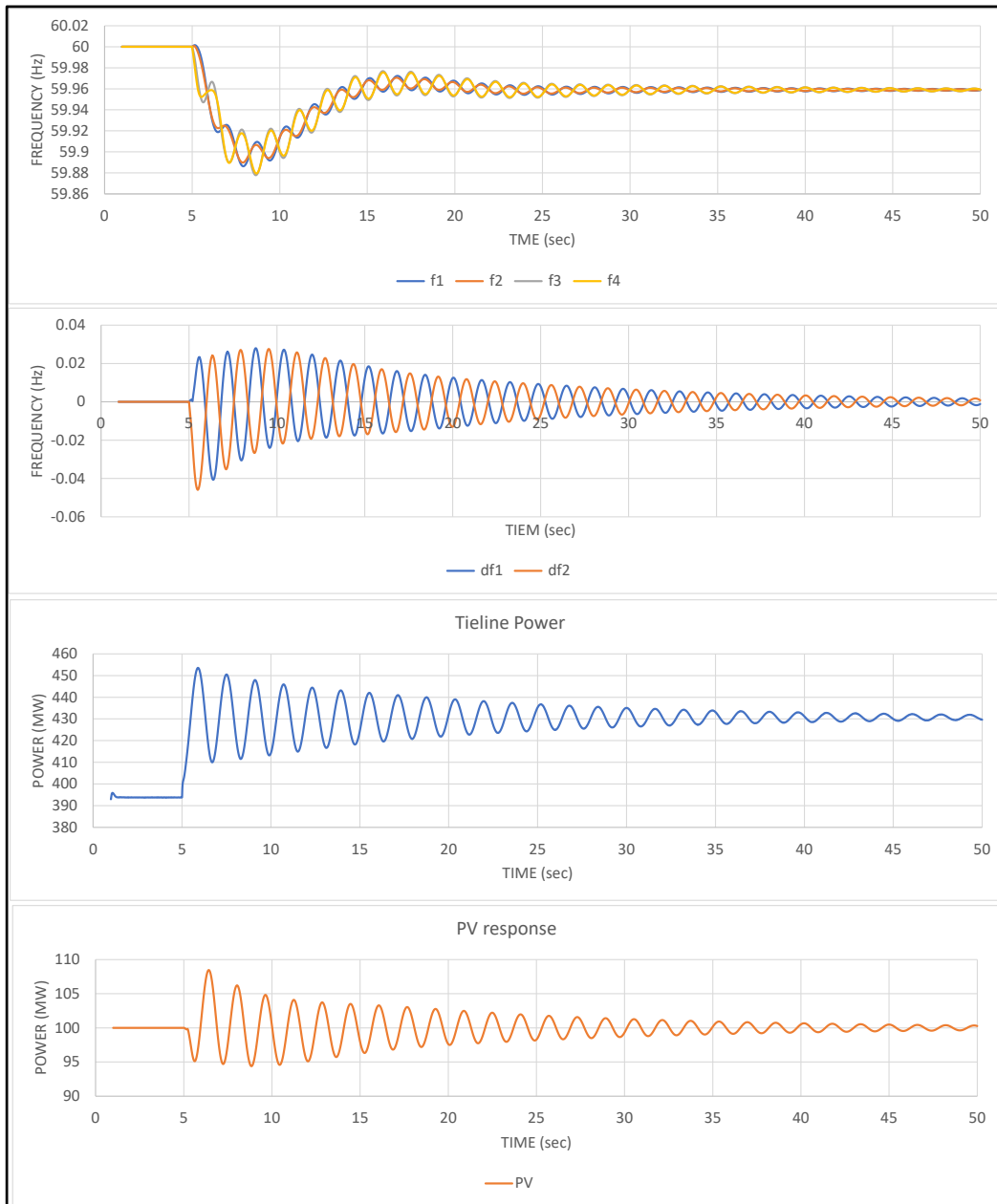


**Figure 69. Oscillations damped by POD control applied to the PV plant (T$_d$=200 ms)**

One important consideration about the provision of power oscillation damping (POD) by PV plants is that they need to have headroom to modulate their output in both directions. To avoid continuous curtailment, a method described in Figure 70 can be used. The PV plant can operate without curtailment at peak power until the interarea oscillations are detected by the POD

controller. At this instance, the controller quickly curtails the plant to a desired level before it starts modulating the output of the plant in accordance with the POD control law. This method has not been implemented in the current work, but it will be demonstrated by the NREL team in the near future.
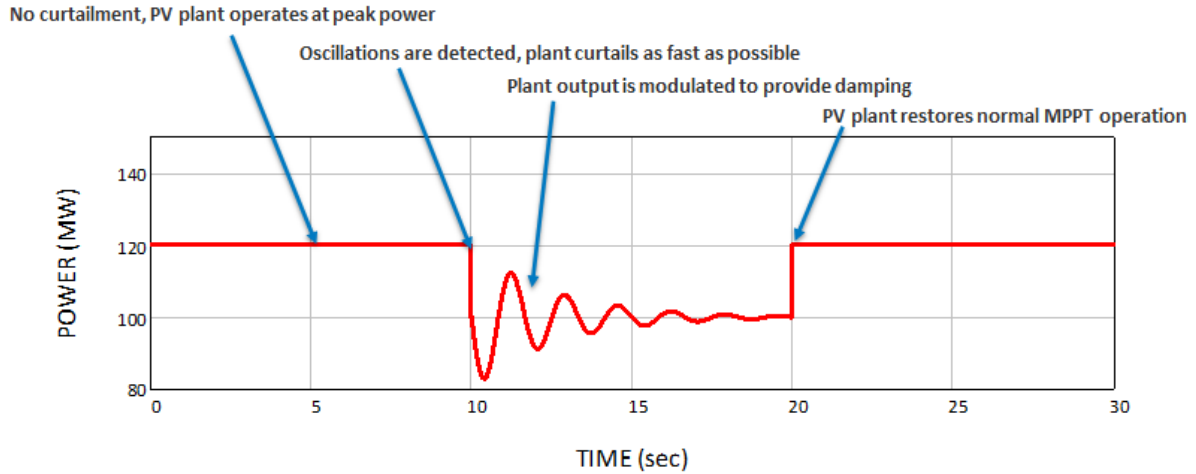


**Figure 70. PV plant providing POD without continuous curtailment**

# 9 Reactive Power Control Tests

The voltage of the North American bulk system is normally regulated by generator operators, which are typically provided, along with voltage schedules, by transmission operators [27]. The increasing penetration levels of variable wind and solar generation have led to the need for them to contribute to power system voltage and reactive regulation because, in the past, the bulk system voltage regulation has been provided almost exclusively by synchronous generators. According to the Federal Energy Regulatory Commission's Large Generator Interconnection Agreement [27], the generally accepted power factor requirement of a large generator is ±0.95. In conventional power plants with synchronous generators, the reactive power range is normally defined as dynamic, so synchronous generators must continuously adjust their reactive power production or absorption within a power factor range of ±0.95. For PV power plants, the reactive power requirements are not well defined. Federal Energy Regulatory Commission Order 661-A is applicable to wind generators but sometimes applies to PV plants as well. It also requires a power factor range of ±0.95 measured at the POI and requires that the plant provide sufficient dynamic voltage support to ensure safety and reliability. (The requirement for dynamic voltage support is normally determined during interconnection studies.) Utility-scale wind power plants are designed to meet the ±0.95 power factor requirements. The common practice in the PV industry is to configure PV inverters to operate at a certain power factor needed to cover the reactive losses and then follow the utility's reactive power or power factor set point (often at unity power factor). It is expected that similar interconnection requirements for power factor range and low-voltage ride-through will be formulated for PV in the near future. To meet this requirement, PV inverters must have MVA ratings large enough to handle full active and reactive current.

The steady reactive power capabilities of the 430-kW PV plant and 1-MW BESS were measured in CGI-connected mode to avoid the voltage stability impact on NREL's medium-voltage, Xcel Energy-connected grid. The CGI provides full isolation for reactive power flows between the test article bus and the regular grid bus; therefore, conducting such experiments on the CGI is a very safe and controlled way to characterize the reactive capabilities of multimegawatt inverters. In many cases, conducting such experiments in the field is not possible because of strictly defined under- and overvoltage limits by utilities.

The measured steady-state reactive power capability of the 430-kW PV plant is shown in Figure 71. The voltage on the low-voltage terminals was set at a 600-V nominal level by the CGI. Despite commanding a full two-quadrant reactive power profile (blue trace), the PV plant, consisting of six string inverters, was capable of delivering only the reactive power profile depicted by the orange trace. This is because of a -0.8…0.8 power factor limit set by the inverter vendors.
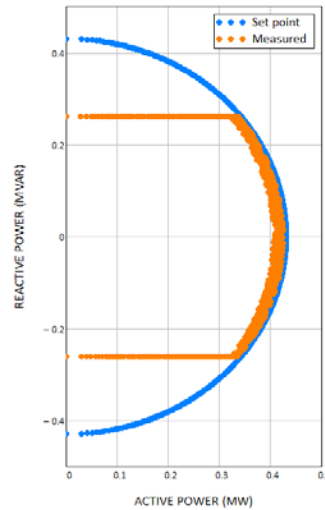
**Figure 71. Measured reactive power characteristics of the PV plant (all inverters)**

The P-Q capability of NREL's 1-MW/1-MWh BESS—consisting of LG Li-ion batteries and an SMA 2.2-MVA, 400-V AC inverter/charger with a 1.1-MVA 13.2-kV/400-V transformer—was verified using the experimental setup shown in Figure 19. The BESS inverter's full four-quadrant, steady-state P-Q characteristic was tested in CGI-connected mode to avoid impacts on NREL's medium-voltage, Xcel Energy-connected grid. The inverter was commanded to use various combinations of active and reactive power set points to cover the whole range of P-Q operation. The results of one such test are shown in Figure 72.

The P-Q characteristic of the BESS system was measured on the medium-voltage side (or CGI side) of the BESS transformer as well. A comparison of both P-Q characteristics is shown in Figure 73. The shift between the two is caused by a 6% impedance of the BESS transformer and some reactive losses in the 100-meter underground collector line. NREL is developing a control to compensate for these reactive losses so the reactive power can be accurately controlled on the medium-voltage side of the BESS transformer. The inverter limits only $P_{max}$ and $Q_{max}$ at the 1-MW and 1-MVAR levels accordingly, but it does not limit the maximum apparent power, $S_{max}$, which is expected to be 1 MVA. Instead, the measured the P-Q characteristic approaches the square shape, as shown in Figure 72. Because of this characteristic, care must be taken not to exceed the $S_{max}$ set point for inverter transformer protection (the 400-V/132-kV step-up transformer is rated at 1.1 MVA).

The overall combined ideal reactive power capability measured for the 430 kW PV plant and the 1-MW/1-MWh BESS is shown in Figure 74. As expected, the aggregate reactive power capability of this hybrid PV-plus-storage plant is larger than the reactive power capability of individual components. The ideal shape, assuming a low-impedance connection and steady grid voltage, can change depending on the characteristics of each POI.
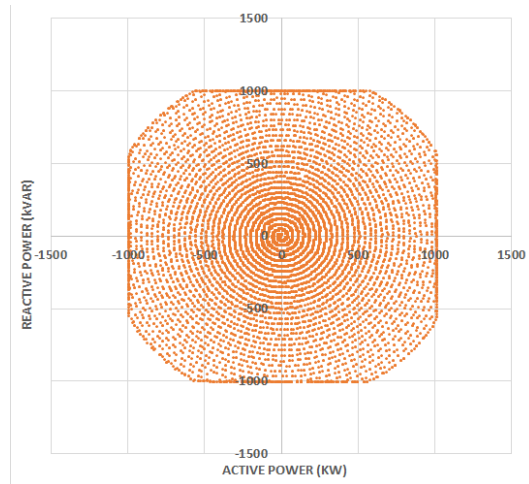
**Figure 72. Measured reactive power capability of the BESS system**
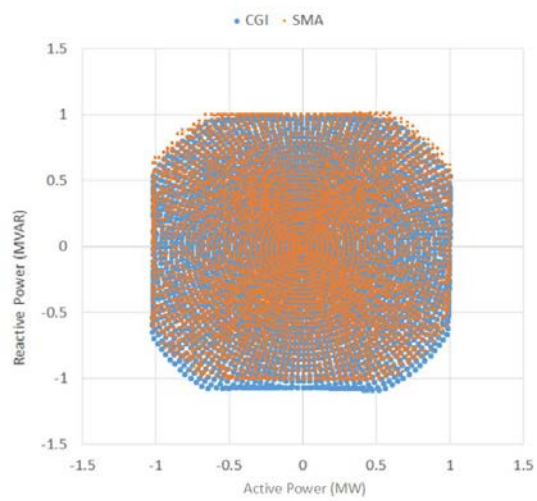


**Figure 73. Reactive power capability measured on the low-voltage (SMA) and medium-voltage (CGI) sides of the BESS transformer**
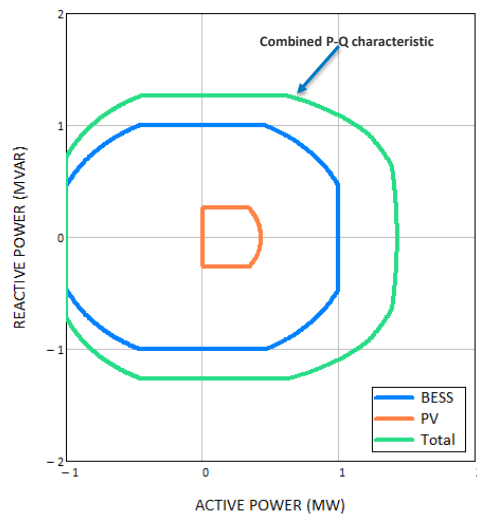


**Figure 74. Combined reactive power capability of the PV-BESS plant**

56

# 10 Impedance Characterization of the PV-BESS Plant

Impedance-based stability analysis studies have proven effective for the evaluation and mitigation of control interactions in wind and PV power plants, including subsynchronous and super-synchronous resonance conditions [50]. Transmission system operators have started demanding that manufacturers provide electromagnetic transient PSCAD models of IBRs to evaluate different stability problems, including low- and high-frequency control interactions, interarea oscillations, and frequency stability. The impedance measurement of wind turbines and PV inverters can be used not only for stability studies but also for the high-fidelity validation of electromagnetic transient models, which can be used for grid integration studies.

In this project, we performed the impedance characterization of a 2.2-MVA SMA inverter interfaced with a 1-MW/1-MWh BESS. We also performed the impedance characterization of inverters interfacing First Solar's 430-kW PV plant. In addition to the impedance measurements, we performed a PHIL experiment to simulate the operation of the First Solar plant under a weak grid condition. Impedance measurements were used to predict the oscillatory instability observed in the PHIL experiment for the operation of the PV plant under a weak grid condition. Details of the impedance measurement and PHIL experiments for weak grid operation are discussed in this section.

The impedance response of an inverter can be measured by injecting voltage or current perturbations at different frequencies from its terminals superimposed on the voltages and currents at the fundamental frequency. The 7-MW grid simulator, called the CGI, at NREL's Flatirons Campus was used for the impedance characterization of the 2.2-MVA battery storage inverter and the PV inverters interfacing First Solar's PV plant.

## 10.1 Impedance Measurement System

This subsection describes different systems used for the impedance characterization of the PV-BESS plant. More details on the impedance measurement system can be found in [51].

### 10.1.1 Grid Simulator

The CGI grid simulator at NREL is rated for 13.8-kV, 7-MVA continuous power, and it is used for injecting voltage perturbations at the terminals of the inverters at frequencies ranging up to 3 kHz for impedance characterization. The control system of the CGI is coupled with an RTDS, which can provide dynamic voltage references for all three phases and the neutral wire for different grid integration tests; the desired perturbations for the impedance measurement of the 2.2-MVA BESS inverter and the PV inverters of the 430-kW PV plant were configured inside the RTDS.

## 10.1.2 GPS-Synchronized Medium-Voltage Measurements



**Figure 75. Hardware in each medium-voltage DAS sensing node: (left) voltage and current sensors; (right) data conditioning built around the National Instruments' cRIO-9030 platform.** *Photos by NREL*

The admittance measurement test bed for utility-scale wind turbines and PV inverters at NREL has a medium-votlage DAS, which is a distributed network of GPS-synchronized measurement nodes sampling three-phase voltages and current waveforms at 50 kHz with 24-bit resolution. Raw 50-kHz voltage and current waveform captures can be triggered by programmable thresholds, supervisory control and automation systems, or asynchronously by user interface, and they can be stored locally for post-event downloading, alignment, and processing. The system is implemented on a National Instruments (NI) CompactRIO (cRIO) platform, and it uses onboard field-programmable gate array hardware for synchronization and processing functions. Figure 75 shows the hardware in a sensor node, including capacitive voltage sensors[3]; Rogowski coil-based current sensors[4]; and a GPS-synchronized, signal-conditioning unit built around the NI cRIO-9030 platform. Medium-voltage DAS nodes are located at different points in the test bed, and they allow for the GPS-synchronized measurement of voltages and currents during the injection of perturbations to obtain impedance responses over a broad frequency range.

## 10.1.3 Impedance Measurement System

To enable the admittance measurement of an inverter, all the components previously described are integrated, as shown in Figure 76. The CGI is controlled by an RTDS using a fast 2-Gbit/s optical fiber interface. The high-bandwidth interface and delay compensation techniques implemented in the CGI control system allow for the injection of perturbations over a wide spectrum of frequencies, from 0.1 Hz to 3 kHz.

---

[3] Jomitek – Power Solutions, "The Jomitek v3 voltage sensor," Datasheet, 2012.
[4] Powertek – RCTi current sensors, "RCTi single-phase current transducer," Datasheet. [Online] www.powertekuk.com/rcti-single-phase-current-transducer.pdf, accessed on July 17, 2019.
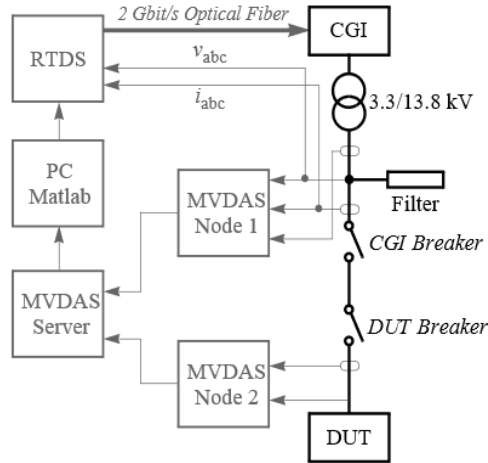
**Figure 76. Impedance measurement system diagram**

## 10.2 Impedance Measurements

Figure 77 shows the components of the PV-BESS plant whose sequence impedance responses are measured using the impedance measurement system described in the previous subsection. For the positive-sequence impedance measurement of a test article, the CGI injects positive-sequence voltage perturbations superimposed on the nominal fundamental trajectory. The measured positive-sequence impedance responses of the 1-MW/1-MWh BESS plant for different magnitudes of the injected voltage perturbations are shown in Figure 78. The positive-sequence impedance responses of the two groups of string inverters (4 kW x 40 kW and 2 kW x 125 kW) at the front end of First Solar's 430-kW PV plant are shown in Figure 79.

The impedance responses of the BESS and PV plants, shown in Figure 78 and Figure 79, respectively, can disclose many important characteristics of inverters interfacing these plants that can be used both for the stability and for the high-fidelity model validation. For example, the impedance responses in Figure 78 and Figure 79 reveal that the current control bandwidth of the BESS inverter is near 100 Hz and that of the string inverters in First Solar's PV plant is near 2 kHz. This is inferred from the fact that the impedance response of an inverter exhibits inductive and capacitive behavior, respectively, above and below the current control bandwidth of the inverter. The capacitive behavior of the inverter's output impedance below its current control bandwidth is because of the integral gain of the current controller, whereas the inductive behavior of the inverter's impedance response above the current control bandwidth is because of the phase reactors after the three-phase bridge in the inverter.

**Figure 77. Inverters for impedance characterization: the (a) 2.2-MVA inverter interfacing the 1-MW/1-MWh BESS and the (b) 430-kW PV plant with six string inverters.** *Photos by NREL*
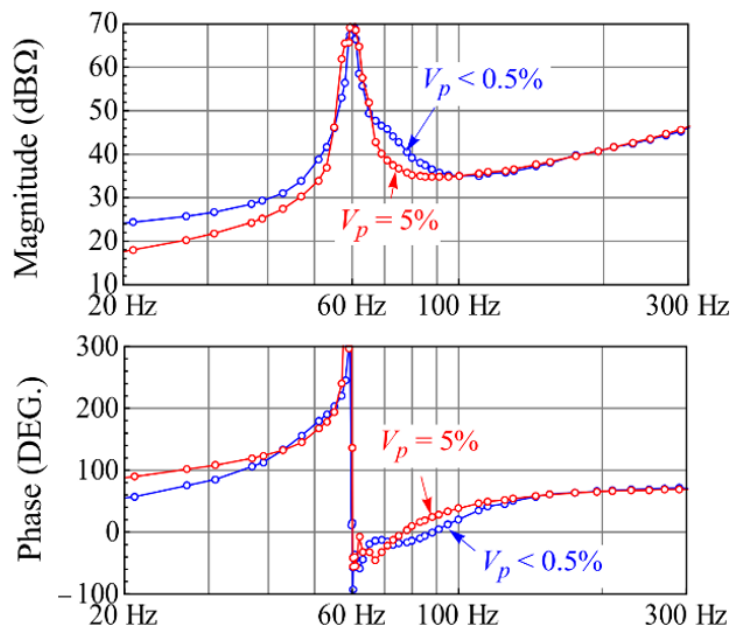


**Figure 78. Positive-sequence impedance response of the 1-MW/1-MWh BESS plant measured for different magnitudes of the voltage perturbation injected by the CGI for the impedance measurement**
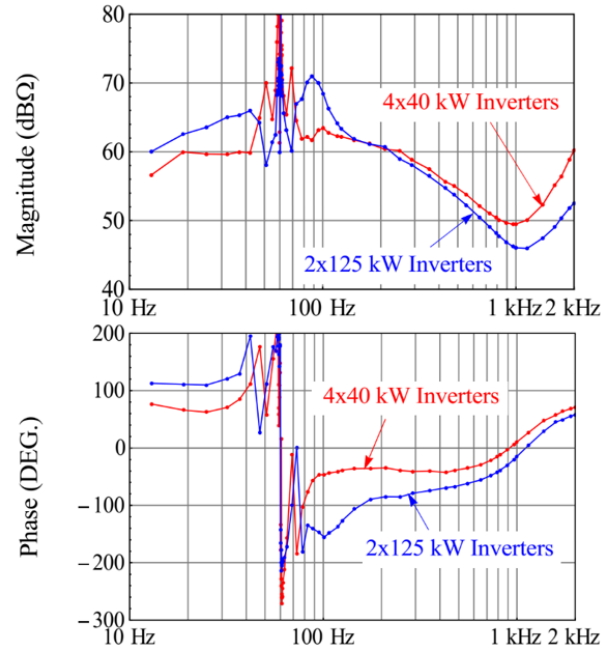
**Figure 79. Positive-sequence impedance response of two sets of string inverters (4 kW x 40 kW and 2 kW x125 kW) interfacing First Solar's 430-kW PV plant**

Because the impedance measurement thoroughly characterizes the behavior of a device from the grid perspective, it can be used for characterizing new technologies developed for improving grid resilience. For example, recently there has been a lot of interest on grid-forming inverters to substantially increase the penetration of IBRs. Different control methods—including droop, virtual oscillators, and virtual synchronous machine-based approaches—have been investigated for implementing the grid-forming functionality in inverters. Impedance characterization can serve as an excellent platform for comparing these methods and evaluating their impacts on grid stability. Figure 80 compares the positive-sequence impedance response of the 1-MW/1-MWh BESS plant shown in Figure 77 (a) when it is operated in standard grid-following and the recently developed grid-forming control modes. The peaking behavior of the impedance response near the fundamental frequency for the grid-following mode shows that the inverter is being controlled as a current source. On the other hand, the dipping of the impedance response near the fundamental frequency for the grid-forming mode shows that the inverter is being controlled as a voltage source. More importantly, the phase response of the impedance stays relatively closer to zero and within ±90 degrees at most frequencies when the BESS inverter is operating in the grid-forming mode; this signifies that the grid-forming mode provides higher positive damping than the grid-following mode, which can avoid potential stability and control interaction problems.

## 10.3 Impedance-Based Prediction of Oscillatory Instability During Weak Grid Operation

Fast and complex controls of inverters can lead to unstable interactions between a PV plant and the grid as well as among the inverters of a PV plant. It is particularly difficult to maintain the stability of an inverter when it operates under a weak grid condition. Different control systems inside an inverter—including PLLs, current controllers, and DC-bus voltage controllers—can interact in an undesired manner, leading to an unstable operation and damage or tripping of the inverters [52], [53].

61
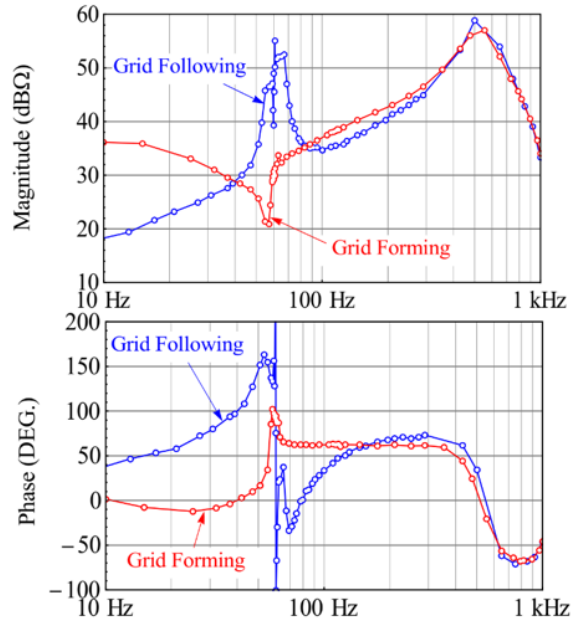
**Figure 80. Comparison of positive-sequence impedance response of the 1-MW/1-MWh BESS plant when it is operating in grid-following and grid-forming control modes**

Based on the impedance response of the PV plant inverters shown in Figure 80, below the current control bandwidth of 2 kHz, the impedance response is capacitive. The capacitive response of the PV inverters can interact with a weak inductive grid and can create an unstable resonant mode. To demonstrate the unstable operation of First Solar's PV plant under a weak grid operation, a set of PHIL experiments were performed by simulating a weak inductive grid using the CGI grid simulator.

Figure 81 shows the impedance-based stability analysis for the operation of the PV plant under a weak grid condition. Figure 81 (a) compares the positive-sequence impedance responses of the PV plant and the grid simulated inside the CGI. The impedance analysis predicts an unstable super-synchronous resonance at 554 Hz. The inverter output currents in Figure 81(b) confirm the presence of an unstable resonance predicted by the impedance analysis. This shows the value of the impedance characterization of the PV inverters to evaluate their stability properties during operation under different grid conditions.
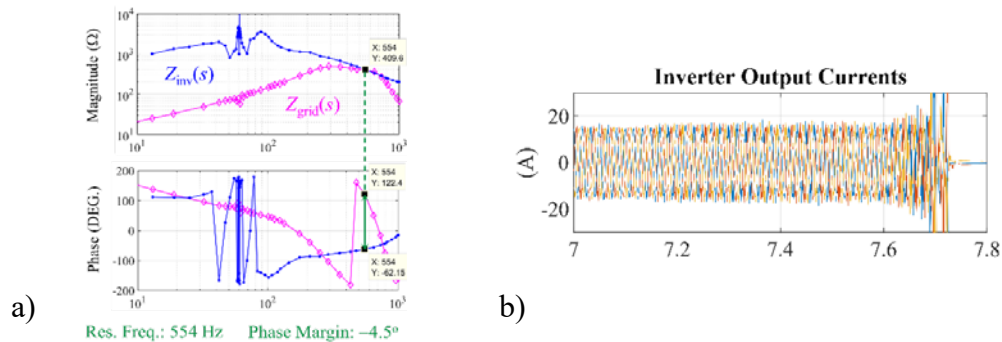


**Figure 81. Impedance-based prediction of instability of First Solar's 430-kW PV plant during operation under a weak grid condition: the (a) impedance analysis comparing the impedance responses of the PV inverters with the grid impedance and the (b) PV plant output current during instability**

62

# 11 Black Start of PV Plant with BESS

## 11.1 Black-Start Experiment with CGI

The first black-start experiment for the PV power plant was performed in 2019 using the CGI as a black-start grid-forming resource. This was done because the black-start controls for the SMA inverter of the BESS were not available until March 2020. In this first black-start experiment, the CGI increased its terminal voltage from 0 kV to 13.2 kV with a slow ramp to avoid inrush currents in the PV plant transformer. The total duration of the black-start process in this mode was approximately 9 min. This was because the programmed delays in both the 45-kW and the 125-KW inverters were near 5 min.

A number of black-start experiments for the 430-kW PV array using the CGI as a black-start resource were conducted in 2019. Results of a few such experiments are shown in Figure 83. The PV plant demonstrated robust black-start performance during all experiments.
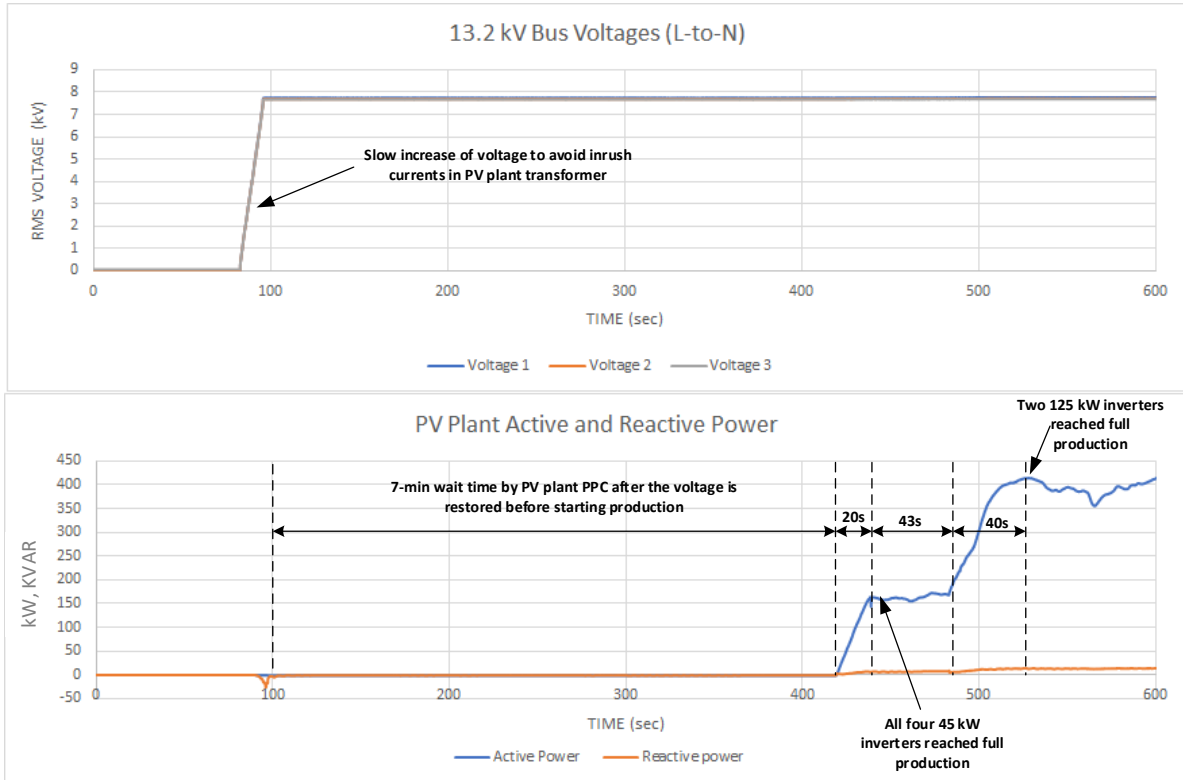
**Figure 82. Black start of PV system with the CGI**



**Figure 83. Series of black-start experiments using the CGI**

64

## 11.2 Black-Start Experiment with BESS

After the completion and commissioning of the black-start controls, new experiments were conducted using the BESS as a black-start resource for the PV plant. The experiment setup is shown in Figure 84. In this setup, medium-voltage side transformers for both the PV plant and BESS are wired as delta, so the whole islanded system does not have a ground reference. To introduce a grounding reference, a grounding transformer was installed in the system, as shown in Figure 84. The experiment was conducted with all assets connected to the CGI bus (the CGI was de-energized and disconnected), so the system was fully isolated from the real grid.
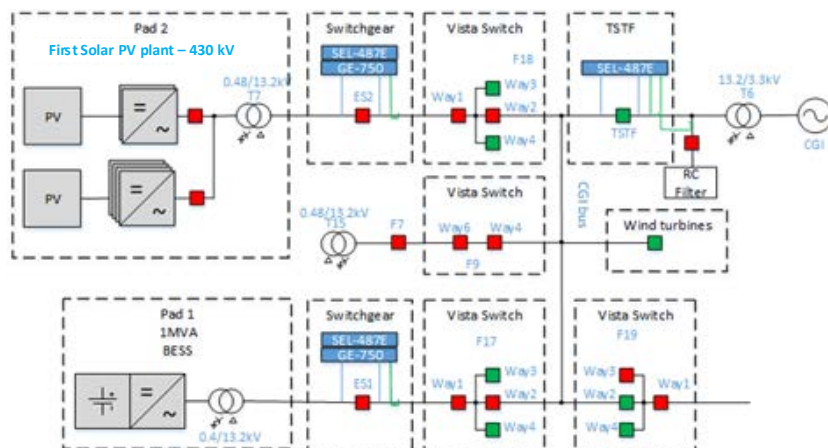


**Figure 84. Test setup for the black start of the PV plant with BESS**

This experiment was conducted with the BESS set in two different voltage control modes:

- Soft black start: The BESS inverter ramped its voltage from zero to the full level during a 200-ms time period to minimize the inrush current in the PV plant transformer, which was connected to the circuit during the whole process
- Hard start: The PV plant transformer was not connected until the BESS inverter reached full voltage, and then the switch was closed to energize the transformer with the full inrush current.

### 11.2.1 Soft Black Start

Results of the soft black start for the 430-kW PV plant using the 1-MW/1-MWh BESS as a black-start resource are shown in Figure 85. The SMA inverter of the BESS increased its voltage with a 200-ms ramp to minimize the inrush currents in the PV plant transformer, as shown in Figure 86. The peak BESS current during the start was only at 5% of the inverter rated current. After the transformer was energized, the initialization timers was triggered in the inverters (60 s for the 45-kW inverters and 80 s for the125-kW inverters). Then the PV plant ramped it power production to the maximum power point (MPP) level. The overall black-start process took approximately 130 s.

65
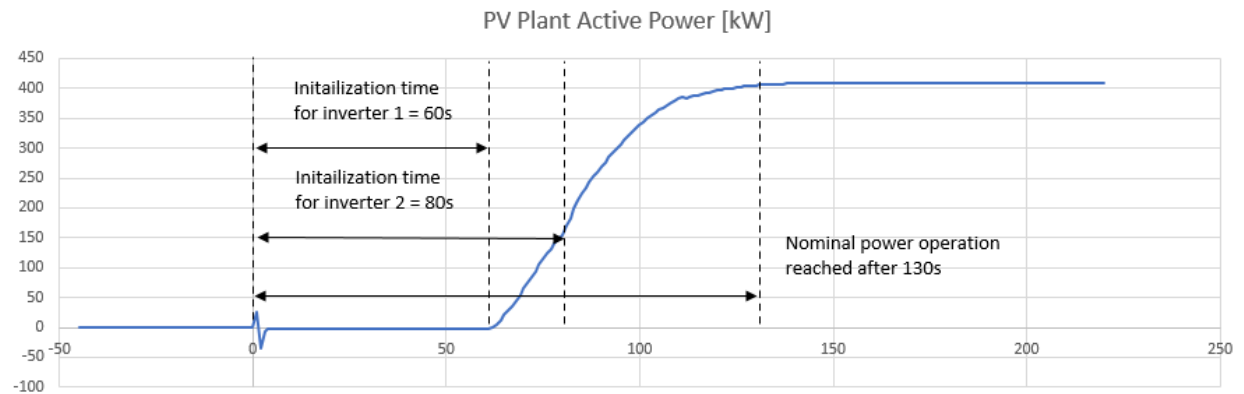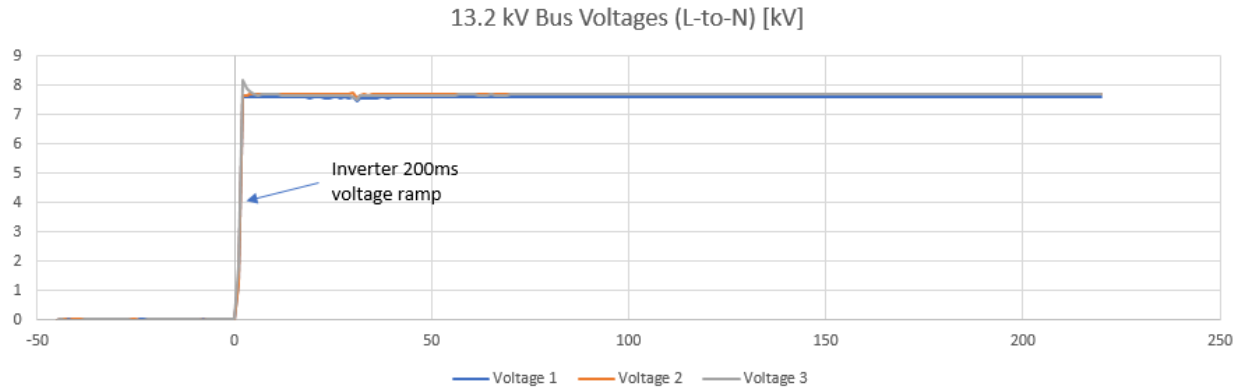
**Figure 85. Soft black start of the PV system using the BESS**
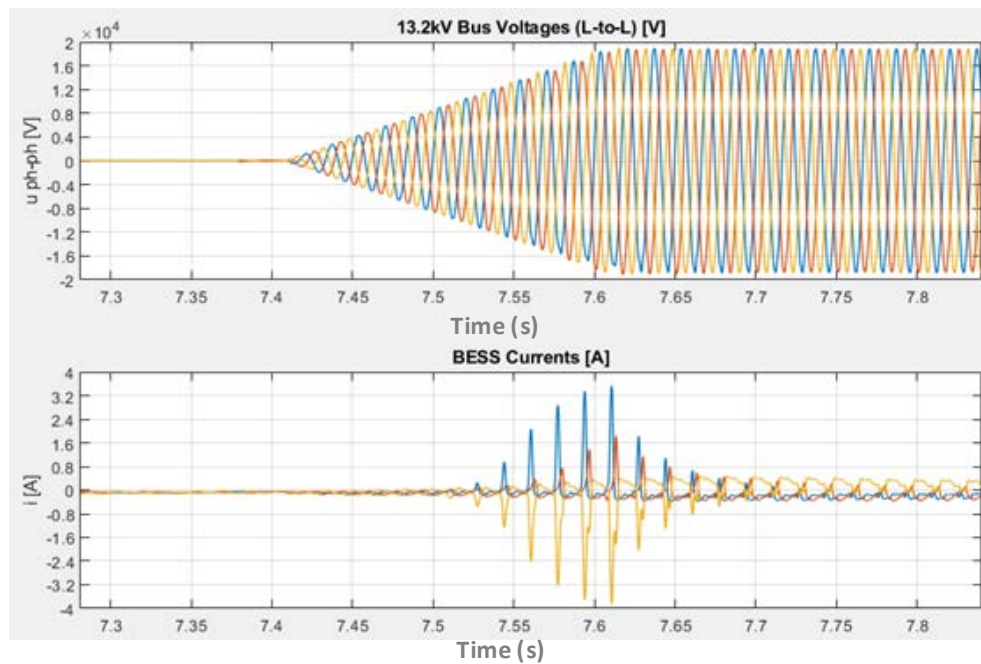


**Figure 86. (Top) Soft black start of the PV system using the BESS and (bottom) magnified view of the voltage ramping by the inverter. The voltage ramp was performed within 200 ms.**

66

### 11.2.2 Hard Black Start

Results of the hard black start are shown in Figure 87. In this case, the inverter first set the voltage in the 13.2-kV collector system with the transformer breaker open. At t=70 s, the breaker of the PV plant transformer was closed. This resulted in a much higher inrush current and voltage transient, as shown in Figure 88; however, even this high inrush current is still within the limits of the BESS inverter. After the transformer was energized, the initialization timers triggered the inverter controls. The inverters came online, and the plant was fully operational within approximately 320 s after the black start.
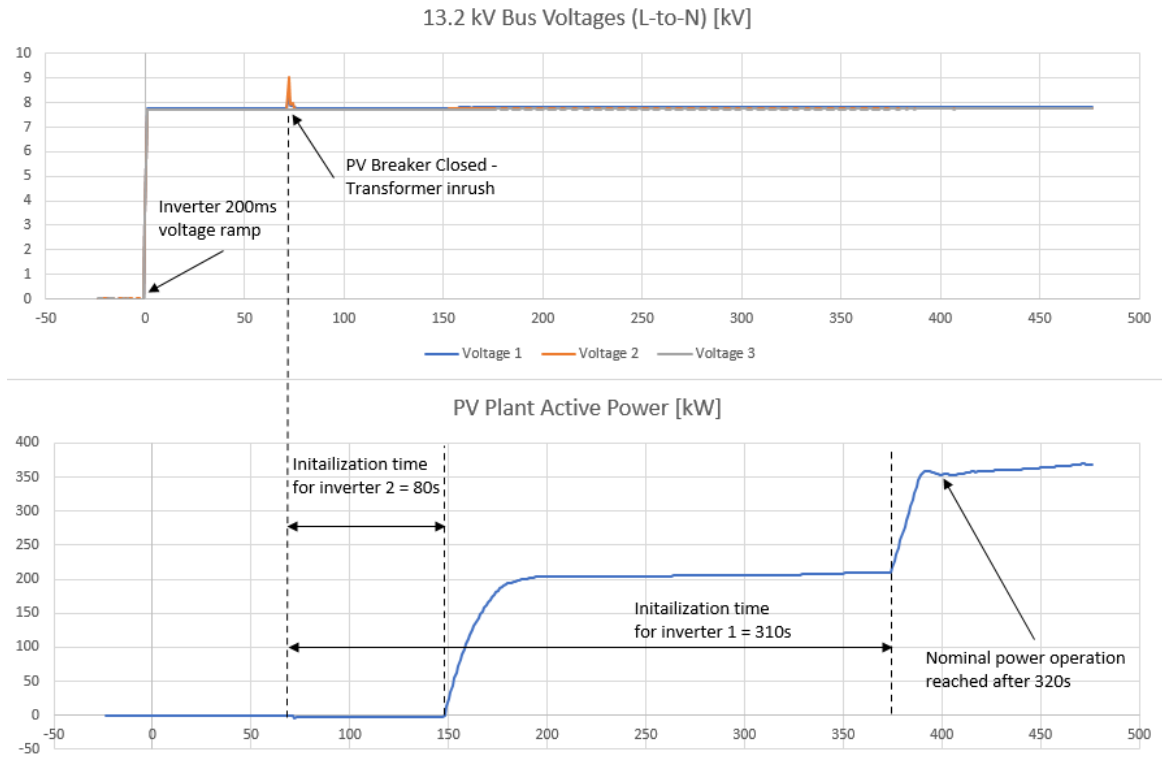


**Figure 87. Hard black start of the PV system by closing the PV breaker on the live voltage bus**
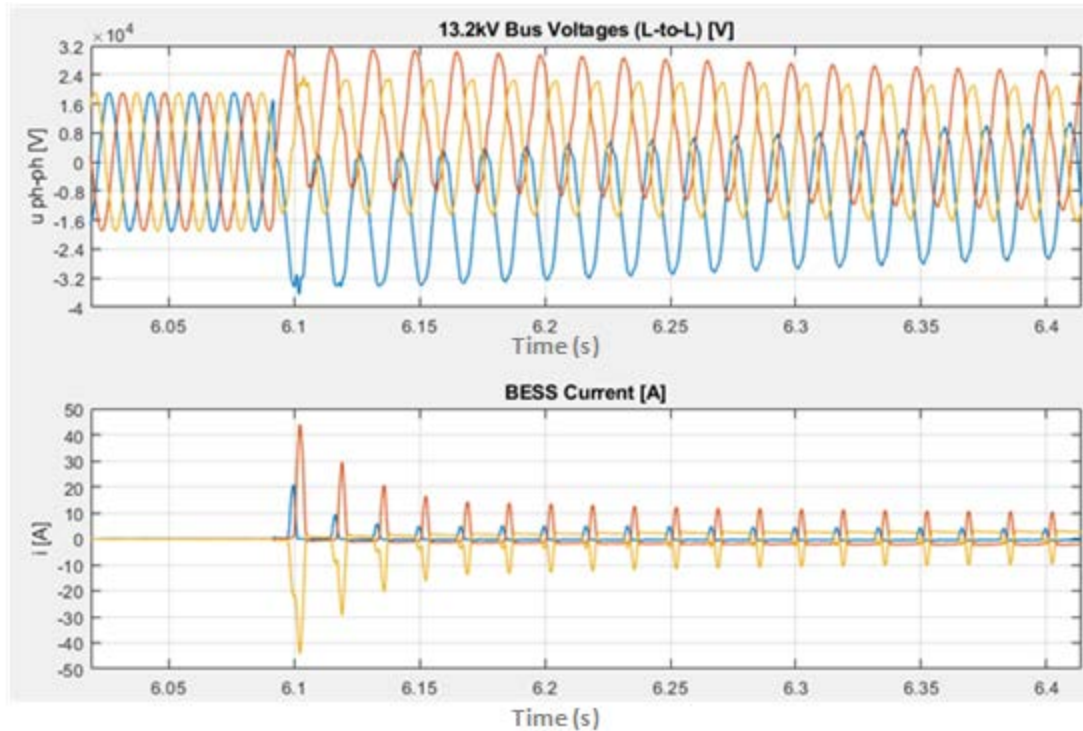
**Figure 88. Hard black start of the PV system by closing the PV breaker on the live voltage bus—magnified view of the voltage and current transient**

## 11.3 Other Black-Start Configurations

The system restoration is a gradual process based on priorities as defined in restoration plans until the totality of customers are re-energized. The system restoration strategies depend on the type of systems being restored. For the bulk transmission system, the restoration can be in the form of re-energizing the full network with black-start units before synchronizing the remaining generators, or it can be in the form of island-by-island restoration with eventual interconnections between them. Mixed strategies are also possible.

On lower voltage distribution levels, the system restoration is essentially a network reconfiguration exercise. The distribution system operators try to transfer the maximum possible loads from faulted feeders to healthy ones; however, in large-scale blackouts, the distribution system might stay in the black condition until the bulk system is restored. From this perspective, the ability of DERs and energy storage systems to provide black start and to participate in restoration schemes can become a critical component of a future resilient grid.

A typical restoration plan for a bulk power system includes the following essential steps:

- System status identification: establishing blackout boundaries and locations with respect to critical loads, the status of circuit breakers, the capacity of available black start-units, etc.
- Starting at least one black-start unit to supply critical loads, such as nuclear or large thermal power plants
- Progressive restoration: providing the step-by-step supply of other loads, avoiding over- and undervoltage conditions.

68

A restoration concept involving distributed generation can be developed if the distributed resources are required to have black-start grid-forming capabilities to form islands with critical loads (Figure 89). In some cases, distribution network reinforcement might be needed depending on the distributed resource locations because more sectionalizing switches would be necessary for feeder reconfiguration during a black start. The availability of distribution management systems and communication networks for distributed generation is also important for successful restoration services.

Another important aspect of black start and grid forming by a distributed inverter-coupled system is power quality issues because interfacing converters generate voltage and current harmonics transmitted to the loads. Harmonic interactions between voltage source inverters and loads can vary significantly depending on the loading levels of the inverters, the types of distribution networks (overhead or underground), and the types of loads (resistive or reactive). In some cases, additional filtering must be installed with black-start-capable inverter units to ensure a reliable restoration procedure because power supplies and auxiliary systems of some loads might fail to start, thus jeopardizing the whole black-start process. Inverter filters are normally designed for specific grid impedance levels, and network reconfiguration during black start might cause undesirable consequences in the form of harmonic resonances or increased distortions.
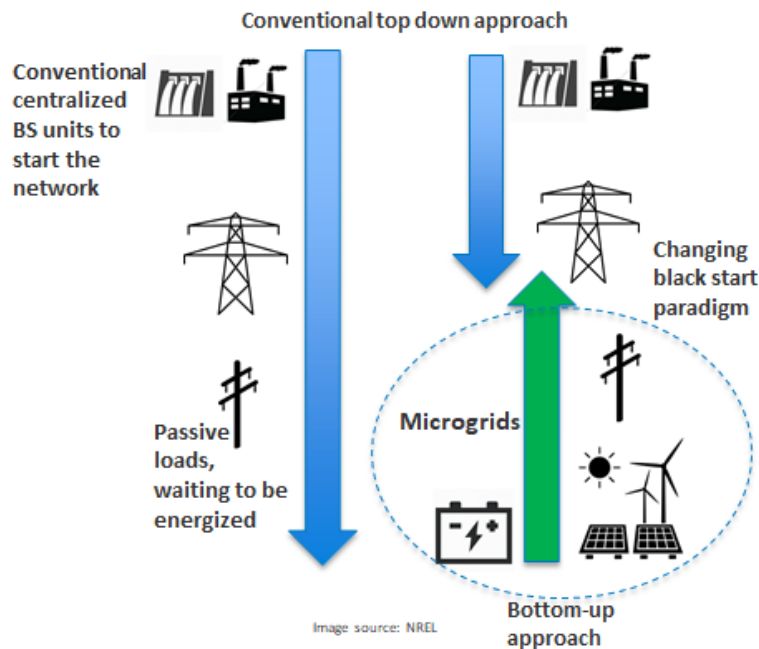


**Figure 89. New black-start paradigm**

The black-start capability by conventional generators requires first energizing the auxiliary equipment to generate the initial voltage, which is normally characterized by long startup times because of slow thermal or hydromechanical dynamics; however, voltage source converters of modern variable-speed wind turbine generators and PV and energy storage inverters, once equipped with black-start capability, can provide fast services for power system restoration. Several configurations of PV-plus-storage systems can serve as a kick-starter for larger conventional plants that are, in turn, designated as black-start resources. This can be achieved

69

either by PV-plus-storage plants that are colocated with conventional plants or by PV-plus-storage plants that are not located in close proximity of a conventional plant, as shown in Figure 90. In addition, a PV-plus-storage plant can be configured as a fully functional black-start resource. The number of PV-plus-storage plants can also be controlled to provide a collective black-start resource.
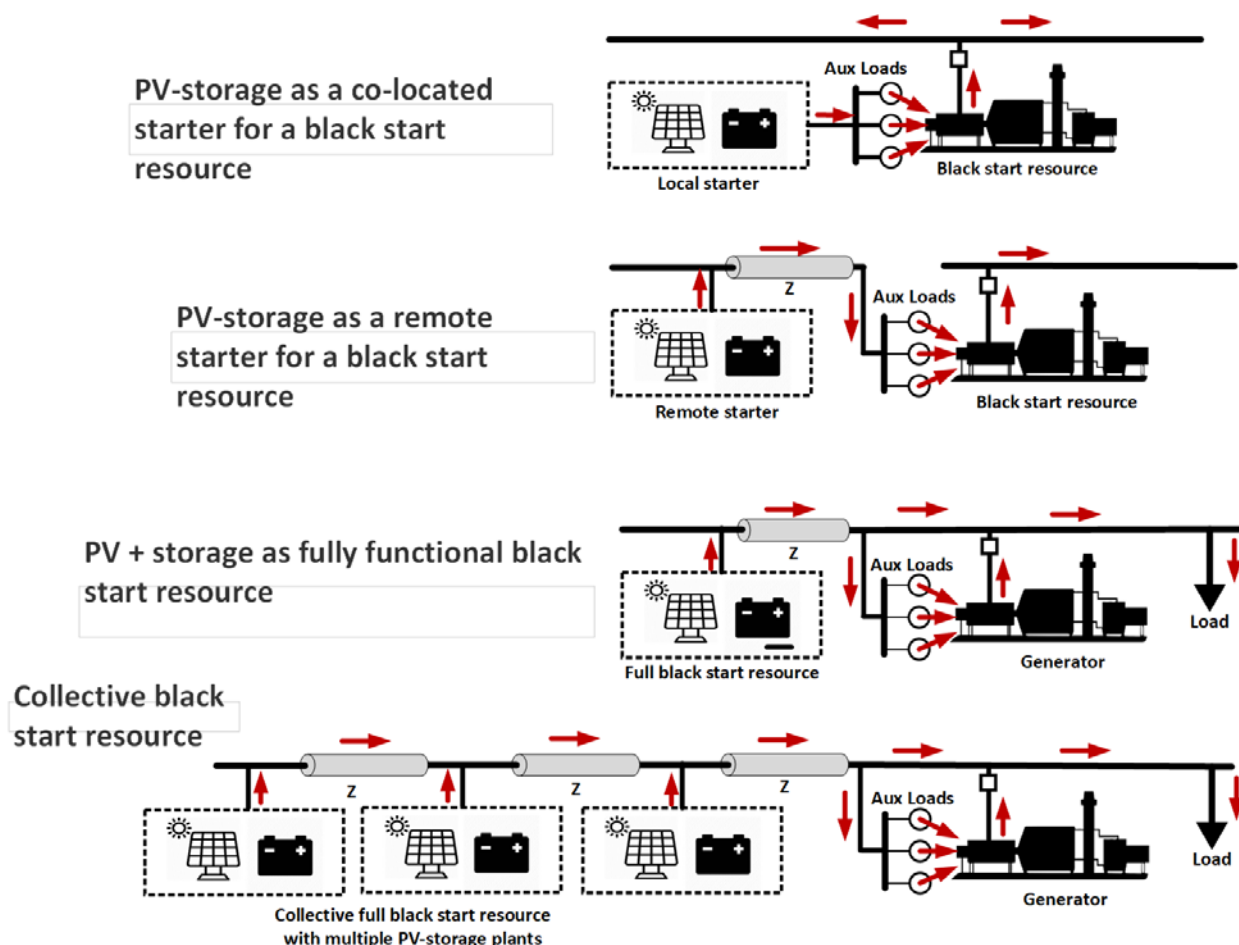


**Figure 90. Configurations of integrated PV-plus-storage plants as black-start resource for conventional plants**

A PV-plus-storage black-start resource that directly energizes high- and medium-voltage transmission lines must be capable of managing the charging currents associated with energizing unloaded transmission lines and must provide inrush current when energizing transformers. Smaller black-start resources that might need to provide cranking power for larger plants might also need to handle the inrush currents associated with the cold-load pickup of auxiliary inductive loads, such as motors at the large plants. For systems similar to the one shown in Figure 91, one main challenge during black start is to provide inrush current when energizing transformers and feeders as well as starting auxiliary motors in power plants; therefore, grid-forming inverters used in a black start need to provide necessary inrush currents. This can be achieved by oversizing the inverters for inrush currents, equipping motors with soft-starters or variable frequency drives, or employing soft-starting solutions in grid-forming inverters.

70
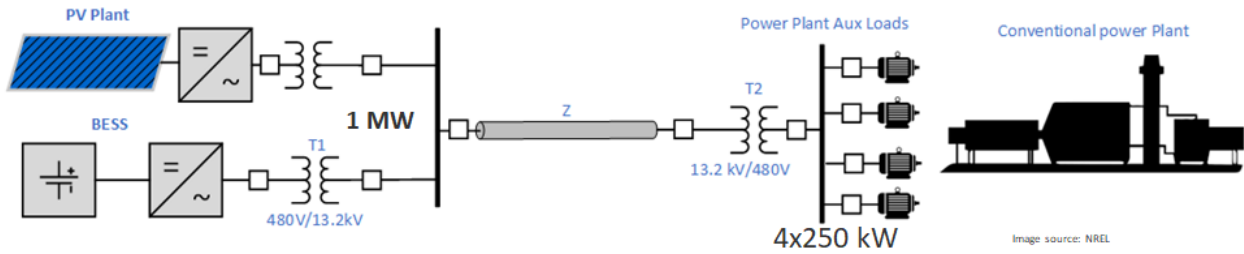
**Figure 91. PV-plus-storage plant to start auxiliary loads in a thermal power plant**

Simulation results for the case with a 1-MW grid-forming PV-BESS system operating at constant frequency starting four 250-kW auxiliary motors are shown in Figure 92. One motor starts at a time, and large inrush current is needed for each motor to start. The level of such inrush current exceeds the rated current for the 1-MW PV-plus-storage plant, even during the start of the first motor, making the black start of the whole plant impossible because the inverters will either trip off because of the overcurrent protection or operate in current-limiting mode, which will make the black start impossible because of voltage collapse.
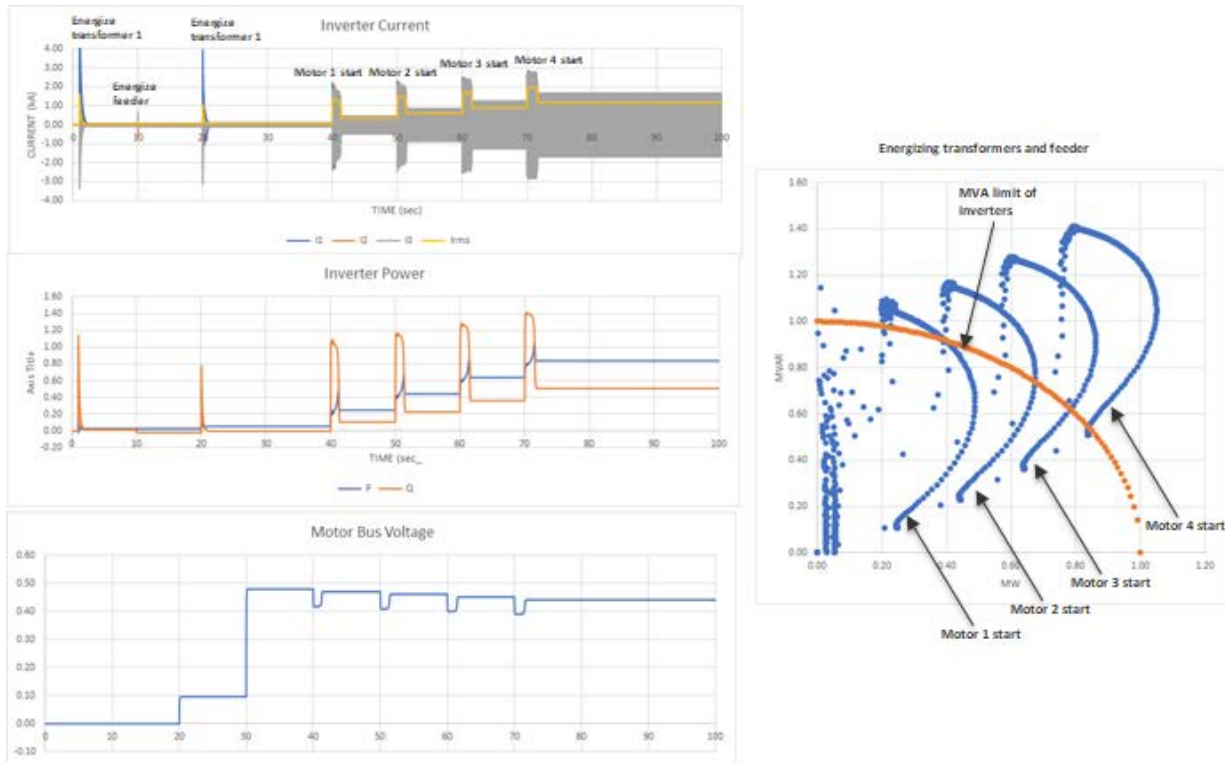


**Figure 92. Consecutive starts of auxiliary motors**

Another method for a soft start is described in Section 11.2, using voltage ramping control for the grid-forming inverter to minimize the inrush currents when energizing the PV pant transformer. One advanced soft-start control method possible for grid-forming voltage source inverters can be based on variable-frequency and variable-voltage operation during a black start. Grid-forming inverters can start at zero voltage and very low frequency, and then increase both the voltage and frequency to nominal levels at a constant volt/Hertz ratio to avoid both inrush current and possible transformer saturation. Simulation results for such advanced "variable-

71

frequency-drive-like" functionality for the grid-forming inverter is shown in Figure 93. The inverter is controlled to ramp up both voltage and frequency during the initial stage of the transformer energization and startup of all four motors without exceeding the current limit during the entire startup process.
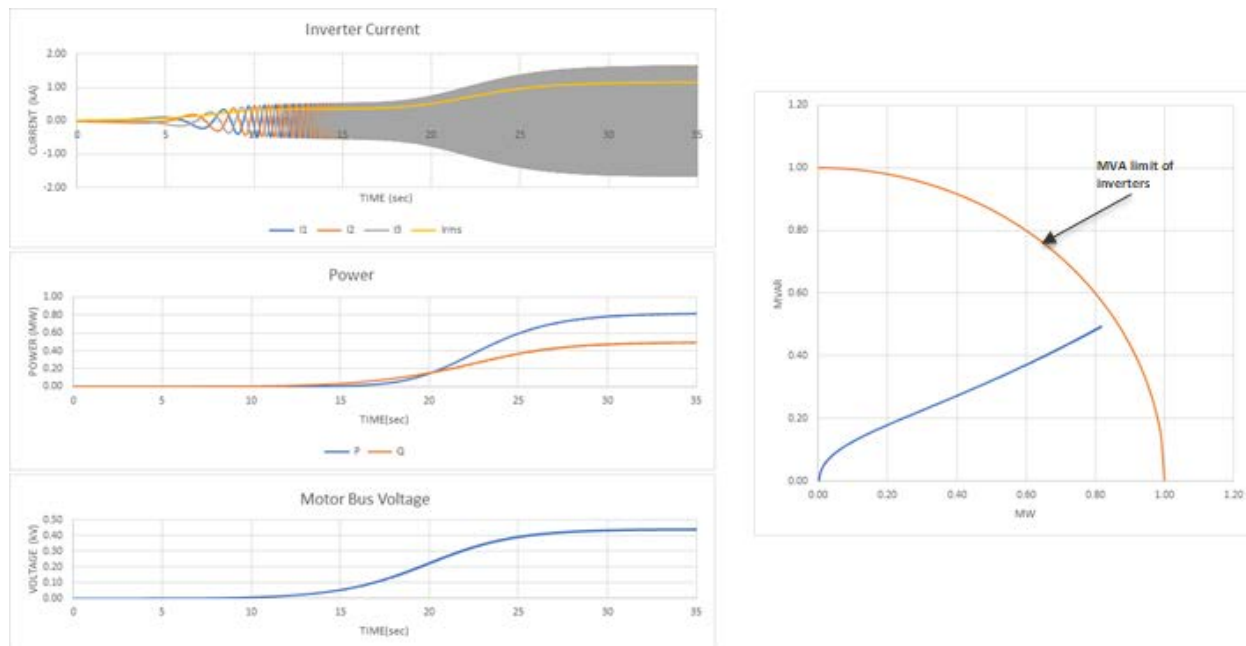


**Figure 93. Constant volt/Hertz startup**

Today's and future restoration strategies should align with the changing network paradigm. Modern grid-forming inverters can contribute to a black start/restoration with superior reactive power capabilities compared to conventional synchronous generators; however, the inherent inverter current limit is one of the most important factors for black-start applications.

Recommendations for future grid-forming and black-start studies using PV-plus-storage at NREL's Flatirons Campus might include:

- Fault performance of grid-forming inverters—needs to be robust and standardized
- Robust seamless transition between grid-forming and grid-following modes
- Continued impedance characterization of grid-forming inverters
- Analysis of grid stability impacts of grid forming
- Validated grid-forming inverter models are needed for various renewable and storage technologies for successful black-start studies.
- At-scale PHIL testing of black-start-capable renewable resources is an important tool to discover potential issues, test mitigating solutions, and validate models.

# 12 Solar Forecast

In 2019, a solar resource forecasting was implemented for NREL's Flatirons Campus by First Solar that produces a PV forecast using a methodology based on National Oceanic and Atmospheric Administration satellite data. The forecast data are being updated on a secure NREL File Transfer Protocol server. Currently, several months of forecast data are available, and more are coming, so long-term statistics on the accuracy and persistence of the solar forecast and its impact on PV-plus-storage system operation for different market scenarios can be evaluated in the future. All components of solar radiation—including global horizontal irradiance (GHI), direct normal irradiance, and diffuse horizontal irradiance—along with ambient temperature are provided as part of an hour-ahead, day-ahead, and 7-day-ahead forecast.

The estimated active power output of the 430-kW PV plant is calculated from forecast data using various performance models of PV arrays, such as a widely accepted model that has been developed and is continuously updated by Sandia National Laboratories [12]. A similar approach was used in [13] for estimating the power production of the NREL 1-MW PV plant using irradiance data. Examples of comparisons between forecasted irradiance time series and estimated power are shown in the following figures. Figure 94 shows the correlation between actual measured GHI at the NREL site and the hour-ahead forecast of GHI for a time period of 2 weeks of operation, and Figure 95 shows the recorded temperature at the site used in the power calculations. There is a strong positive correlation between the measured and the forecasted GHI, as shown in Figure 94. The accuracy of the estimated power time series compared to the actual measured power is shown in Figure 96. The values of the absolute errors in the hourly power production forecasts are quite high, reaching +138 W and -211 kW during certain days. NREL is currently working with First Solar and a forecast provider to understand the nature of such inaccuracies. The comparison between the estimated and the measured hourly power profiles is shown in Figure 96 for a whole week of operation.
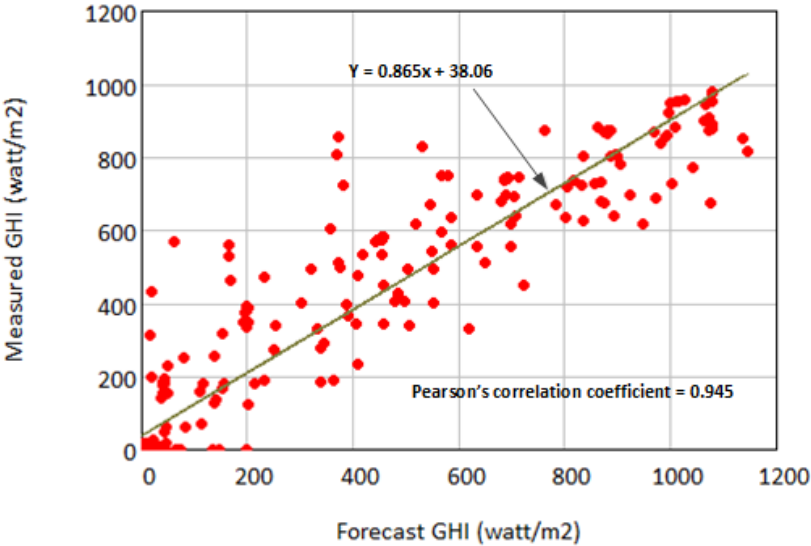


**Figure 94. Correlation between the measured hourly and the forecasted GHI**
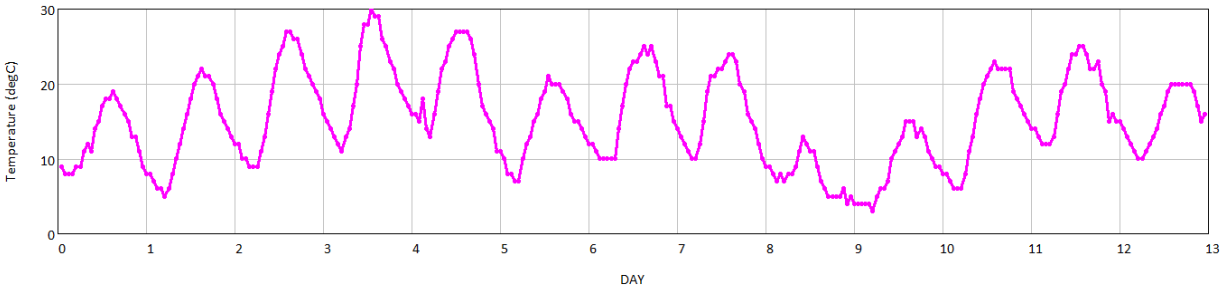
**Figure 95. Measured hourly average site temperature during a two-week period**
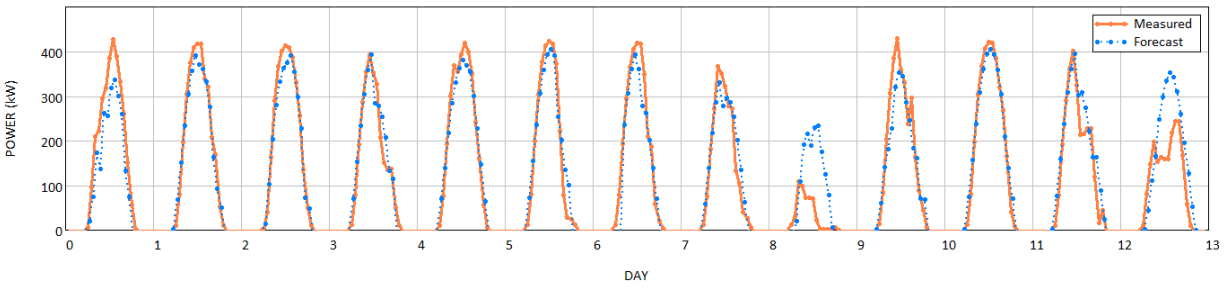


**Figure 96. Example of the forecasted and the measured PV plant hourly power production during 2 weeks of operation**
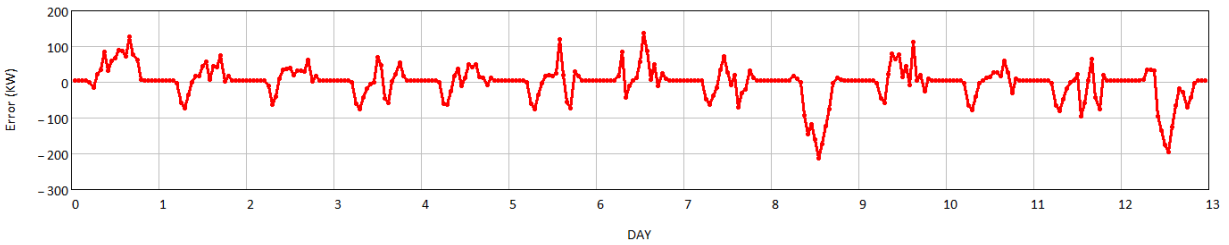


**Figure 97. Absolute error in the estimated power using an hour-ahead forecast**
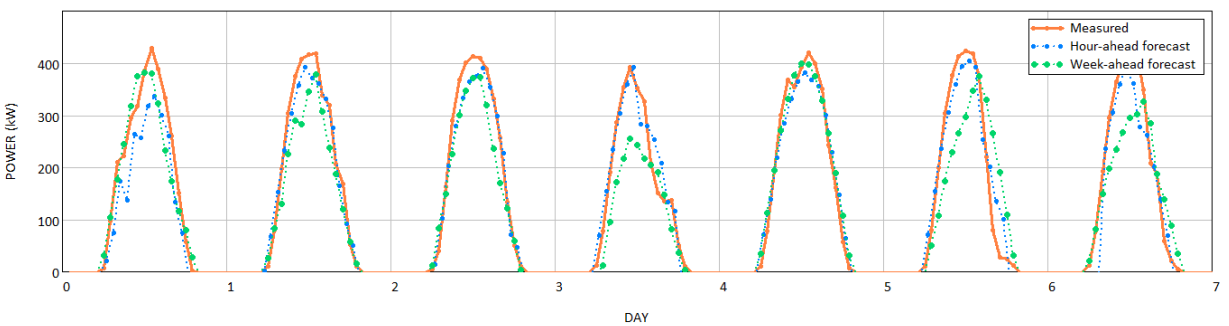


**Figure 98. Example comparison of an hour-ahead and a week-ahead forecast**

74

# 13 Accurate Method for Real-Time Power Reserve Estimation for Utility-Scale PV Power Plant

## 13.1 Importance of Accurate Estimation of Available PV Power

All around the world, system operators and utilities are continually adapting their grid codes, interconnection requirements, operational practices, and market mechanisms to make the integration of shares of fast-growing variable renewable generation both reliable and economic [4]. As power systems continue to evolve, the Federal Energy Regulatory Commission noted that there is an increasing need for a refined understanding of the services necessary to maintain a reliable and efficient system. In orders 755 and 784, the Federal Energy Regulatory Commission required improving the mechanisms by which frequency regulation service is procured and enabling compensation by fast-response resources, such as energy storage. The NERC Integration of Variable Generation Task Force made several recommendations for requirements for variable generators (including solar) to provide their share of grid support, including active power control capabilities [16], [17]. Similar requirements for renewable energy plants have been introduced in Europe at both the transmission and distribution levels [18], [19]. In 2018, Federal Energy Regulatory Commission Order No. 842 amended the *pro forma* interconnection agreements to include certain operating requirements, including maximum droop and deadband parameters in addition to sustained response provisions [23].

NERC's standard BAL-003-1, Frequency Response and Frequency Bias Setting, establishes target contingency protection criteria for each North American interconnection and individual balancing authorities within interconnections [24]. Balancing authorities need to meet a minimum frequency response obligation, so the generating resources that are operated in a mode and range to meet their frequency response obligation need to have adequate headroom to respond to frequency transients and load-frequency control set points. Establishing this headroom is not a problem for the conventional generation fleet, but the varying nature of solar and wind generation makes it challenging to set and maintain adequate headroom for these varying resources. In general, all system operators have processes and procedures in place to ensure grid reliability by monitoring market participant operation. For example, provisions of the CAISO tariff [28] set penalties for deviations from the dispatch and the regulation capacity for market participants that fail to comply. The permitted area of variation for the performance requirements of resources used for various purposes is provided in the CAISO tariff [28]. The tolerance band is expressed in terms of energy (MWh) for generating units and imports from external dynamic system resources for each settlement interval, and it equals the greater of the absolute value calculated using either of the following methods: (1) 5 MW divided by the number of settlement intervals per settlement period; or (2) 3% of the relevant generating unit's maximum output ($P_{max}$), as registered in the master file, divided by the number of settlement intervals per settlement period.

This CAISO tariff and similar requirements from other system operators imply that the accurate real-time estimation of available maximum power from a curtailed PV plant is important for avoiding excessive penalty payments if utility-scale PV plants become market participants for energy and various reliability services related to active power controls.

A typical modern utility-scale PV power plant is a complex system of large PV arrays and multiple power electronic inverters, and it can contribute to mitigating the impacts on grid stability and reliability through sophisticated, automatic "grid-friendly" controls [28]. To provide active power reserves (or a headroom margin) for up-regulation that can be automatically dispatched as needed, a PV plant needs to operate below its MPP; however, evaluating that MPP in curtailed mode is not a trivial task, especially for large PV power plants during various types of variable conditions caused by clouds. One paper [29] proposed an experimentally validated maximum power point estimation (MPPE) method, which operates in real time using irradiance and cell temperature measurements to ensure that sufficient reserve power is available. Another paper [30] proposes an advanced real-time MPP estimation algorithm by applying curve fitting on voltage and current measurements obtained during inverter operation. Some previously proposed MPPE methods used offline prediction and employed regression analysis or neural networks [31], [32]. These methods seem to be accurate but might require excessive processing power. Others have proposed methods for real-time calculation ([33]–[35]) by making assumptions that reduce the accuracy of the PV model or, in some cases, require knowledge that is not typically available on PV module data sheets [33], [36]. Another important limitation of MPPE estimation methods is that modifications are needed based on inverter types and topologies. For example, in single-stage inverters (no DC/DC conversion), the power reserve capability can be achieved by inverter control modifications [30]–[37]; however, in two-stage systems (inverter and DC/DC converter), the DC/DC converter control needs to be modified [38]. This makes the use of maximum peak power estimation for curtailed PV systems challenging and highly dependent on inverter make and topology, the types of modules used in PV plants, and accurate knowledge of the inverter and PV module parameters.

The variability of PV output in the regulation reserve time frame among various arrays within a large-scale (~50-MW) PV plant in the southwestern United States was explored in [39]. Although the distributions of changes in aggregate power output throughout all timescales considered were clustered around a strong peak at zero, the distributions at all timescales exhibited significant instances of higher magnitude ramps in the tails of the histograms. The results achieved in [39] were very important because the method presented in this report was also tested using the data from the same PV power plant [50].

In 2015, a demonstration project was conducted in the U.S. territory of Puerto Rico using a 20-MW grid-connected PV power plant [40]. This plant was controlled to provide different types of reliability services to the island's grid, including various types of active power controls. Testing on this plant provided "real-world" data on levels of uncertainty that can be introduced by traditional MPPE estimation methods based on irradiance and temperature measurements as well as inverter I-V characteristics. One example of such uncertainty is shown in Figure 99 during operation when the PV plant was responding to an AGC signal sent from the system operator. The AGC system assumed that there was still some available headroom for up-regulation because its evaluation was based on the available plant power value that was communicated by the PPC; however, the calculated available power was overly optimistic, and the inverters were not able to produce that much power because they were already operating at the maximum peak power point.
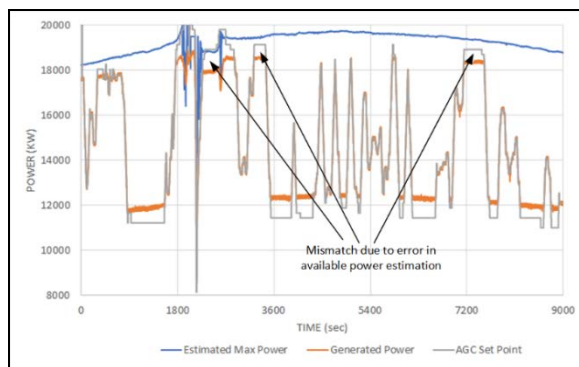
**Figure 99. Example of inaccurate maximum peak power estimation**
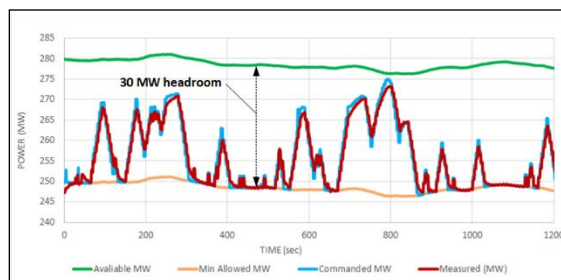


**Figure 100. Example of maximum peak power estimation using a single reference inverter**

A different method for estimating the maximum power was used during a demonstration test of a 300-MW PV power plant in California [4]. In this case, a single 4-MVA inverter was taken from the AGC scheme and set to operate at the power level determined by its MPPT algorithm. The measured AC power of this inverter was used as an indicator of available power for the other 79 inverters (80 inverters total), so the plant was able to operate with a fixed 30-MW headroom (Figure 100). This method also has inherent uncertainties because it assumes uniform solar irradiation conditions across the whole 300-MW plant. Fortunately, cloud conditions were favorable for this method to be acceptable because there was a clear sky above the plant during most of the day of testing.

The method proposed in this project is also based on using dedicated reference inverters within a curtailed PV power plant for estimating the maximum available power; however, it is based on using multiple reference inverters to achieve high levels of real-time, maximum peak power estimation under extreme variability conditions. The method was first validated using data from an approximately 50-MW PV plant in the western United States [50], and it showed a high level of accuracy for large utility-scale PV plants. In this report, the method was further improved to provide accurate estimation of available peak power for smaller distributed PV plants that have larger per-unit magnitudes of fast changes in plant outputs compared to larger utility-scale plants because of smaller footprints.

The concept of active power reserve estimation is explained in Figure 101 for a curtailed PV plant. The estimated available headroom should be accurate to ensure that the plant can avoid penalties for not meeting its dispatch and regulation capacity, and deviations are within tolerance bands. For example, if a curtailed plant is requested to release its estimated spinning reserve, then care must be taken to ensure that the PV plant can reach the commanded power set point with a high level of precision.
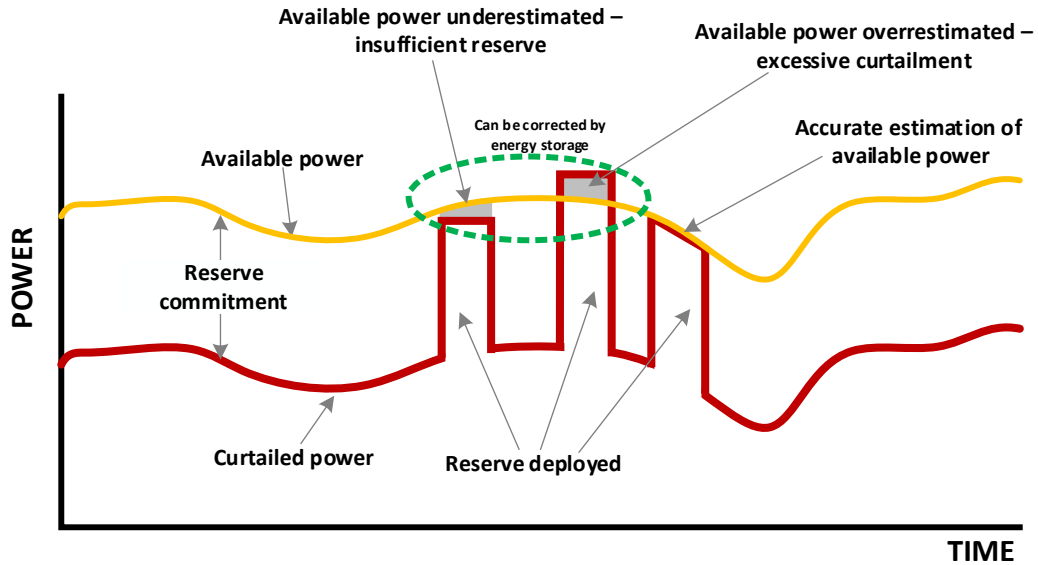
**Figure 101. Estimation of available power for a PV power plant**

## 13.2 Proposed Method

For utility-scale PV power plants to be able to maintain the desired regulation range or spinning reserve levels, the plant controller must be able to estimate the available aggregate peak power that all the plant's inverters can produce at any point in time. The available power is normally estimated by an algorithm that considers solar irradiation, the PV modules' I-V characteristics and temperatures, inverter efficiencies, etc.; however, this method has many uncertainties, among them a dependence on the availability of accurate system models, and it does not account for other factors, such as panel soiling because of dust. The proposed method can determine the available peak power of the PV plant and maintain the desired reserves with high levels of accuracy without the use of external sensors or devices. The existing plant hardware and controls can perform this task after the addition of the new optimized control algorithm in the PPC software.

Under clear-sky conditions, a single PV inverter can be used as a reference for the whole plant to determine the available power at any point in time (Figure 102, upper graph); however, under variable cloud-cover conditions, a single inverter method will not be accurate enough for large PV power plants. Instead, we propose a concept that can accurately allocate reserves for PV power plants by:

- Creating dynamic virtual control zones in the PV plant
- Determining which PV inverter will serve as a reference by operating at MPP
- Determining the optimal dispatch interval for the reference MPP inverters based on the rate of change of power in each zone (indicator of cloud movement)
- Determining the optimized combinations of curtailment set points for participating inverters in each zone for maximum aggregate inverter efficiency (or minimum electric losses in the plant) for every control interval.

78

The idea for this method is shown in the lower graph in Figure 102. The plant controller allocates virtual dynamic control zones consisting of two or more inverters depending on the cloud conditions over the plant. Then, a single inverter in each virtual group is operated at MPP and is used as a reference for determining the maximum available power for the zone so that appropriate curtailment set points can be sent to all participating inverters within that zone. After a certain time interval, the process is repeated, ensuring accurate reserve allocation by the whole plant and avoiding excess curtailments.

In this report, we use the following abbreviations:

- $N_{total}$: total number of inverters in a PV power plant
- $N_{zones}$: number of control zones (same as the number of reference inverters, $N_{ref}$)
- $N_{inv} = \frac{N_{total}}{N_{zones}}$: number of inverters in each control zone
- $P_{total.max}$: total power production of the plant when all inverters are operating at MPP
- $P_{max,i}$: power production of zone $i$ when all inverters in the zone are operating at MPP
- $P_{mppt,i}$: power production by a single inverter operating at MPP in zone $i$.



**Figure 102. Large PV power plant divided into control zones during cloud conditions**

The estimated maximum available power from the plant using the instantaneous power produced by single MPPT inverters in each zone (blue inverters shown in Figure 102) is obtained by:

$$P_{total.max}^{est} = \sum_{i=1}^{N_{zones}} N_{inv} \cdot P_{mppt,i} \qquad (13.1)$$

The plant curtailment set point as a percentage of the estimated maximum available power from the plant is determined by:

$$P_{total}^{set} = (1 - \Delta P) \cdot P_{total.max}^{est} \qquad (13.2)$$

where $\Delta P$ (in per units) is a curtailment set point. For example, $\Delta P = 0.1$ means that the plant is expected to operate with a 10% active power reserve margin or at 90% of $P_{total}^{set}$. The power set points to all individual inverters in zone $i$ that are participating in the curtailment scheme (orange inverters in Figure 102) can then be calculated:

$$P_{inv,i} = P_{mppt,i} \cdot \frac{N_{inv}(1 - \Delta P) - 1}{N_{inv} - 1} \qquad (13.3)$$

Therefore, the power production of zone $i$ can be calculated as:

$$P_{zone,i} = P_{mppt,i} + (N_{inv} - 1) \cdot P_{inv,i} \qquad (13.4)$$

And the total power production of the plant operating with the curtailment set point, $\Delta P$, is:

$$P_{plant} = \sum_{i=1}^{N_{zones}} P_{zone,i} = [N_{inv}(1 - \Delta P) - 1] \times \sum_{i=1}^{N_{zones}} P_{mppt,i} \qquad (13.5)$$

As part of this project, the validity of this method for utility-scale PV power plants was demonstrated by using field measurement data from an approximate 50-MW PV plant in the western United States The results of such analysis were published in a separate NREL report in 2019 [51]. In this report, we explore the possibility of using the same method when applied to smaller distributed PV power plants (similar to the 430-kW plant at NREL's Flatirons Campus) that are exposed to faster output power ramps caused by moving clouds because of the smaller footprint of such plants compared to large utility-scale projects. The accurate estimation of available power in PV plants that happened to be curtailed for any reason is also important for integrated PV-plus-storage operation so that the plant controller can have precise information on the available spinning reserve from PV and can dispatch energy storage accordingly.

## 13.3 Implementation of Reserve Estimation Method on the 430-kW PV Power Plant

In this work, we examined the applicability of the proposed method using PV output power data from different arrays in a single utility-scale 430-kW PV plant at NREL. The plant consists of 6 individual inverters, two rated at 125 kW and four rated at 45 kW. We used 1-s power data from each individual inverter collected from the plant, allowing us to analyze the accuracy of the proposed method under different resource variability scenarios. Example production profiles for the plant are shown in Figure 103 for 2 days of operation with different variability patterns for the whole plant and individual inverters (the output of the 45-kW inverters is shown in aggregate). The 1-s changes in total plant power are shown in Figure 104, indicating the

magnitudes of the 1-s variability, which is quite high compared to larger utility-scale solar power plants, as observed in the analysis conducted in [4] and [51]. The maximum 1-s change for this 430-kW plant can reach more than ±10% of capacity per second.
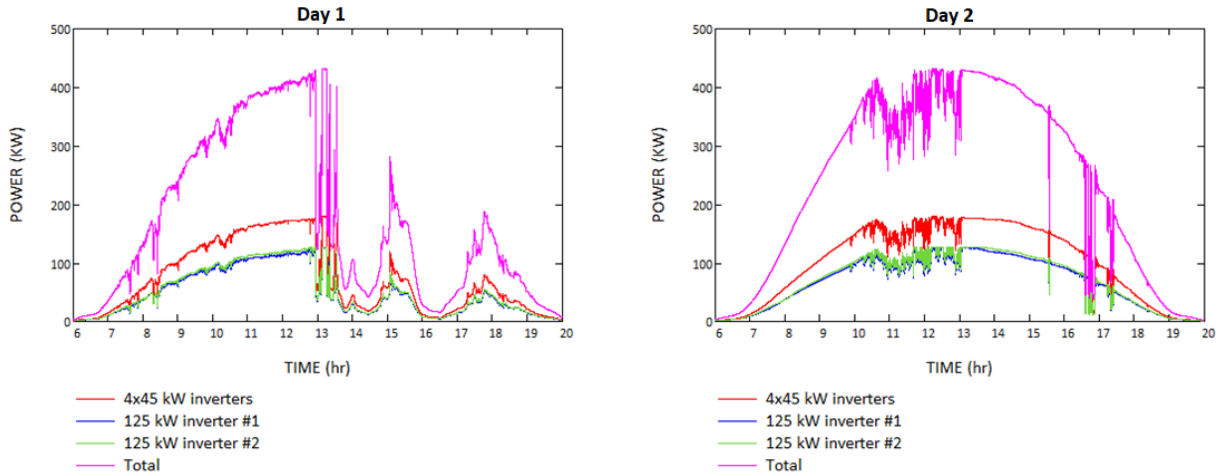


**Figure 103. Examples of 430-kW plant daily production profiles**
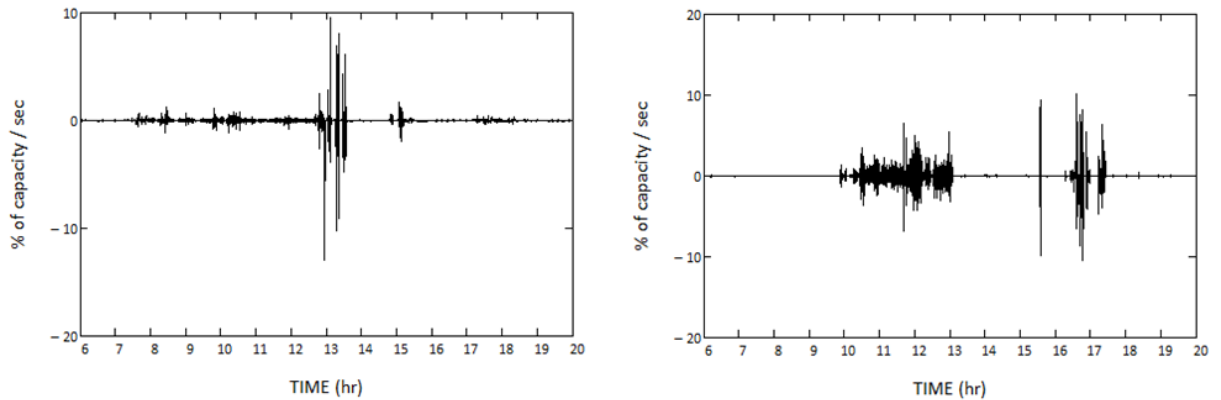


**Figure 104. Measured 1-s total power ramps**

Because the 430-kW PV plant has only 6 string inverters, the evaluation of the available power estimation method was done with only one 125-kW reference inverter, unlike up to the 48 reference inverters used in the larger plant [50].

We evaluated the accuracy of the method using a simple equation for calculating the available total plant power derived from the real-time power output of a single 125-kW operating at MPP:

$$P_{est}(t) = P_{125}(t) \cdot K_{scale} \tag{13.5}$$

where $P_{est}(t)$ is the estimated maximum total plant power [kW], $P_{125}(t)$ is the measured output power of a single 125-kW inverter operating at MPP [kW], and $K_{scale}$ is a constant scaling coefficient defined as 430 kW / 125 kW = 3.44.

After applying the active power estimation method described in the previous section (henceforth, we refer to it as the "simple" method), a larger than expected estimation error was observed,

81

especially during the periods of high variability, as shown in Figure 105 and Figure 106. For comparison, the same simple method applied to the 50-MW plant produced estimation errors within ±1.5% of the rated plant capacity. For this much smaller 430-kW plant, however, the estimation errors exceeded ±10% of rated plant capacity, which might not be acceptable for the accurate evaluation of available spinning reserves from distributed PV plants.
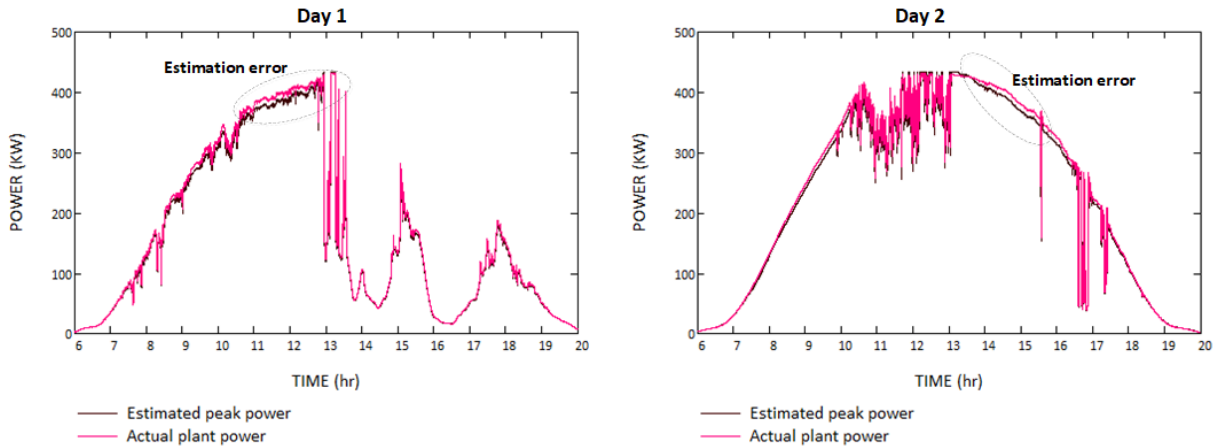


**Figure 105. Comparison of estimated and measured power using simple method**
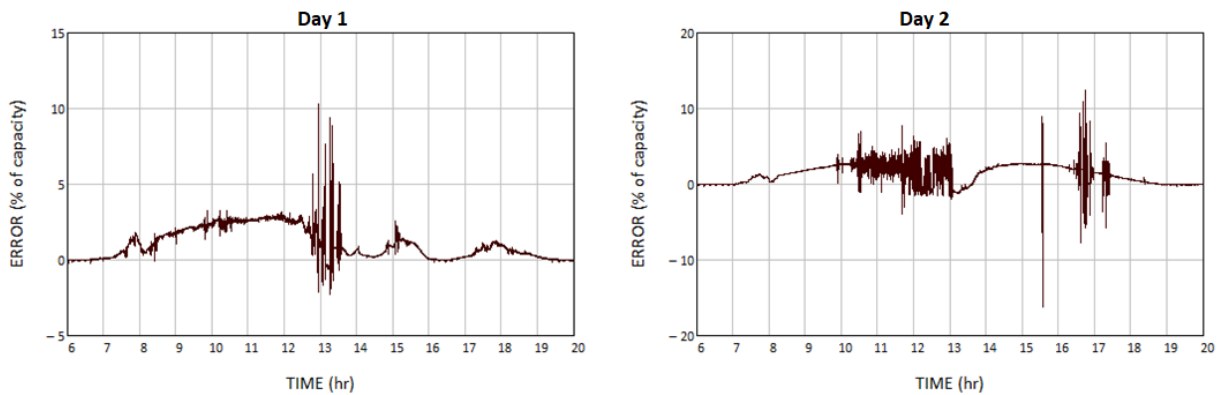


**Figure 106. Peak power estimation error**

This error was caused by using a constant value for the $K_{scale}$ scaling coefficient, which did not account for fast changes in power across the various sections of the plant because of its small footprint. In fact, it was observed from further analysis that the estimation error had a strong linear correlation with the 1-s changes in power output of the reference inverter, as shown in Figure 107. This fact allows introducing a dynamic scaling coefficient that accounts for such fast variability in plant power.
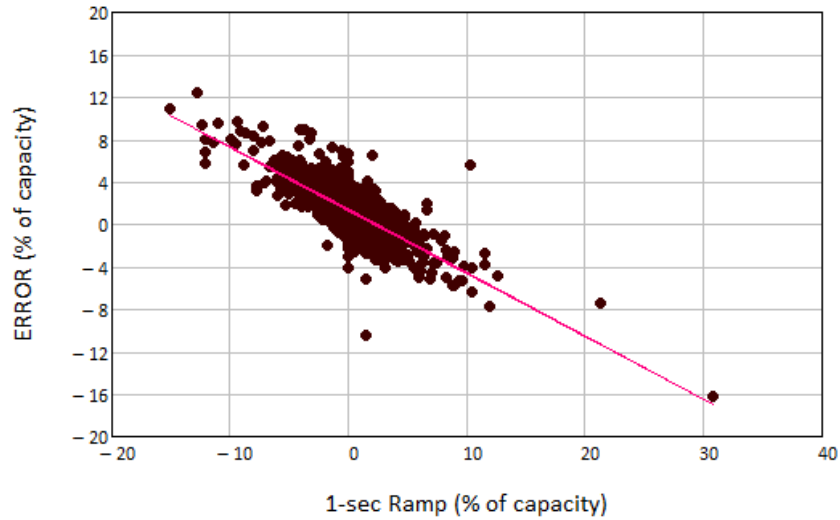
**Figure 107. Correlation between the estimation error and the 1-s variability in the power output of the reference inverter and linear regression**

The slope, $a$, and intercept, $b$, of the linear regression estimation were used to introduce a dynamic scaling factor as a function of 1-s changes in power for the reference inverter, defined as:

$$R_{ref}(t_i) = P_{ref}(t_i) - P_{ref}(t_{i-1}) \tag{13.6}$$

where $R_{ref}(t_i)$ is the 1-s ramp rate of the reference inverter (% of capacity/s) measured at time instance $t_i$; and $P_{ref}(t_i)$ is the measured power output of the reference inverter operating at MPP.

The dynamic scaling factor then can be defined as:

$$K_{scale}(t_i) = a \cdot R_{ref}(t_i) + b \tag{13.7}$$

Therefore, the improved estimated power at each time step, $t_i$, can be defined as:

$$P_{est}(t_i) = P_{125}(t_i) \cdot K_{scale}(t_i) \tag{13.8}$$

This is a very simple approach but one that does not require complex calculations in the PV plant controller and provides substantial improvement in the estimated maximum available power for the entire plant using real-time power measurements from a single reference inverter that operates at MPP. The results of such improvements are shown in the estimation error histograms depicted in Figure 108. For both the less variable Day 1 and more variable Day 2 profiles, the estimation error of the improved method helps keep the maximum 1-s peak power estimation error within ±5% of the rated plant capacity, which is adequate for a plant of this size.

The accuracy of the method will improve with time if long-term plant data are analyzed to derive a more precise regression for a dynamic scaling factor that can also be scheduled based on the season. This will be a subject of future research.
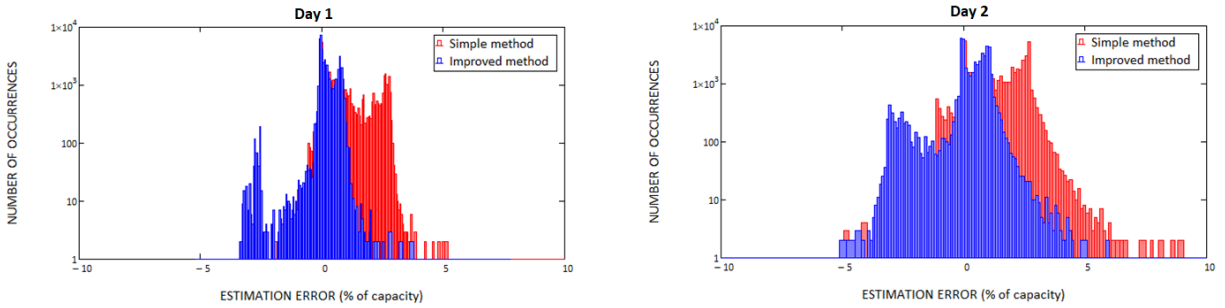
**Figure 108. Distribution of peak power estimation errors**

## 13.4 Evaluation of Peak Power Estimation Method for a Large 300-MW PV Power Plant

During this project, we continued evaluating the reference inverter method for estimating the available peak power in large PV plants with curtailed headroom. We used 1-s production data from one approximately 300-MW PV plant located in the western United States. The plant consists of 79 inverters, each rated at 4 MW, with PV arrays covering large geographic area.
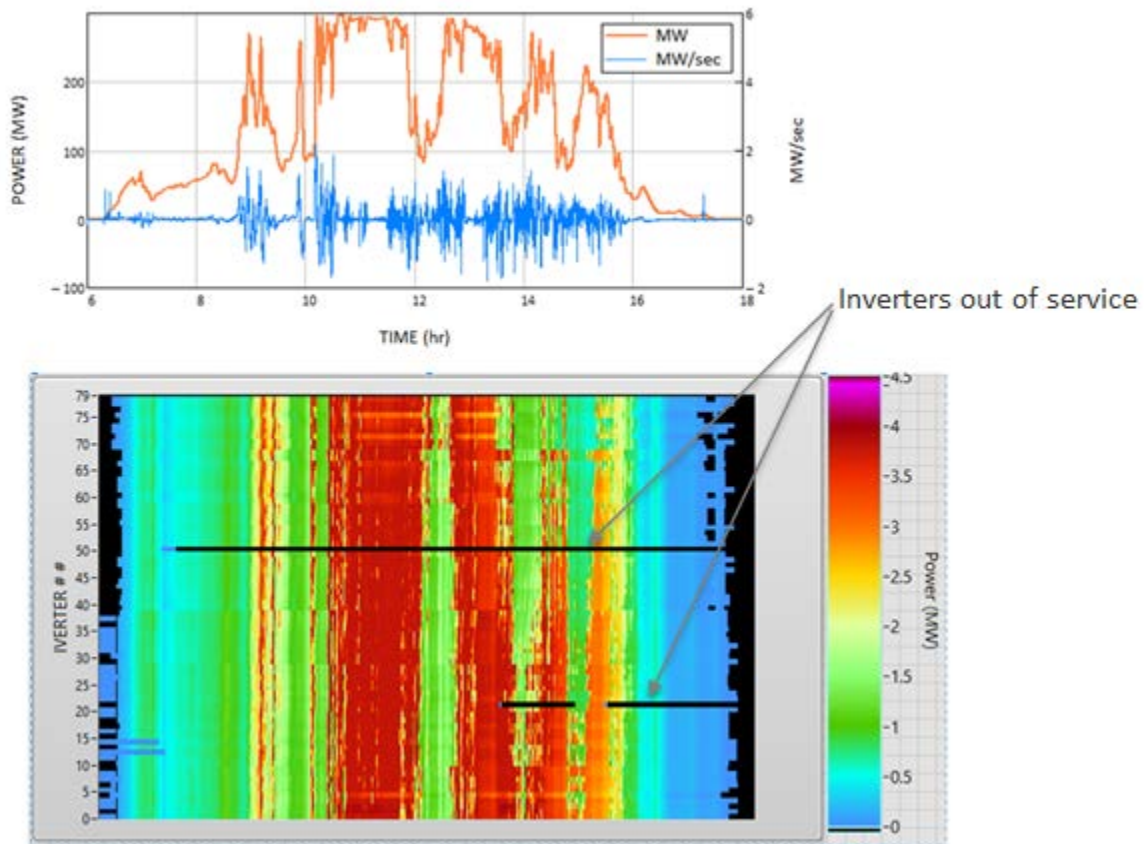


**Figure 109. Example of the daily operation profile of a 300-MW PV plant**

Figure 109 shows an example of 1 day of production of the plant, with the plant total power and total 1-s changes in power (upper graph) and a more detailed view of the performance of each individual inverter during that day (lower heat map). The horizontal axis of the heat map

84

represents the time of day, the vertical axis indicates the inverter number, and the color of the heat map indicates the power production level of each individual inverter during every second of the day. We analyzed several similar days of production with different variability patterns. The total plant 1-s production data and data from the 79 individual inverters for four variability cases were used to evaluate the ability of the proposed method to accurately predict the maximum available power from the entire plant for different numbers of reference inverters.

The following numbers of control zones with a single reference inverter in each zone were used in the analysis of the number of reference inverters: $N=1, 2, 4, 8, 12, 24, 38$. A simple algorithm was developed to select the locations of the reference inverters using an equidistant approach. Another innovative approach used in this analysis was to implement dynamic control zones in the PV plant. The designated reference inverters can be selected dynamically by the plant controller based on various factors. One of these factors can be the array temperatures of curtailed zones. By cycling the reference inverters every specific time interval, excessive heating of the array sections can be avoided to reduce losses. Such operation is shown in Figure 110. In this example, the reference inverters are cycled every 10 min, which explains the checkers-like heat map because the same inverters are switching between peak power and curtailed operation every 10 min.
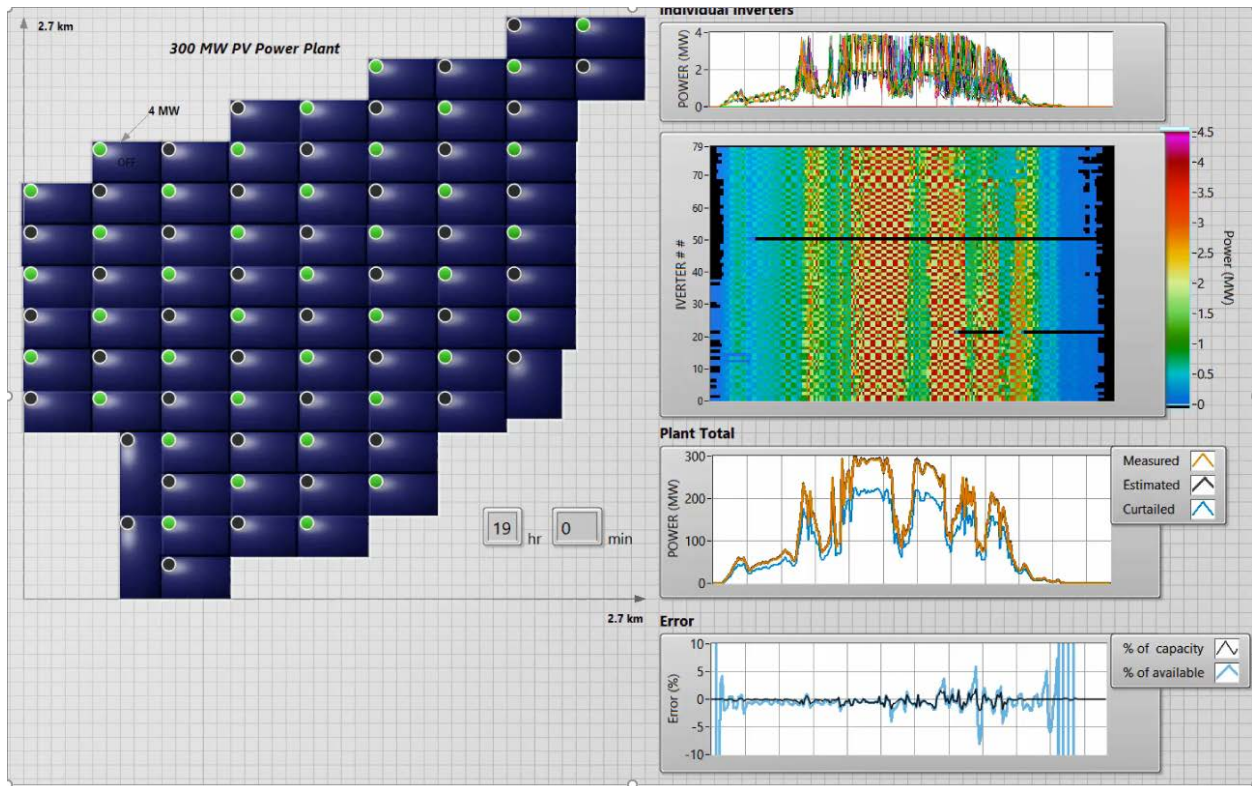


**Figure 110. Dynamic reference inverters (light green circles represent reference inverters)**

The accuracy of the peak power estimation under high-variability conditions for different numbers of reference inverters is shown in Figure 111 in the form of histogram plots. As expected, the highest accuracy of estimation is achieved for a larger number of reference inverters ($N=38$). The maximum positive estimation error is 7.82 MW (or 2.6% of the plant capacity), and the minimum negative estimation error is -7.61 MW (or 2.53% of the plant capacity).
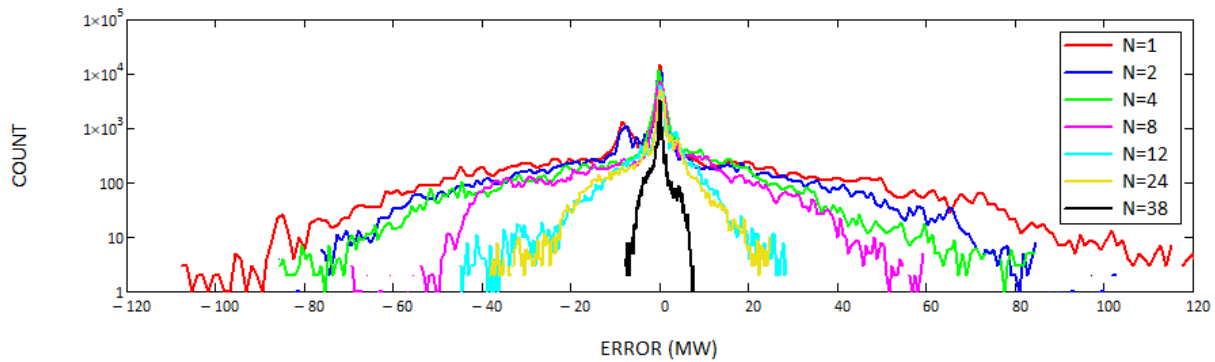
**Figure 111. Peak power estimation errors**

The examined peak power estimation method for curtailed PV power plants is based on using dedicated reference inverters within a plant. The proposed technique does not require deploying any additional equipment or sensors and is based only on the addition of new control logic to the existing PPC. Based on our calculations using measured 1-s power production data from the entire PV power plant and individual inverters, the method has the potential to produce highly accurate real-time estimates of available aggregate peak power that all the plant's inverters can produce at any point in time and can ensure that the control error stays within the desired tolerance bands at all times. The method, by default, accounts for external factors, such as dust accumulation on portions of the modules and the presence of snow or ice patches on the modules, without any additional computations when estimating the available peak power.

The NREL-developed method for active power reserve estimation in curtailed PV plants has been successfully implemented in several utility-scale PV projects worldwide. One such example is the Luz del Norte 141-MW PV power plant owned by First Solar in Chile's Atacama region [42]. This PV plant was used as a pilot to enable PV generation to provide ancillary services to the SEN grid in Chile.

# 14 Test Platform for PV-BESS Systems in Distribution Grids

During this project, we developed a test bed for testing the PV-BESS system in a distribution system and for microgrid applications. The test bed was developed in collaboration with Pacific Gas & Electric Company using a model of their typical distribution circuit. The distribution system model was provided by Pacific Gas & Electric Company, and the NREL team carried out the RSCAD implementation of the distribution system model and implemented it in RTDS (a simplified diagram of the system is shown in Figure 112).

The CGI POI is on the 13.2-kV side of the PV-BESS transformers. An additional voltage-matching transformer was placed in the RSCAD model to match the PV and BESS with a voltage level of 12.47 kV. This point, shown in Figure 112, is the virtual POI of the PV-BESS system with the RSCAD distribution model. Various types of one, two, and three-phase voltage faults can be introduced in the RSCAD model on the 13.2-kV terminals, so the CGI can emulate the exact voltage waveforms on the 12.47-kV bus under such fault conditions. The distribution system model also has submodels of other distributed PV plants, the distribution grid, and various types of loads. A real hardware relay (SEL-351) is connected to the RTDS model as well. The distribution circuit can operate as a stand-alone microgrid after opening Circuit Breaker 1 (CB1). This way, the ability of the grid-forming control of the PV-BESS plant can be tested for islanded operation. One example of such a test event is shown in Figure 113, with the BESS operating in grid-forming mode. After Circuit Breaker 1 trips, the BESS starts tracking the load and automatically injects power into the island. The measured voltage waveforms do not show any transient behavior during this process (upper plot in Figure 113).

Another useful outcome of the test bed is the ability to evaluate the impacts of PV-BESS systems on currents and voltages in the microgrid during transient events. One example of such an evaluation is shown in Figure 114. It combines results on both peak current and minimum voltage levels in different measurement points in the circuit during a line-to-line faut in one of the system buses. NREL developed an automated test and visualization system that allows for producing these types of plots for any desired fault and transient event scenarios, identifying the most "stressed" nodes in the system, and determining the appropriate settings for protection and coordination between various protection devices under each scenario.

This test bed is a unique tool for conducting "at-scale" integration testing of various types of PV-BESS configurations and associated controls in distribution grids and islanded systems. NREL plans on using this platform in future SETO-funded research and collaborative projects with industry.
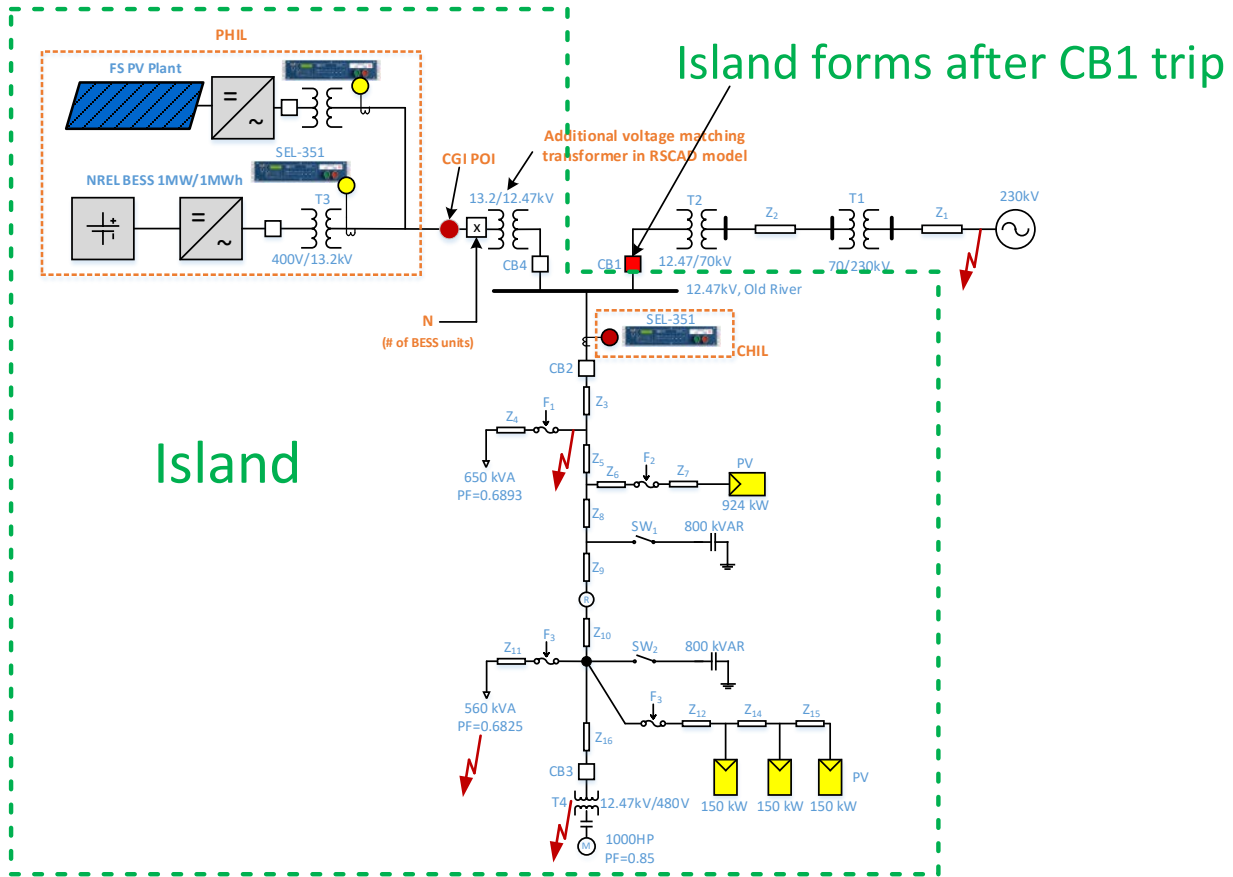
**Figure 112. Test bed for PV-BESS systems in distribution microgrids and islanded grids**
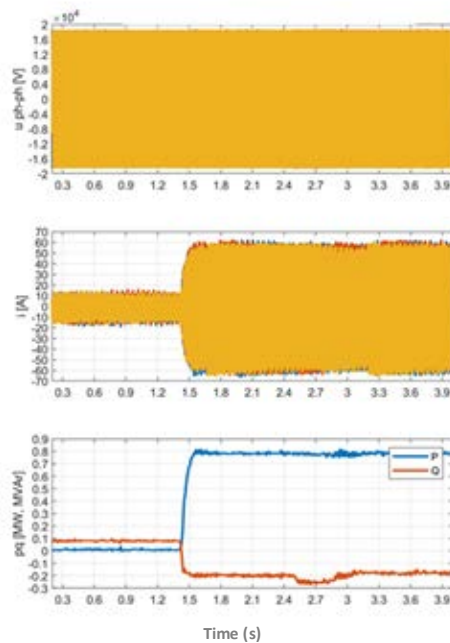


**Figure 113. Measured response of grid-forming BESS after Circuit Breaker 1 trips in the PHIL model**
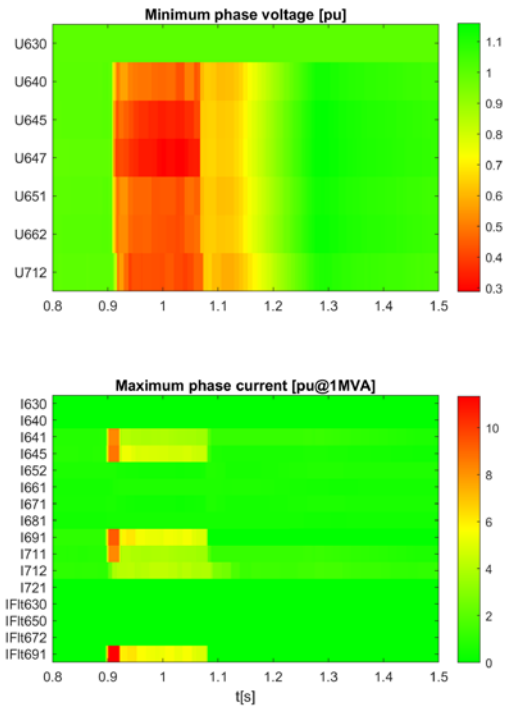
**Figure 114. Minimum voltages and maximum currents recorded in all buses during a line-to-line low-impedance fault in Bus 691**

# 15 Conclusions

This NREL-First Solar cooperative research-and-development agreement project leveraged and benefited from the prior collaboration of large-scale demonstration projects for the provision of reliability grid service by PV plants, knowledge and field experience accumulated from NREL's previous work with First Solar and other partners (CAISO, ERCOT, AES, PREPA, etc.), and advanced prior work by creating new capabilities at NREL's Flatirons Campus for the validation and testing of advanced controls for PV-BESS plants and the demonstration testing of such controls under both real and controllable grid conditions. Specific accomplishments of this project are:

- Constructed, interconnected, and commissioned a real 430-kV PV plant with string inverters. The plant was designed for easy expansion to larger power capacities (up to 1 MW), if needed in the future.
- Integrated the PV plant into NREL's PHIL validation platform based on the CGI and RTDS systems
- Combined the PV and BESS controls under the hybrid plant controller framework to provide existing and evolving ancillary service products for various balancing authorities and system operators in the U.S. interconnections and island systems
- Developed controls with increased complexity because of the multi-technology nature of the PV-BESS operation
- Enhanced the PV PPC based on the SEL RTAC platform by adding new algorithms to include BESS controls and provide many types of essential reliability services
- Demonstrated the operation of the PV-BESS plant with a robust controller interacting with three types of inverters from different vendors
- Demonstrated new PV-BESS controls that can be used by existing and future ancillary service markets (inertial response, PFR, FFR, down-ramp control, provision of spinning reserve, dispatchable operation, voltage control, different types of ramp controls, etc.)
- Demonstrated the ability of PV-BESS plants to provide wide-area stability services in the form of interarea oscillation damping
- Demonstrated that grid-forming controls by BESS can provide resilience services (black start, islanded operation, system restoration) to hybrid PV-plus-storage plants
- Developed and demonstrated methods for the impedance characterization of PV-BESS systems using the 7-MVA CGI coupled with the RTDS
- Demonstrated the black-start capabilities of grid-forming BESS as part of the PV-BESS plant
- Developed a new accurate method for the real-time estimation of available active power reserve in curtailed PV plants. The method has been implemented in serval utility-scale projects worldwide.

The project resulted in the development of a new valuable test and validation asset—a grid-scale PV-plus-storage hybrid system test bed that can be used by the industry and research communities for the validation and demonstration of new control concepts, stakeholder engagement, workforce education, and as a validation platform for the future standardization of hybrid technologies. It will lead to the development of both technology- and vendor-neutral, plug-and-play hybridization guidelines and control architectures openly available at all segments of stakeholder communities.

This project was the first research effort that demonstrated the multi-technology aspect of grid integration research possible at NREL's Flatirons Campus, and it facilitated the shift toward the development of new research platforms, such as IESS and ARIES. Capabilities developed under this project were also foundational for continued hybrid systems research conducted at NREL and were used in other DOE -funded research work, such as the Grid Modernization Laboratory Consortium FlexPower hybrid plants project.

# 16 Future Opportunities

The emergence of new integrated energy systems provides many opportunities, and it also presents urgent challenges that must be addressed to ensure that these new integrated energy systems meet evolving consumer expectations and continue to be economic, reliable, resilient, and secure. From this perspective, integrated PV-BESS systems can play a crucial role for power systems in the transition to high shares of IBRs. New, upcoming capabilities of NREL's Flatirons Campus will establish new, unique research opportunities for PV-plus-storage systems in terms of storage technology diversity, increased capacity, and increased voltage levels for integrated systems, allowing for the study of at-scale interactions among PV generation, storage, advanced controls, and cybersecurity in hybrid energy systems—at both the integration and planning stages. A new 19.9-MVA CGI will be a major addition to the ARIES research platform, enhancing NREL's capabilities to conduct more advanced PHIL experiments for integrated PV-plus-storage systems involving not only BESS but also other storage technologies, such as hydrogen storage, flow batteries, flywheels, and ultracapacitors. The main technical characteristics of the new CGI are shown in Figure 115. There is currently no other research platform like the Flatirons Campus anywhere in the world that can support research at the scale and integration necessary to make a global impact in the marketplace.



**Power rating**
- Continuous AC rating - 19.9 MVA at 13.2kV and 34.5 KV
- Overcurrent capability (x5.7 for 3 sec, x7.3 for 0.5 sec)
- 4-wire 13.2 kV or 35.4 kV taps
- Continuous operational AC voltage range: 0 - 40 kVAC
- Continuous DC rating – 10 MW at 5 kVDC

**Possible test articles**
- Types 1, 2, 3 and 4 wind turbines
- PV inverters, energy storage systems
- Conventional generators
- Combinations of technologies / hybrid systems
- Responsive loads

**Voltage control (no load THD <1%)**
- Balanced and unbalanced voltage fault conditions (ZVRT, LVRT and 140% HVRT) – independent voltage control for each phase on 13.2 kV and 34.5 kV terminals
- Response time – less than 1 millisecond (from full voltage to zero, or from zero back to full voltage)
- Programmable injection of positive, negative and zero sequence components
- Long-term symmetrical voltage variations (+/- 10%) and voltage magnitude modulations (0-10 Hz) – SSR conditions
- Programmable impedance (strong and weak grids, wide SCR range corresponding to a POI with up to 250 MVA of short circuit apparent power)
- Injection of controlled voltage distortions
- Wide-spectrum (0-2kHz) impedance characterization of inverter-coupled generation and loads
- All-quadrant reactive power capability characterization of any system

**Frequency control**
- Fast output frequency control (3 Hz/sec) within 45-65 Hz range
- 50/60 Hz operation
- Can simulate frequency conditions for any type of power system
- PHIL capable (can be coupled with RTDS, Opal-RT, Typhoon, etc.)
- Coupled with PMU-based wide-area stability controls validation platform
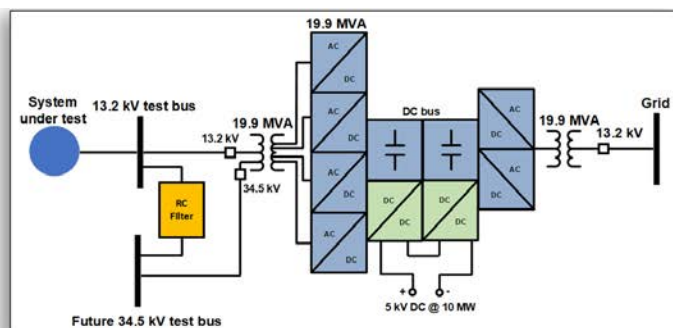
**New features**
- 5 kV MVDC grid simulator (PHIL capable)
- Voltage or current source operation
- Seamless transition between voltage and current source modes
- Emulation of full set of resiliency services:
  - Black start
  - Power system restoration schemes
  - Microgrids
- Flexible configurations are possible when combined with CGI#1:
  - Two independent experiments
  - Parallel operation
  - Back-to-back operation
  - Emulation of isolated, partially or fully grid-connected microgrids

**Figure 115. Main characteristics of the 19.9-MVA CGI**

92

# References

[1]  https://www.cpuc.ca.gov/rps/

[2]  P. Denholm, R. Margolis, "Energy Storage Requirements for Achieving 50% Solar Photovoltaic Penetration in California". NREL report, August 2016

[3]  V. Gevorgian, B. O'Neill *Advanced Grid-Friendly Controls Demonstration Project for Utility-Scale PV Power Plants*. NREL report, 2016. www.nrel.gov/docs/fy16osti/65368.pdf

[4]  V. Gevorgian, C. Loutan, M. Morjaria, et.al. "Demonstration of Advanced Ancillary Service Controls by a Large Utility-Scale PV Power Plant in California". NREL draft report in review, December 2016

[5]  P. Denholm, J. Eichman, R. Margolis, "Evaluating the Technical and Economic Performance of PV Plus Storage Power Plants" NREL technical report, August 2017

[6]  R. Fu, T. Remo, R. Magolis, "2018 U.S. Utility-scale PV-plus-Energy Storage System Costs Benchmark", NREL technical report, November 2018

[7]  W. Gorman, A. Mills, M. Bolinger, R. Wiser, N. Singhal, E. Ela, E. O'Shaughnessy, "Motivations and options for deploying hybrid generator-plus-battery projects within bulk power system", The Electricity Journal, 33/2020.

[8]  M. Bortolini et al., "Technical and economic design of photovoltaic and battery energy storage system," Energy Conversion and Management, vol. 86, pp. 81 – 92, 2014.

[9]  Y. Khawaja, D. Giaouris, H. Patskis, M. Dahidah, "Optimal Cost-Based Model for Sizing Grid-Connected PV and Battery Energy System", 2017 IEEE Jordan Conference on Applied Electrical Engineering and Computing Technologies (AEECT), October 11-13, 2017

[10] C.S. Lai, M. D. Mcculloch, : LCOE for PV and Grid Scale Energy Storage Systems, Applied Energy, Elseiver, volt 190©, pages 191-203

[11] V. Gevorgian et. al. "WGRID-49 GMLC Project Report", NREL, August 2019, https://www.osti.gov/biblio/1558905

[12] Kratochvil, J.A.; Boyson, W.E.; King, D.L. Photovoltaic Array Performance Model; Technical Report; Sandia National Laboratories: Albuquerque, NM, USA, 2004.

[13] L. Petersen, F. Iov, G. C. Tarnowski, V. Gevorgian, P. Koralewicz, D.-I. Stroe, "Validating Performance Models for Hybrid Plant Control Assessment", Energies 2019, 12, 4330

[14] "EPIC 2.05: Inertia Response Emulation of DG Impact Improvement", EPIC Final Report, Pacific Gas and Electric Company, February 20, 2019

[15] X.-Q. Guo, H.-R. Gu, "Phase locked loop and synchronization methods for grid interfaced converters", PRZEGLĄD ELEKTROTECHNICZNY (Electrical Review), ISSN 0033-2097, R. 87 NR 4/2011

[16] NERC, Integration of Variable Generation Task Force Report (Technical Report) (Washington, D.C.: 2012).

[17] NERC, Essential Reliability Services Working Group and Distributed Energy Resources Task Force Measures (Technical Report) (Washington, D.C.: 2012),

[18]   ENTSO-E, "ENTSO-E network code for requirements for grid connection applicable to all generators," ENTSO-E, Brussels Belgium, Tech. Guideline, March 2013

[19]   Technical Requirements for the Connection to and Parallel Operation with Low-Voltage Distribution Networks, VDE-AR-N 4105

[20]   H. Villegas Pico, V. Gevorgian, "Ultra-fast Freqeucny Response of Converter-dominant Grids using PMUs", Conference paper presented at Wind and SOalr Integration Workshop in Dublin, Ireland, October 2019

[21]   WECC Governor Droop Seeting Criterion, PRC-001-WECC-CRT-1.2

[22]   P. Denholm, E. Ela, B. Kirby, "The Role of Energy Storage with Renewbae Electricity Generaion", NREL technical report, January 2010

[23]   "Essential Reliability Services and the Evolving Bulk-Power System – Primary Frequency Response", Federal Energy Regulatory Commission's Order No. 842

[24]   "BAL-003-1 Frequency Response and Frequency Bias Setting Standard", NERC, 2016

[25]   J. C. Neely, R. H. Byrne, R.T. Elliott, C. Silva-Monroy, D. Schoenwald, D. Trudnowski, M, Donnely, "Daming of Inter-area Oscillations using Energy Storage", IEEE PES GM meeting paper, July 2013

[26]   P. Kundur, Power System Stability and Control. New York: McGraw-
[27]   Hill, Inc., 1993

[26]   P. Kundur, Power System Stability and Control, New York, KcGraw-Hill, Inc., 1993

[27]   Federal Energy Regulatory Commission (FERC), "Large Generator Interconnection Agreement," www.ferc.gov/industries/electric/indus-act/gi/stnd-gen.asp.

[28]   M. Morjaria, D. Anichkov, V. Chadliev, and S. Soni, "A Grid Friendly Plant," IEEE Power and Energy Magazine (May/June 2014)

[29]   CAISO 5th Replacement Electronic Tariff, Appendix A: Master Definition Supplement, February 1, 2017

[30]   A. Hoke, E. Muljadi, D. Maksimovic, "Real-time Photovoltaic Plant Maximum Power Point Estimation for Use in Grid Frequency Stabilization", 2015 IEEE 16th Workshop on Control and Modeling for Power Electronics

[31]   E. Batzelis, G. Kampitsis, S. Papathanassiou, "Power Reserves Control for PV Systems with Real-time MPP Estimation via Curve Fitting", IEEE Transactions on Sustainable Energy, Vol. 8, No.3, July 2017

[32]   T. Hiyama and K. Kitabayashi, "Neural network-based estimation of maximum power generation from PV module using environmental information," Energy Convers. IEEE Trans. On, vol. 12, no. 3, pp. 241–247, 1997.

[33]   M. Taherbaneh and K. Faez, "Maximum power point estimation for photovoltaic systems using neural networks," in Control and Automation, 2007. ICCA 2007. IEEE International Conference on, 2007, pp. 1614–1619.

[34]   J.-C. Wang, Y.-L. Su, J.-C. Shieh, and J.-A. Jiang, "High-accuracy maximum power point estimation for photovoltaic arrays," Sol. Energy Mater. Sol. Cells, vol. 95, no. 3, pp. 843–851, 2011.

[35] A. Garrigós, J. M. Blanes, J. A. Carrasco, and J. B. Ejea, "Real time estimation of photovoltaic modules characteristics and its application to maximum power point operation," Renew. Energy, vol. 32, no. 6, pp. 1059–1076, 2007.

[36] J. Ma, K. L. Man, T. O. Ting, N. Zhang, S.-U. Guan, and P. W. Wong, "Dem: direct estimation method for photovoltaic maximum power point tracking," Procedia Comput. Sci., vol. 17, pp. 537–544, 2013.

[37] G. Kumar and A. K. Panchal, "Geometrical prediction of maximum power point for photovoltaics," Appl. Energy, vol. 119, pp. 237–245, 2014.

[38] B.-I. Craciun, T. Kerekes, D. Sera, and R. Teodorescu, "Frequency support functions in large PV power plants with active power reserves,"*IEEE J. Emerg. Sel. Topics Power Electron.*, vol. 2, no. 4, pp. 849–858, Dec. 2014.

[39] V. A. K. Pappu, B. Chowdhury, and R. Bhatt, "Implementing frequency regulation capability in a solar photovoltaic power plant," in *Proc. North Amer. Power Symp. 2010*, Arlington, TX, USA, Sep. 2010, Art. no.5618965

[40] S. Shedd, B.-M. Hodge, A. Florita, and K. Orwig, "A Statistical Characterization of Solar Photovoltaic Power Variability at Small Timescales", 2nd Annual International Workshop on Integration of Solar Power in Power Systems Conference, Lisbon, Portugal, Nov 12-13, 2012

[41] V. Gevorgian, B. O'Neill, "Advanced Grid-Friendly Controls Demonstration Project for Utility-Scale PV Power Plants", NREL technical report, January 2016.

[42] V. Gevorgian, "Highly Accurate Method for Real-Time Active Power Reserve Estimation for Utility-Scale Photovoltaic Plants", NREL report, February 2019

[43] S. Michels Alvaro, T. Avila Araya, G. Ortiz Mercado, N. Milan, "Demonstration of Ancillary Service Provision Capabilities of PV Power Plants: Study Case Luz Del Norte", LABORELEC report, April 2019

[44] "Innovative Ancillary Services", IRENA report, 2019

[45] M. Singh, A. J. Allen, E. Muljadi, V. Gevorgian, Y. Zhang, and S. Santoso, "Interare oscillation damping controls for wind power plants," *IEEE Trans. Sustain. Energy*, vol. 6, no. 3, pp. 967-975, July 2015.

[46] "Oscillation Event 03.12.207 – System Protection and Dynamics WG," ENTSO-E, Brussels, Belgium, 2018.

[47] F. R. Schleif and J. H. White, "Damping for the northwest – southwest oscillations— an analog study," *IEEE Trans. Power App. And Syst.*, vol. 85, no. 2, pp. 1239-1247, Dec. 1966.

[48] E. Rehman, M. Miller, J. Schmal, S. H. Huang, "Dynamic stability assessment if high penetration of renewable generation in the ERCOT grid," ERCOT, Taylor, TX, USA, 2018. [Online]. Available: http://www.ercot.com/content/wcm/lists/144927/Dynamic_Stability_Assessment_of_High_Penetration_of_Renewable_Generation.pdf

[49] E. Rehman, M. G. Miller, J. Schmall, S. H. Huang, and J. Billo, "Stability assessment of high penetration of inverter-based generation in the ERCOT grid," in *Proc. 2019 IEEE Power and Energy Soc. Gen. Meeting*, Atlanta, GA.

[50]  S. Shah, W. Yan, V. Gevorgian, and W. Gao, "Power-domain impedance theory for the analysis and mitigation of interarea oscillations," in Proc. 2020 IEEE Power and Energy Soc. Gen. Meeting. [Online]. Available: https://www.nrel.gov/docs/fy20osti/75273.pdf

[51]  S. Shah, V. Gevorgian, P. Koralewicz, R. Wallen, and W. Yan, "Impedance methods for analyzing stability impacts of inverter-based resources," in *Proc. NSF Workshop Power Electron. Enabled Operation of Power Syst.*, Chicago, IL, Nov. 2019.

[52]  S. Shah, P. Koralewicz, V. Gevorgian, and R. Wallen, "Impedance measurement of wind turbines using a multimegawatt grid simulator," in *Proc. 18th Wind Integr. Workshop*, Dublin, Ireland. [Online]. Available: https://www.nrel.gov/docs/fy20osti/74890.pdf

[53]  S. Shah and L. Parsa, "Impedance modeling of three-phase voltage source converters in dq, sequence, and phasor domains," *IEEE Trans. Energy Conv.*, vol. 32, no. 3, pp. 1139-1150, Sep. 2017.

[54]  S. Shah, P. Koralewicz, V. Gevorgian, and L. Parsa, "Small-signal modeling and design of phase-locked loops using harmonic signal-flow graphs," *IEEE Trans. Energy Conv.*, vol. 35, no. 2, pp. 600-610, June 2020.